THE ELECTROSPINNABILITY OF SACCHARIDES

PABLO GERARDO TORRES LEPE

A thesis submitted in partial fulfilment of the requirements for the

Degree of Doctor of Philosophy in Mechanical Engineering in the

University of Canterbury, Christchurch, New Zealand

March 2017

To my Family and Friends

ACKNOWLEDGMENTS

Firstly, I would like to express my sincere gratitude to Dr. Mark Staiger and Professor Antony Fairbanks for their guidance, supervision and patience during my PhD. Without their support and advice, I could have never achieved the completion of my research. Also, special thanks to Dr Nick Tucker who always believed in me, even before the beginning of this PhD project. Moreover, thanks to the Plant and Food Research biomaterials team, headed by Dr Nigel Larson. Without their scientific support, characterisation infrastructure and editing services assistance, I would not have achieved my PhD Thesis.

Above all, I would like to offer my gratitude to Dr Nick Tucker, his personal support and extended professional friendship have always encouraged me to never give up your personal goals. The professional supervision of Nick Tucker was crucial at every stage of my PhD.

Furthermore, I would like to express my gratitude to Ian Hosie and to the Revolution Fibres team for their extended support during my research and writing. Moreover, special thanks to the Feasey and Hosie families for opening their hearts and homes every time I was in Auckland. Working with the Revolution Fibres team has been the greatest adventure that any student could dream of.

Special thanks to Dr Jonathan Stanger, Dr Nurfaizey A. Hamid, Scientist, Dr Deborah Le Corre and everybody that was part of the Canterbury University and Plant and Food Research electrospinning teams. Without their advice and counselling I would not have had the peer support every PhD student needs throughout their research. Likewise, many thanks to Mike Flaws, Dr Takanori Sato, Kevin Stobbs, Julian Phillips and to all the Canterbury University technicians that were always prompt to help me every time I needed their advice. Thank you for your constructive discussions, valuable comments, general support and practical help during my research work.

Also, I would like to express my earnest gratitude to the governments of Mexico and New Zealand, for their financial support during my studies. I will always be grateful and honoured by their credence, confidence and faith in my persona.

Above all, I would like to express my foremost gratitude to my beloved family back in Mexico, who always believed in me. Specially my only sister, Beatriz Lepe, and my adoptive mother, Lupita Munguia. Even though they were on the other side of the world, they always believed in me and encouraged me to never give up. Thank you!

Lastly, I would like to thank all of my friends for their personal support throughout the years away from home. Thanks to all of the above and to all my beloved ones that are no longer here with me. I know, as they would also acknowledge, that achieving this PhD would mean a lot to me.

ABSTRACT

The electrospinnability of concentrated aqueous solutions of glucose, fructose and sucrose was combinatorially studied by physicochemical and rheological characterisation methods, and by subsequently examining the fibre morphology via scanning electron microscopy. Furthermore, the significance of intermolecular forces (van der Waals versus hydrogen bonding) in the electrospinnability of saccharides was investigated as a function of the substitution of sucrose (e.g., octa-*O*-acetyl sucrose and octa-*O*-methyl sucrose), using an aqueous sucrose solution as the control.

Discussions on secondary bonding driven electrospinnability for saccharide materials are presented throughout the thesis. However, the physical-chemical and molecular mechanisms in the electrospinnability of saccharide materials are still non-obvious.

Furthermore, the electrospinnability of cyclodextrin solutions was also studied in order to explore the effects of hydrogen bonding on supramolecular materials with complex visco-elasticity. Therefore, the electrospinnability of 2-hydroxypropyl-β-cyclodextrins (2HP-β-CD) was investigated by comparing a 2HP-β-CD peroxide-aqueous/acetone-ethanol/$NaHCO_3$ solution and an aqueous urea solution, as a function of 2HP-β-CD concentration. Furthermore, the rheological behaviour of all 2HP-β-CD solutions was characterised by a frequency-independent stress relaxation plateau such as that observed in cross-linked polymer networks and reversible polymer gels with extensive intermolecular bonding.

Moreover, electrospinnability models based on chain entanglement and visco-elasto-capillary theories were compared with experimental results. Visco-elasto-capillary theory showed a better relationship to experimental data, suggesting that longer relaxation times or the capacity to remain electrically stressed for longer periods of time, correlated to improved electrospinnability.

However, neither critical concentration nor visco-elasto-capillary theory can offer an explanation as to how bounded water and aqueous phase separation (aggregate formation) relates to hydrogen bonding or van der Waals interactions during electrospinning.

The commercial application of the research on the electrospinnability of saccharide materials, is exemplified with the development of mānuka honey-glucose syrup nanofibre composite membranes. Commercially sensitive formulations are not reported in this thesis, as products based on the research mentioned on this PhD are currently entering the market.

TABLE OF CONTENTS

LIST OF TABLES

LIST OF FIGURES

GLOSSARY OF SYMBOLS

ρ = Fluid density

g = Gravity acceleration

h = Height of the meniscus on the *y*-axis

p = Pressure

ε = Vacuum permittivity

E = Electric Field strength

r = Droplet, jet or molecular radius

σ_s = Surface and bulk charge

V_{avg} = Average velocity of the flow

K = Boltzmann constant ($K_b = 1.38 \times 10^{-23} J$)

T = Absolute temperature

$\mathfrak{x}$ = Surface tension

L = Most relevant physical length scale

W = Thermodynamic work

A = Relevant area

Δp = Change of pressure

Pc = Capillary pressure

Pe = Electric pressure

$R_{X,Y}$ = Droplet radii of curvature per parallel axis to the surface

z = Position respective to the jet axis

a = Capillary length

b = Vertical (x) droplet displacement

ω = Angular frequency

π = Pi

v = Volume

c = Concentration

d = Distance

Na = Avogadro's number

V = Applied Voltage

R = Gas constant

D = Debye's length

G = Gibbs energy

$л$ = Molecular mean free path

E_{cr} = Critical electric field strength

λ = Wavelength, relaxation time

k = Wave number, ion mobility

e = Natural logarithm

q = Wave amplitude

R_o = Original radius of the cylinder

R_d = Droplet radius

Q = Volume flow rate

v = Axial velocity

I = Current, Ionic flux, Ionic wind

Φ = Electric or electrostatic potential

M = Chemical potential, dipole moment

Λ = Intra-jet distance

c^* = Critical concentration

n_{sp} = Specific viscosity

$[\eta]$ = Intrinsic viscosity

M_w = Molecular weight

η = Viscosity

τ = Relaxation time

G' = Storage modulus

G'' = Loss modulus

R_g = Radius of gyration

μ = Dynamic viscosity

η = Shear viscosity

CHAPTER 1

INTRODUCTION

1.1 Background

Electrospinning is a method of producing fibres in the micro and nano scale, this is between 1 x 10^{-9}m (1 nm) and 1 x 10^{-7}m (0. 1 μm). During the electrospinning process, a high voltage is applied to a droplet of a polymer solution (or melt), stretching the droplet into a conical shape (known as the Taylor cone) by means of electrostatic repulsion. A jet of polymer solution is emitted from the tip of the Taylor cone if the build-up of internal electrical charge overcomes the surface tension of the droplet.

Given an appropriate combination of electro-viscoelastic properties, the polymer jet initially follows a stable, linear trajectory that resists the Plateau–Rayleigh instability, enabling it to be drawn into a fibre. Otherwise, the solution will break-up into small droplets during flight, as described by the Rayleigh instability (aka electrospraying). Following stable jet formation, the jet typically undergoes a chaotic bending instability that leads to extensive jet thinning through solvent loss. A solid polymer fibre is then collected at an earthed electrode if sufficient solvent has been evaporated during the flight from tip to collector.

The ability of a polymer solution to resist the Plateau–Rayleigh instability during flight is usually attributed to the entanglement of polymeric molecules, and chain entanglement, or critical concentration theory, is commonly proposed to be the most commonly accepted explanation of fibre formation during electrospinning of polymeric systems. The formation of uniform electrospun polymeric fibres is thought to rely on the presence of at least 2 to 2.4 entanglements per chain, based on the critical "theta" concentration and pervaded volume threshold of each polymer–solvent system.

However, some polymers may transition from electrospraying to electrospinning (as evidenced by the formation of beads-on-a-string) at concentrations between the critical overlap concentration (c^*) (e.g., semi-dilute, un-entangled) and the entanglement concentration (*Ce*) (e.g., semi-dilute, entangled), where *Ce* is typically ~10 × c^*.

An alternative approach used to describe the concept of electrospinnability is the visco-elasto-capillary theory. According to visco-elasto-capillary thinning theory, non-Newtonian fluids

that undergo shear thinning and where $G' > G''$ at higher angular frequencies are able to better resist extensional capillary thinning and filament break-up when compared with Newtonian fluids for which $G' < G''$ at lower angular frequencies. According to the visco-elasto-capillary theory, when the inverse of the fluid relaxation time exceeds the rate of capillary thinning (wave propagation), Rayleigh instabilities can be suppressed, resulting in uniform filaments.

Oligosaccharides are carbohydrates that consist of monosaccharide units linked together to form short chains of varying length (di-, tri-, tetra-, pentasaccharides, etc.). The potential of concentrated saccharide solutions to create metastable "supramolecular-like" architectures may underpin the electrospinnability of such materials. Elasticity for supramolecular materials is often related to electrospinnability, through gelation or colloid aggregation via hydrogen bonding networks and van der Waals mechanisms.

The results presented throughout this thesis indicate that the electrospinnability of concentrated saccharide solutions is in agreement with visco-elasto-capillary theory, as described by the Deborah (De) and Ohnesorge (Oh) non-dimensional numbers relating elasto-capillary thinning rates to the characteristic relaxation time of the material. Moreover, the results presented in this thesis, confirm the hypothesis that intermolecular interactions (van der Waals forces and hydrogen bonding) are critical for the electrospinnability of saccharide solutions.

Novel experimental evidence is provided on the electrospinnability of nonpolymeric saccharides that might have implications for the development of new bionanomaterials for medical, healthcare and pharmaceutical applications; as exemplified by the development of mānuka honey and glucose syrup composite nanofibre prototypes (Chapter 6).

1.2 Research motivation

The need for new healthcare products (e.g., air filtration facemasks and repair skincare patches) based on locally sourced functional biomaterials (e.g., mānuka honey) is increasing as worldwide air pollution and health problems continues to rise due to several man-made and natural causes.

In contrast, common manufacturing techniques for microfibre (e.g., spun bonded, co-extrusion, melt-spinning, etc.) do not easily allow for the integration of chemical and biological functionality within the fibre matrix and resulting membrane. In contrast, electrospinning of biomaterials allows for the addition of natural extracts with antimicrobial properties, which can be subsequently used for many air filtration and healthcare applications. Medical patches and industrial respirators based on microfibre technology do not offer the breathability and efficacy that nanofibre technology can provide.

In particular, mānuka honey is regarded as an efficient natural product with high antimicrobial efficacy in many Asian markets. Subsequently, mānuka honey–nanofibre formulations could be a sensible business opportunity with many positive health impacts for skincare and healthcare applications.

The industrial challenges of scaling up the electrospinning process have been previously overcome by our research group (Plant and Food Research, biomaterials group and the University of Canterbury, materials science department) in collaboration with the industrial partner of this research project – Revolution Fibres Ltd.

The manufacturing challenges of prototyping a functional nanofibre facemask have also been overcome by me and Revolution Fibres. The resulting and confidential Intellectual Property (IP) presented in Chapter 6, is the result of five years of research and business development work of all parties involved in this research project.

The main goal of this research is to further understand the electrospinnability of saccharide materials at an industrial scale for the emerging nonwovens nanofibre industry. The physical-chemical mechanisms during the electrospinning of nonpolymeric, low molecular weight biomaterials is of critical significance for the antimicrobial functionality of resulting nanofibre.

This thesis provides further insights into the processability of honey and sugar syrups as novel biomaterials for the production of nonwoven media for healthcare applications.

This PhD was developed by the University of Canterbury and Plant and Food Research Ltd, through a joint PhD studentship received from the Ministry of Business Innovation and Employment of New Zealand (MBIE) granted through Revolution Fibres Ltd. The intent of the funding provided by Ministry of Business Innovation and Employment of New Zealand

(MBIE) for this study, was to develop innovative new products using New Zealand waste biomaterials using new nanotechnology delivery platforms. Also, to develop proprietary kiwi electrospinning technology, as co-developed by the author in collaboration with the industrial partner of this project - Revolution Fibres Ltd.

1.3 Objectives

The principal objective of this thesis is to further understand the electrospinnability of saccharide materials for industrial nanofibre manufacturing. Also, understanding the rheological properties of saccharide materials is of crucial significance to the industrial processability of such materials, as the flow dynamics of complex fluids are a determining factor in their processability. Moreover, the use of commercial, food-grade glucose syrups as a promoting electrospinnability agent for honey is of particular importance in lowering the cost restrictions of the raw materials. In general, the research and development objectives pursed on this thesis are the following:

- Explore the electrospinnability boundaries of common sugars and its ability to form continuous filaments.
- Explore the electrospinnability boundaries of modified sucrose solutions to further understand the physical-chemical mechanism for the electrospinnability of sugars.
- Explore the electrospinnability of cyclodextrins in the presence of salts to further understand the electrospinnability behaviour of the physical-chemical properties of dense supramolecular fluids with complex rheological properties.
- Explore the electrospinnability boundaries of a food-grade glucose syrup as an alternative material for supporting honey extracts.

Also, further understanding on the applicability of current electrospinnability models (e.g., critical concentration or chain entanglement theory, and visco-elasto-capillary theory), for nonpolymeric materials has been explored and extensively discussed throughout the thesis.

1.4 Thesis scope

An extensive literature review of the electrospinning process, with a strong focus on the physical-chemical peculiarities of the process, is presented in Chapter 2. Also, a review on current electrospinnability theories (e.g., critical concentration and visco-elasto-capillary theory). Detailed experimental procedures and characterisation methods are presented in Chapter 3. However, in each chapter a brief list of materials, experimentation methodology and equipment used is also offered. Chapters 4 and 5 present the bulk of the experimental results generated throughout this investigation based on the electrospinnability of concentrated saccharide solutions, modified sucrose compounds and cyclodextrins. Chapter 6 presents a brief description of a current application for the electrospinnability of saccharide materials e.g., mānuka honey nanofibres.

Finally, Chapters 7 and 8 present the discussions and conclusions of the thesis, and a brief analysis on the perspectives needed to advance future research on this area. The Appendix provides a list of all graphs needed to calculate the non-dimensional numbers required by the visco-elasto-capillary theory, and based on relaxation time approximations using a simplified version of the tube model.

CHAPTER 2

LITERATURE REVIEW

2.1 The electrospinning process

During the electrospinning process, a high voltage is applied to a droplet of a polymer dissolved in a solution (or polymer melt), stretching the droplet into a conical shape (also known as the Taylor cone) by means of electrostatic repulsion. A jet of polymer solution is emitted from the tip of the Taylor cone if the build-up of internal electrical charge overcomes the surface tension of the droplet. Given an appropriate combination of electro-viscoelastic properties, the polymer jet initially follows a stable, linear trajectory that resists the Plateau–Rayleigh instability, enabling it to be drawn into a fibre.

Following stable jet formation, the jet typically undergoes a chaotic bending instability that leads to extensive jet thinning that is accompanied by solvent loss. A solid polymer fibre is then collected at an earthed electrode if sufficient solvent has been evaporated during the flight from tip to collector (Figure 2.1).

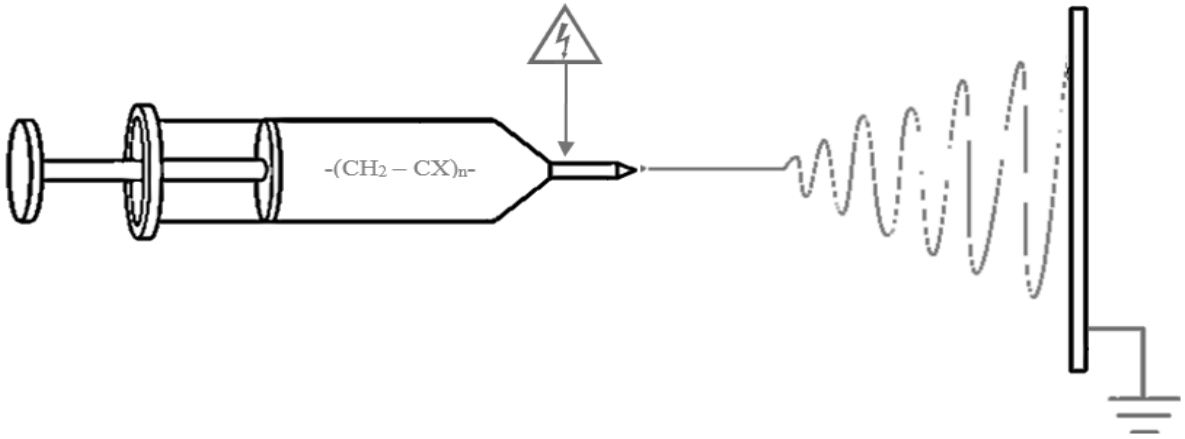

Figure 2.1 – Schematic of the electrospinning process.

Most reviews on the electrospinning process are based on the mathematical descriptions between idealised boundary conditions. [12, 16, 18-21]. Usually, process descriptions are performed by statistical parametric analysis of the relationships between experimental results and fibre morphology. Common techniques are scaling law [22-24], regression analysis [25], independent variables parametric analysis [26-28], and computer simulations [29].

The experimental characterisation of the electrospinning process is also limited in that only some of the variables (e.g., flow, voltage and distance) that affect the evolution of the overall process can be studied and properly quantified. Parametric analysis based on the relationship between measured variables is the basis for most of the proposed mathematical models [25, 30-38].

The electrospinnability of a given material is thought to be mainly dependent on the ability of the solution or melt to resist the Plateau–Rayleigh instability during the flight of the jet. Chain entanglement is commonly proposed to be the leading mechanism for electrospinnability [30-38]. Moreover, the formation of uniform electrospun polymeric fibres is thought to rely on the presence of at least two entanglements per chain [39, 40].

However, conventional polymer electro-hydrodynamic descriptions of the process (the basis for chain entanglement theory) are often incomplete when describing charge transfer mechanisms by ionic convection only, without taking into consideration intermolecular forces, surface charge migration (convection and diffusion) or electronic diffusion by means of chemical potential flow (phase transition) [41].

2.1.1 Historical background to electrospinning

Early studies on the phenomena of electricity and magnetism can be dated as far back as 600 B.C. (e.g., Thales of Miletus and his studies on the properties of rubbed amber). However, in the 1600s, William Gilbert discovered that a small piece of electrostatically charged amber, when moved towards a droplet of water, forces a cone-like shape to form [1]. In 1749 Nollet observed that during electrical discharges in vacuum, small droplets could be emitted from the tip of this fluid cone, which became the first recorded case of electrospraying [2].

Further understanding of the behaviour of electrified liquid jets and point discharges was brought about by the work of Zeleny between 1907 and 1917 [3,4]. Research on the electrospinning process was continued by Taylor et al. in the late 1960s, with extensive work on electrified droplet geometry and jet emission [5].

Subsequently, the above studies formed a basis for the development of electrohydrodynamics theory and the Taylor–Melcher leaky-dielectric model, which explains the behaviour of droplets deformed by an electric field [6]. Research on electrodynamics for continuous media was extended by Landau and Lifshitz in 1984 by the rescaling of time as a complex constant [7].

In 1971, Baumgarten described the basic mathematical relationships in the electrospinning of acrylic submicron fibres and was first to photograph the expanding helix of a pure fibre during electrospinning [8]. In 1981 Larrondo and Manley studied electrified polymer melts and solutions that, under high electric potential, solidify prior to disintegrating into droplets [9].

However, this behaviour was already predicted by Rayleigh, as the Plateau–Rayleigh instability since 1870 [10, 11]. Increasing interest in nanotechnology over the last two decades has led to many potential applications of electrospun nanofibre. This in turn has drawn attention to the electrospinning process as a versatile method of producing nanofibres.

The journal paper entitled “Process and Applications of Electrospun Fibres” by Doshi and Reneker in 1995 [12], stimulated a strong surge in interest in electrospinning, as shown by a subsequent explosion in the number of scientific publications (Figure 2.2). However, a considerable amount of research on the industrialisation of the electrospinning process has been carried out by Russian scientists at the Karpov Institute of Physical Chemistry in Moscow since 1930. Much of this work is continued at Esfil-Tehno on Sillamäe, Estonia [13].

The electrospinning research by the Russians was not widely available, due to the secrecy that surrounded scientific development during the Cold War. However, a substantial amount of this knowledge was eventually shared with the rest of the world through the translation of a book entitled “Electrospinning of Micro and Nanofibres” [14].

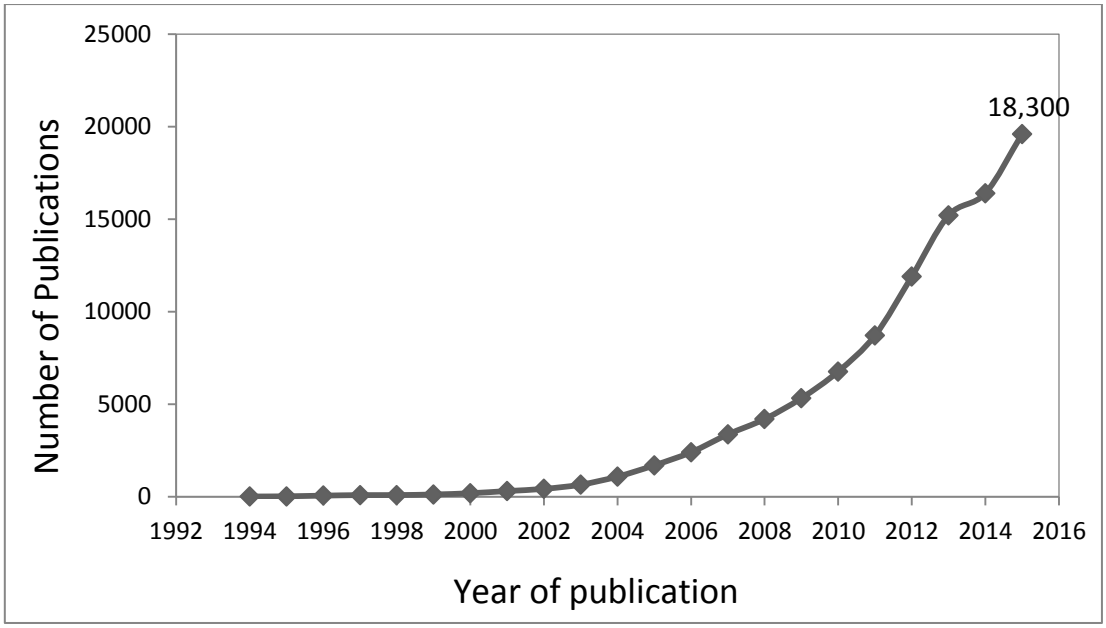

Figure 2.2 - Annual number of publications with the key word "electrospinning" as provided by Google scholar (data survey made on 1 December 2016).

The renewed interest in developing new electrospinning IP is due to the large number of potential applications of this technology [15-18]. Furthermore, the ability to scale up the electrospinning process, as demonstrated by the Russians, has encouraged the continuous development of further commercial opportunities for electrospun nanofibre (Chapter 6).

2.1.2 Polymer flow

Capillary flow can be pressure driven,

$$p = \rho g h \qquad \text{Equation 2.1}$$

where pressure p, equals the fluid density ρ multiplied by the height of the meniscus h and the gravity acceleration; and electro-kinetically driven,

$$Ne = \epsilon E^2 r/\sigma \qquad \text{Equation 2.2}$$

where the electric bond number *Ne*, equals the permittivity ϵ, multiplied by the square of electric field strength E^2, by the fluid radius r and by the total surface and bulk charge energy of the fluid σ.

The balancing electric and capillary mechanism can act as a pushing force (inertia viscous-fluidity) at the same time that as a drawing force (electro kinetic-capillary) [42]. For instance, higher voltages usually yield higher flow rates during electrospinning [39-40]. Nonetheless, both mechanisms of capillary flow are based on the assumption of laminar flow and do not consider the onset of turbulence, as described by the Reynolds number

$$Re = \frac{\rho L V_{avg}}{\eta} \qquad \text{Equation 2.3}$$

where *L* is the most relevant length scale, η is the viscosity, ρ is the fluid density and V_{avg} is the average velocity of the flow.

The small dimensions of the syringe capillaries typically used in electrospinning and the viscoelastic properties of semi-dilute entangled polymer solutions ($Re < 1$) are conditions that typically do not promote turbulent flow [42, 43]. In this Reynolds spectrum, most fluids will flow as steady Newtonian liquids, as described by the classical Navier–Stokes equations.

However, there is no need for turbulent flow (high Reynolds numbers) to stress a molecule, since it is possible to have molecular-momentum phenomena, even at moderate temperatures (e.g., flow separation due to Brownian motion) [50]. Moreover, nonlinear terms such as convective acceleration (advection and diffusion flow mechanisms) cannot always be neglected [44], particularly if the fluid is accelerated in a convergent nozzle (e.g., fluid flowing from a syringe through smaller capillaries into a needle) [45].

Barber et al., have shown that in standard micro-fluidic environments, the slip flow regime can still be modelled using the Navier–Stokes equations, provided that appropriate tangential slip-boundary velocity conditions are implemented along the walls of the flow domain [46]. The use of stochastic partial differential equations with nonlinear solutions can yield more accurate results [47-49].

Furthermore, Brownian motion can be observed in large molecules such as dilute polymeric solutions, such that their flow is no longer driven by their own thermal energy but by collisions with nearby solvent particles. Hence, Brownian molecular turbulence can add momentum to semi-dilute entangled polymer chains, invariably creating a difference in the electrochemical potentials of the species [51]. In contrast, zero voltage is often used as the initial condition for the energy equation in electrospinning, commonly used as the basis of most electrospinnability models (e.g., chain entanglement) [39, 40].

2.1.3 Droplet formation

As the polymer solution continues to flow through the syringe capillary, it gradually generates a droplet at the end of the needle that subsequently becomes the base of a Taylor cone. The evolution of droplet formation is typically described as the capillary forces F_{γ} balancing the gravitational Fg and electric forces Fe [52], such that

$$F_{\gamma} = Fe + Fg \qquad \text{Equation 2.4}$$

Droplet formation in the absence of an applied electric field has been widely studied in microjet printing and genomics microarray devices [53-55]. Microjet printing has been extensively studied over the past few years, commonly modelled using simplified versions of the complete 3D Navier–Stokes equations, assuming isotropy in the material, idealised boundary conditions and Newtonian fluid behaviour. However, computational models for low viscosity and dilute polymer solutions, have shown that relaxation times of polymer chains due to an extensional change in filament radius far exceed the estimated values using conventional Rouse–Zimm theory [54].

2.1.4 Taylor cone formation

Taylor cone formation from pendant drops subjected to external electric fields is usually described as the result of the nonlinear convective mechanism of ionic charge redistribution with respect to voltage [56-62]. The droplet and subsequent jetting is assumed be either a perfect conductor or in a more realistic case, a “leaky-dielectric” medium. Leaky dielectrics

differ from ideal conductors in that the free charge that accumulates on the fluid interface is continuously changing the electric field on the surface of the body [6].

However, when the leaky-dielectric model is applied to electrospinning, it results in discontinuous solutions for some of the proposed equations for velocity, electric field strength and free-surface configurations [63, 64]. The leaky-dielectric model assumes that ionic mobility within the solution is due to conductive and convective mechanisms of charge redistribution only. However, electrophoresis theory predicts that droplet polarisation can occur instantly, as soon as the droplet interacts with an external electric field [65].

Droplet polarisation causes a nonuniform distribution of electrons within the molecules and, as a result, mutual attraction is created between two neighbouring molecules (dipole-dipole) [66]. Subsequently, permanent or induced dipole moments are formed within the bulk of the molecular conglomerate. The width of the ionic atmosphere surrounding the surface of the polarised droplet is called the Debye length. In turn, the Debye length can be further polarised often forming a double layer within the ionic atmosphere and surface of the droplet (Figure 2.3).

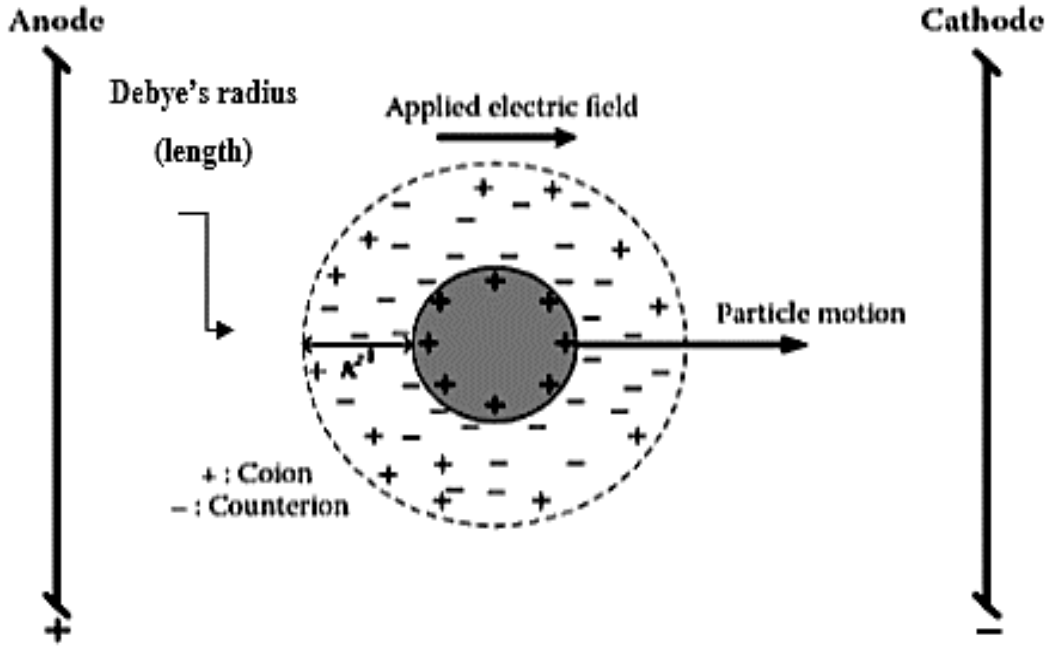

Figure 2.3 - Electrophoresis of a positively charged colloidal particle subject to an applied external electric field [65].

The Debye length is ultimately a consequence of the solvent-polymer intermolecular interactions throughout the bulk of the solution and particularly at the liquid-air interface. In other words, the tendency of the system to balance its surface energy (capillary pressure) relative to the external applied electric field (electric pressure), can be regarded as the main phenomenon driving the visco-elasto-capillary thinning of the stable part of the jet during the electrospinning process [41].

2.1.5 Jet formation

Classical thermodynamics states that the mechanical work W needed to increase surface area A is given by the relationship

$$dW = \gamma \, dA \qquad \text{Equation 2.5}$$

where surface tension γ equals the Gibbs free energy per unit surface area at constant temperature and pressure [67]. Also, classical equilibrium thermodynamics requires that all spontaneous changes of state are accompanied by a decrease in Gibbs free energy.

In other words, decreasing the surface area of the jet is always a spontaneous process under an applied electric field, since the surface tension of any two-layer boundary medium cannot be zero ($\Delta G < 0$). In the case of electrospinning and for isotropic materials, when the electric pressure and surface tension balance each other, the enthalpy of the system corresponds to the Gibbs free energy, as the surface of the jet increases linearly with jet length [67]. Further stretching of the jet stresses the molecules, increasing their relative molecular potentials at the liquid-air interface, creating a pronounced electric bilayer effect (the Debye length), in turn increasing the overall Gibbs free energy.

Lukas et al., [41] arrived at the conclusion that jetting will occur when electric pressure pe exceeds capillary pressure pc, $pe \geq p$c, by assuming the potential field gradients at the surface and inside the bulk of the fluid counteract each other due to the electrical bilayer effect [41]. As the electric pressure keeps exceeding the total capillary pressure of the fluid jet, the electric field will curve the jet until the electric pressure overcomes the total cohesive energy of the fluid jet, eventually breaking it up into smaller droplets as described by the Rayleigh instability (Figure 2.4).

Moreover, as surface tension balances capillary forces, the jet geometry becomes a curved shape, to minimise the exposed surface area to the externally enforced high voltage electric field [68]. When all the forces are balanced, the resulting equilibrium can be described by the Young–Laplace equation

$$\Delta p = \gamma \left(\frac{1}{R_x} + \frac{1}{R_y} \right) \qquad \text{Equation 2.6}$$

where Δp is the pressure difference, γ is surface tension and R_X and R_Y are the radii of curvature in each of the axes that are parallel to the surface [69].

The apparent resulting sinusoidal behaviour of the jet and Δp fluctuations can be ultimately related to the intermolecular electrostatic potentials experienced by the polymer–solvent molecules in the outer layers of the jet in direct contact with the high voltage electric field [69].

Furthermore, when the Δp perturbations are resolved into their sinusoidal components, it has been found that some components grow with time while others decay [70]. Such apparent contradictory behaviour may be associated, under specific conditions, with the nonlinear additivity of van der Waals forces when subjected to external electric fields [71, 72].

For example, electron-dynamic interactions such as Lifshitz–van der Waals interactions can promote an asymmetric electronic configuration of the molecules within the solution when aqueous solutions of nonpolar molecules are subjected to high voltage electric fields [71, 72].

Moreover, Lifshitz–van der Waals interactions can arise from permanent dipole-dipole interactions (Keesom interactions), dipole-induced dipole (dispersion) interactions (London forces), and dipole-induced dipole (induction) interactions (Debye polarisation).

The orientation of charged water molecules is in turn associated with the high density of opposing electron-donors, often a sizeable distance away from the hydrophobic (electron-donating) surfaces – a mechanism associated with hydrogen bonding [71, 72].

2.1.6 Rayleigh instability

Generally, the disintegration of a liquid jet of radius r into small droplets occurs due to the development of wave perturbations on the surface of the jet. The wavelength λ must be greater than π r for the perturbation to trigger disintegration of a cylindrical liquid jet ($\lambda > \pi$ r) [41].

Figure 2.4 - Jetting showing the Rayleigh instability [56].

The Rayleigh instability of a liquid jet is the consequence of a temporal development and subsequent magnification of intermolecular perturbations referred to as capillary waves. These waves are described by Chandrasekhar and others as surface perturbations or sinusoidal capillary waves [73-77].

In other words, the external electric field helps to reduce the Rayleigh instability during the stable part of jet, since it is hindering the destructive capillary pressure of the liquid jet curving the surface into a droplet (the most stable geometry under such conditions).

For the subsequent thinning of the jet, the intermolecular forces of the jet might oppose further Rayleigh instabilities [78]. In practice, this occurs when the fibre attains diameters of less than 100 nm, as supported by the lack of evidence of bead formation in electrospun fibres below the diameter of 100 nm. Surface tension drives the thinning, and either viscosity or elasticity resist necking in a capillary thinning process such as electrospinning. Therefore higher De and Re numbers are needed for electrospinnability, since both imply that a higher or longer relaxation time of the overall system is present in respect to the capillary perturbation wavelength [79-81].

Typically, relaxation times for polymers are in the range of 1 to 3 seconds [79]. Chain entanglement models for electrospinning are based on the Rouse–Zimm model of polymer physics, using the Rouse relaxation times predicted by this theory.

However, relaxation processes that occur on smaller time scales than 10–100 ms cannot be unambiguously resolved [82]. Hence, Rouse relaxation times are only approximate at best, when predicting stress relaxation in processes with large strains in very short times (typical of electrospinning); the effective time for the molecules to relax the applied stresses during the flight of the jet is typically less than 10 ms [79-82].

2.1.7 Jet stretching

The stability of the initial linear jet region is associated with high electrical conductivity of the ionic species within the solution during this stage of the process such that Rayleigh instability wavelengths are usually not present. As a result, the jet diameter decreases linearly according to various relationships derived from the mass and charge conservation laws [83-87].

The apparent symmetric scaling of the stable jet is typically deduced from the conservation of energy in the form of the modified Bernoulli theorem, used to describe the dependence of the jet radius (*r)* on position (*z)* with respect to the jet axis [41]. However, loss of surface charge through the air/jet interface increases as the surface area increases during stretching of the jet.

Subsequently, the energy of the electric pressure can no longer be dissipated by further linear elongation when the charge mobility inside the bulk of the solution is restricted by the reduced jet diameter, resulting in the whipping instability as described by the Earnshaw theorem [88].

2.1.8 Whipping instability

During the whipping instability, the highly charged electrospun jet experiences long-range electronic and viscoelastic interactions, due to its long cylindrical shape (high surface area) and inherit molecular anisotropy. As first described by the Earnshaw theorem: *"A charged body placed in an electric field of force cannot rest in a stable equilibrium under the influence of the electric forces alone."* [88].

In other words, self-attraction and self-repulsion effects between surface charge carriers occurs as the jet elongates due to inertia looping and viscoelastic bending, leading to a rapid whipping instability expansion [89].

The whipping instability is a very rapid phenomenon, with axial strain rates of about 10^5 s^{-1} [89]. At this strain rate, the whipping instability leads to further reduction of the jet thickness from around 100 μm down to 100 nm, in less than a fraction of a second [90].

Moreover, the jet elongation is not axisymmetrical, since the viscoelasticity of the material acts as a compressive force on the overall jet structure [90]. The accumulation of localised electric charge can also produce further capillary wave instabilities, generating secondary jets that can theoretically reduce the jet diameter in an infinite fractal manner [91-96].

2.1.9 Phase transition

Energy conservation during electrospinning may be derived from the Thomson-Kelvin principle based on the ideal condition of thermodynamic equilibrium, characterised by the balance of pressures, temperatures and chemical potentials throughout a reversible system [97].

However, small solvent molecules, which are self-propelled by their own thermal energy, do not necessarily require a concentration gradient to flow away from the fibre matrix; they move randomly and frequently collide with each other and nearby molecules on the boundary layer [102, 103]. Hence, kinetic temperature variations and mass density irregularities, due to molecular diffusion and subsequent evaporation, should not be neglected [104].

In the case of, the electrospinning process, thermodynamic equilibrium occurs by of solvent evaporation [99]. Solvent molecules flow from areas of higher chemical potential (whipping jet) to lower chemical potential (ambient air or vacuum) [98,99]. Hence, the evaporation of the solvent tends to accelerate as the radius decreases during jet thinning and the surface-area-to-volume ratio increases. Sometimes, the solution tends to evaporate selectively as the solvent molecules escape to the ambient air, while only entangled polymeric chains are retained in the jet, forming a porous fibre [100, 101].

2.2 Electrospinnability

2.2.1 Introduction

The electrospinnability of a filament is controlled by the relaxation time and tensile strength of the material, according to the theory of cohesive fracture [105]. Instability due to cohesive fracture commonly occurs in melt-spinning of high molecular weight polymers due to their relatively long relaxation time (1 s). Cohesive fracture is a form of viscoelastic instability, for which the loss modulus is higher than the storage modulus. In general, longer relaxation times, higher stretching velocities and larger draw ratios will tend to encourage cohesive fracture [105, 106].

However, there are many other types of flow instabilities that affect filament formation, such as hydrodynamic instabilities [46, 71, 72, 115]. For example, the Marangoni effect results in flow slip at a fluid/fluid interface due to gradients in the surface tension coefficient [108]. Furthermore, Ziabicki showed that the capillary wave mechanism was the determining factor in the electrospinnability of polymer solutions having low viscosity and jet velocity. In contrast, the elastic modulus appears to be the limiting condition for electrospinnability at higher viscosity or velocity [105].

There are several approaches used to describe the concept of electrospinnability, namely chain entanglement theory and visco-elasto-capillary theory. Chain entanglement or critical concentration theory states that the electrospinnability of a given polymer solution will depend on whether there are more than two entanglements per chain [109]. In contrast, the visco-elasto-capillary theory sets different boundaries for electrospinnability that depend on the rheological properties of the solution (Figure 2.5). This can be generally described by the intrinsic Deborah number (De)

$$De_{\text{intrinsic}} = \frac{\lambda}{[\rho*(\frac{L}{\text{ɤ}})]^{1/3}} \qquad \text{Equation 2.7}$$

where $De_{intrinsic}$ equals the relaxation time λ divided by the cubic root of the density ρ, multiplied by the factor of the length scale L divided by the surface tension ɤ; and by the Ohnesorge number (Oh)

$$Oh = \frac{Ca}{Re} = \frac{(\eta*v)/_{\text{ɤ}}}{(v*L*\rho)/_{\eta}} \qquad \text{Equation 2.8}$$

where the capillary number Ca equals the zero-shear viscosity η multiplied by the jet speed *v* and in total, divided by the surface tension ϰ. According to the visco-elasto-capillary theory, a solution can be considered electrospinnable, if the rheological properties comply with the following condition De (elasticity) ≥ Oh (viscosity) ≥ 1 [82].

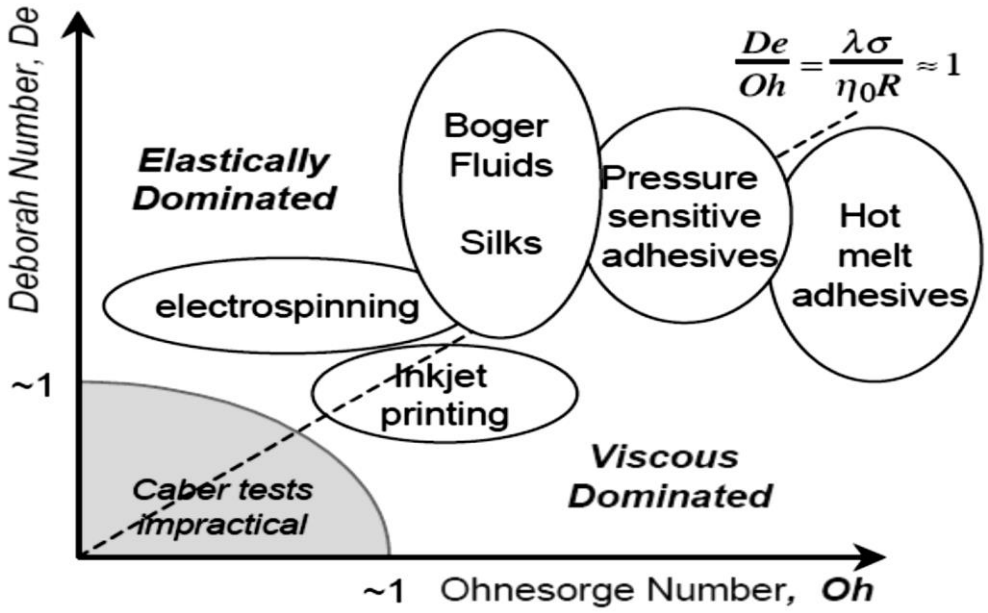

Figure 2.5 - An "operating diagram" for capillary self-thinning and break-up of complex fluids; organized in terms of the natural time scales for capillary, viscous, and elastic phenomena. Sketched are the loci for some common representative free-surface flows of complex fluids [80].

2.2.2 Chain entanglement theory

Polymer rheology has been extended to formulate a semi-empirical analysis to explain the transition from electrospraying to electrospinning based on random (Gaussian) chain conformations, commonly used in the Flory–Huggins theory. The formation of uniform electrospun polymeric fibres is thought to rely on the presence of at least 2 to 2.4 entanglements per chain, based on the critical theta concentration or pervaded volume threshold of each polymer–solvent system [109-111].

The free volume in a polymer solution is the unoccupied physical volume between polymeric chains. Outside the theta condition, solvent molecules might pervade the excluded volume generated within the polymer chains in the solution, increasing the chain contour length and resultant geometrical configuration of the polymer molecule [112].

Covalent bonds with typical energies of 300 to 500 kJ/mol are thought to be responsible for the molecular cohesion needed for each polymer chain to maintain their interconnected structures during entanglement and subsequent electrospinning. Chain entanglement is not limited to a pair of monomeric units on the same chain (intra-chain interaction). Chain entanglement exists equally between monomeric units on different chains (inter-chain interactions) [109].

However, polymer physics regards secondary noncovalent intermolecular forces to act only as virtual chain entanglements, swelling the already interconnected polymeric chains into gels (Figure 2.6) [154]. Similar to a theta condition where solvent-polymer molecular interactions are negligible in terms of the excluded volume effects and ideal chain model parameters (e.g., radius of gyration) can be used to model the chain entanglement interactions.

From this point of view, secondary bonding mechanisms (e.g., hydrogen bonds with typical energies of 10–50 kJ/mol) can act only as a complementary cohesion force to the already covalently cross-linked polymeric chains. However, at higher polymer concentrations, the inter-chain interactions, driven by noncovalent bonding, are the dominant mechanism of chain entanglement (Figure 2.6).

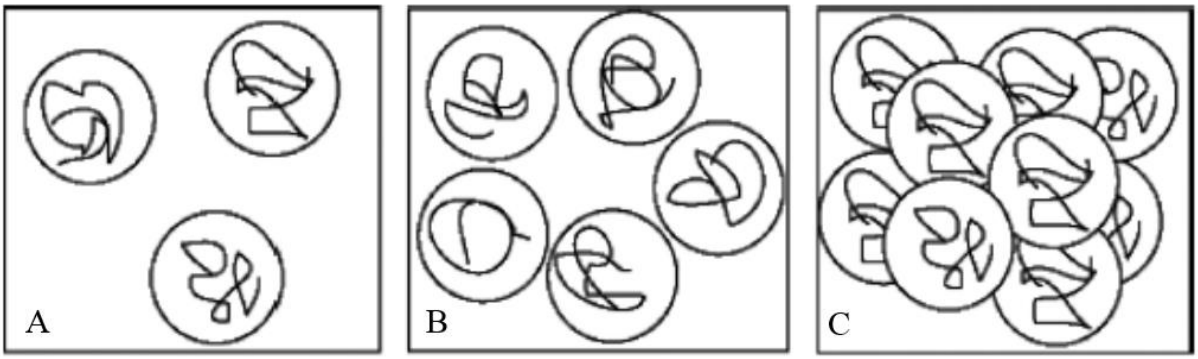

Figure 2.6 - Graphical representation of the three solution regimens; A) dilute ($c \leq c*$) B) semi-dilute ($c* \leq c$) and C) concentrated ($c^* << c$), the quantity (c^*) is the critical concentration [112].

Fibre formation predicted by chain entanglement theory states that it is necessary to have at least one entanglement per polymer chain, while stable fibre formation requires two or more entanglements per chain.

However, some polymers may transition from electrospraying to electrospinning (as evidenced by the formation of beads-on-a-string) at concentrations between the critical overlap concentration c^* (e.g., semi-dilute, un-entangled) and the entanglement concentration *Ce* (e.g., semi-dilute, entangled), where *Ce* is typically ~10 × c^*.

The critical overlap concentration for entanglement c^* corresponds to the maximum number of polymer chains with a radius of gyration r that can be fitted inside the volume of a sphere ($v=\frac{4}{3}\pi * r^3$) where steric exclusion due to increased excluded volume effects starts to overlap the chains. However, chain entanglement theory does not consider the long-range van der Waals interactions of the molecules.

Moreover, chain entanglement theory does not consider the importance of viscoelasticity on the electrospinnability of the material. In addition, the chain entanglement model does not take into account the fluid inertia caused by the cumulative effects of the molecular relaxation of the material while being electrically stressed during the process, which is another key factor in the development of continuous filaments [81].

2.2.3 Visco-elasto-capillary theory

For non-Newtonian fluids, the relative importance of inertial effects and elastic stresses with respect to viscous stresses is characterised by the Reynolds number Re and the Weissenberg number Wi. The Reynolds number is given by the equation

$$\mathrm{Re} = \frac{\rho v \mathrm{L}}{\eta} \qquad \text{Equation 2.9}$$

Where ρ is the fluid density, *v* is the axial velocity, L is the axial length scale and η is the shear viscosity; and the Weissenberg number is given by the equation

$$Wi = \frac{\lambda v}{\mathrm{L}} \qquad \text{Equation 2.10}$$

where λ is the relaxation time of the fluid, *v* is the axial velocity, and L is the axial length scale. In analogous fashion, free-surface flows of Newtonian fluids can be characterised by the magnitude of the Reynolds number and the capillary number Ca [79], given by the equation

$$\text{Ca} = \frac{\eta v}{\text{ɤ}} \qquad \text{Equation 2.11}$$

where ɤ is the surface tension of the fluid, *v* is the axial velocity and η is the shear viscosity. Inertia-less flows of elastic fluids with free-flowing surface can be represented by the combined importance of elastic and capillary effects compared with viscous stresses, as described by the elasto-capillary number

$$Ec = \frac{Wi}{Ca} \qquad \text{Equation 2.12}$$

where Wi is Weissenberg number the and Ca is the capillary number. An increase in Ec often results in a strong stabilisation of the jet [79-81]. The Deborah number is indicative of the relaxation time of the material under an applied stress and the Ohnesorge number indicates the viscous response of a material to a given stress, as given by the inverse of a Reynolds number based on a characteristic capillary velocity [82].

However, the inertia of the fluid is important in the development of the beaded morphology since the capillary waves in the neck region must grow sufficiently fast to exceed the rate of capillary thinning in the primary filament.

In other words, a build-up of electrical stresses in the jet will suppress Rayleigh instabilities if the extensional deformation rate caused by the electrical stresses is faster than the inverse of the relaxation time of the fluid, resulting in uniform filaments [81]. In turn, the elasto-capillary thinning rate of the filament should scale with λ^{-1}, where λ is the characteristic material relaxation time (Figure 2.7). Subsequently, the growth rate of the filament disturbances, should also scale with the inverse of the Rayleigh time scale for inertia capillary break-up

$$\lambda = \frac{1}{\sqrt{\frac{\rho L^3}{\text{ɤ}}}} \qquad \text{Equation 2.13}$$

where ρ is the density of the fluid, L^3 is the volume of the capillary and $\mathfrak{x}$ the surface tension between the fluid and air. Hence, λ^{-1} requires the intrinsic Deborah number to be greater than 1 [79-81]. In contrast, for Deborah numbers below unity, elastic effects do not stabilise the jet and Newtonian-like break-up dynamics are observed. For Ohnesorge numbers below unity, capillary wavelength instabilities are observed in the form of beaded filaments.

For example, in a capillary thinning process, surface tension drives the thinning, and either viscosity or elasticity resists the necking [113]. In other words, the relaxation of elastic stresses should be greater than the response to viscous forces in order for a continuous non-beaded filament to be formed (Figure 2.7) [82].

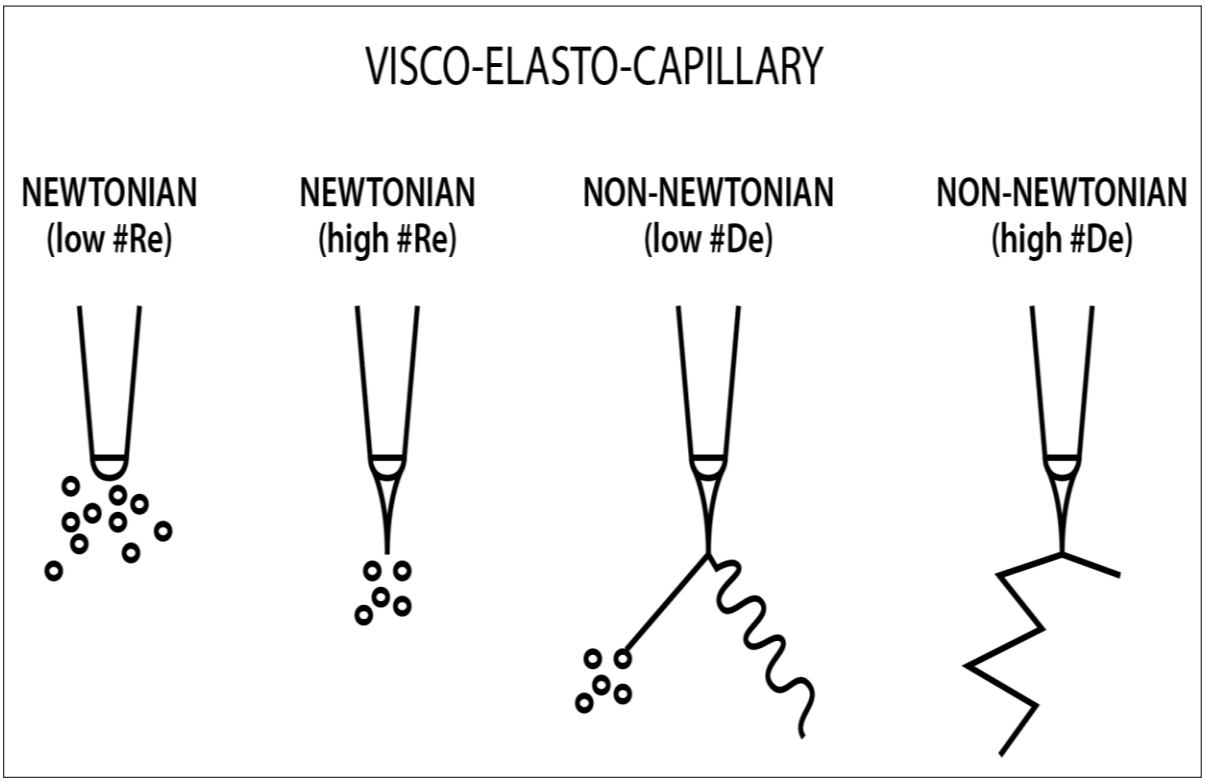

Figure 2.7 - Representation of the visco-elasto-capillary theory and its correlation to jet formation, showing the transition from intermittent spraying (low # Re) to stable spinning (high #De). Re is the Reynolds number ($Re = (\rho Lv)/\eta$) and De is the intrinsic Deborah number ($De = (\lambda \text{ material})/(\text{Rayleight time scale})$) [79].

2.3 Electrospinning of low molecular weight biomaterials

2.3.1 Materials

Fructose is an isomer of glucose, both have the same molecular formula ($C_6H_{12}O_6$) but differ structurally. Fructose has a more stable furanose structure (five carbon ring), called ketose. Glucose has a more flexible pyranose (six carbon ring) configuration, called aldose. Glucose (D-glucopyranose) in aqueous solution exists mostly in its cyclic pyranose form, as it readily undergoes isomerism [153]. In contrast, fructose (D-fructo-furanose), being the most stable isomer, does not dissociate (donates a proton) as easily as glucose.

In other words, isomerism is caused by the chirality (D-, L-) of the anomeric carbon (C-1) per monosaccharide resulting in two different stereoisomers (*trans* α-, *cis* β-*)* which can in turn exists in either pyranose (6-ring) or furanose (5-ring) form [117]. Both glucose and fructose are reducing sugars because of the capacity to convert to their open-chain form through isomerization (e.g., aldehyde group in glucose) or tautomerization (e.g, ketone group in fructose) of its structure their (glucose) and (fructose), as these group readily undergo mutarotation [114].

Mutarotation can momentarily produce dihexose sugars and other metastable and more intricate carbohydrate chain structures [116]. In contrast, disaccharides like sucrose ($C_{12}H_{22}O_{11}$), have glyosidic bonds between the glucose (C-1) and fructose (C-4) anomeric carbons and thus cannot convert to an open-chain form [115]. However, maltose ($C_{12}H_{22}O_{11}$), typically produced during glucose caramelisation (e.g., sugar syrups) and an isomer of sucrose, is a reducing sugar as they are linked by a (C1-C4) glyosidic bond [153].

Oligosaccharides are carbohydrates that consist of monosaccharide units linked together by short chains of varying length (di-, tri-, tetra-, pentasaccharides, etc.) [153]. Each monosaccharide unit (6 carbons) may exist in either the pyranose (6-ring) or furanose (5-ring) form [114].

For example, raffinose ($C_{18}H_{32}O_{16}$), composed of glucose, fructose and galactose is the most common naturally occurring trisaccharide. Oligosaccharide and polysaccharide materials are well known for their ability to form fibres by electrospinning [128, 145, 150-152].

The electrospinning of biopolymers and their applications is widely reported in the literature [128, 147, 170]. The electrospinning of complex oligosaccharides and cyclic polysaccharide materials such as cyclodextrins have also been broadly reported [163-170]. Likewise, the electrospinnability of emulsions, sol-gel systems and complex supramolecular materials have been also reported in the literature [152, 222-225, 233-235]. However, no published evidence on the electrospinnability of mono-, di- and trisaccharide materials has been previously reported.

Interestingly, reported evidence on the electrospinnability of nonpolymeric systems suggests that their capacity to be electrospun is dependent on complex secondary chemical bonding and on the electro-viscoelastic interactions between individual molecules [130, 147, 162-166, 209-211]. However, no experimental evidence on the relationship between hydrogen bonding and van der Waals forces on the electrospinnability of biopolymers, polysaccharide or supramolecular materials has been reported.

For example, polysaccharide electrospinnability has been reported to be particularly dependent on hydrogen bonding [166, 167, 200]. Also, the presence of hydrogen bonding mechanisms is thought to influence the electrospinnability of food-grade polysaccharide solutions [150-151].

Likewise, hydrogen bonding between α-, β- and γ- cyclodextrin (CD) molecules and hydrocolloids are thought to be responsible for the electrospinnability of highly concentrated aqueous solutions of CDs [163-170, 204]. Furthermore, some authors have reported that bounded water in aqueous solutions of CDs can be as high as 100% for solutions over 60% CDs by weight [163].

Moreover, the formation of molecular aggregates of aqueous CDs can be attributable to depletion flocculation by extensive hydrogen bonding networks [164-166]. However, the effect of van der Waals forces in the electrospinnability of such materials is not acknowledged.

Similarly, the potential of saccharides to create metastable supramolecular-like architectures may underpin their molecular aggregation [117]. However, no evidence on the relationship between hydrogen bonding and van der Waals interactions to saccharide aqueous solutions electrospinnability has been previously reported.

2.3.2 Applications

The electrospinning of biopolymers such as chitosan [118-123, 130] and cellulose-based materials [124-127] has been widely reported in literature for various applications [118-127]. The electrospinning of proteins such as collagen [128-131], zein [132-137, 140], bovine serum albumin [138], gelatin [141, 142] and others [139, 143] are often focused on medical and cosmeceutical applications [129, 145, 149]. Low molecular weight saccharides have applications in medicine, biology and microbiology [153] as well as in electrochemistry and nanotechnology [117].

Commercial applications of biopolymer-based materials for smart nanofibre composite membranes are rapidly growing, especially for tissue engineering, medical wound dressings, and cosmetic patches [128, 142-144, 145-149]. Also, polysaccharide applications have commercial significance [150, 151], both as dynamic materials for complexation [199, 128] and as functional carriers for bio-active compounds [144, 219].

A particularly significant effect of using biomaterials in aqueous systems during electrospinning, is the possibility of reducing the environmental and human health impact of toxic solvent systems in commercial nanofibre manufacturing [225].

Additionally, the possibility to create nanofibre membranes by emulsion electrospinning is particularly significant to the growing nanofibre manufacturing industry [222, 224, 226, 230], as emulsion systems could require less regulatory constrains during production.

Also, the relative ease for the complexation of drugs in emulsions and colloidal systems facilitates the commercialisation of new delivery technologies to the medical and pharmaceutical markets [227-229. 231, 232].

However, supramolecular systems (e.g., emulsions), depend on complex physical-chemical variables between external and internal system conditions that are not yet fully understood [152, 175, 233-235].

Nonetheless, such complex macromolecular processes could be further described by studying the nonlinear viscoelastic interfacial and extensional rheological properties of the solutions and the relationships between their physical-chemical properties and electrospinning processing parameters [236, 237].

Pharmaceutical, cosmeceutical and biotechnology applications for polysaccharide materials are often successfully commercialised in the food, pharmaceutical and cosmeceutical industries [117, 128, 150-152].

For example, polysaccharide electrospun nanofibre (e.g., alginates, cellulose, chitin, chitosan, hyaluronic acid, starch, dextran, heparin and levan) could be used for enzyme immobilization for biotechnology processes or as new drug delivery mechanisms for wound dressings [150-152]. Also, the electrospinning of new saccharide solutions could potentially lead to the development of new devices for bio-sensing, skin scaffolds, and personal health products [145, 153].

Remarkably, no evidence of mono-, di-, and trisaccharides electrospun fibres or their application as functional sugar membrane composites for air filtration and healthcare materials has been previously reported in the literature. Sugar based formulations undergoing nanotechnology processing (e.g., electrospinning), being commercialised in air filtration and cosmetic applications, are highly innovative (Chapter 6).

CHAPTER 3

EXPERIMENTAL PROCEDURES

3.1 Materials

D-glucose D-sucrose), D-fructose, raffinose, and maltose were used as supplied (Sigma-Aldrich, Germany) without further purification. Urea (CH_4N_2O, > 99.5%, CAS # 57-13-6), sodium hydrogen carbonate ($NaHCO_3$, > 99.7%, CAS # 144-55-8) and aqueous hydrogen peroxide (H_2O_2, > 50 wt. %, CAS # 7722-84-1) were also used as supplied (Sigma-Aldrich, Germany) without further modification (Table 3.1).

Table 3.1. Materials used in this experimentation

Name	Molecular formula	CAS	Manufacturer
Glucose - 99.5% pure D-(+)-glucose	$C_6H_{12}O_6$	50-99-7	Sigma
Sucrose - 99.5% pure A-d-glucopyranosyl β-d-fructofuranoside* α-d-gl-(1 2) - β-d-fructose	$C_{12}H_{22}O_{11}$	57-50-1	Sigma
Fructose - 99% crystalline D-(-)-fructose	$C_6H_{12}O_6$	57-48-7	Sigma
Maltose - 99% pure D-(+)-maltose monohydrate, 4-o- α-d-glucopyranosyl-d-glucose	$C_{12}H_{22}O_{11} \cdot H_2O$	6363-53-7	Sigma
Raffinose D-(+)-raffinose pentahydrate	$C_{18}H_{32}O_{16} \cdot 5H_2O$	17629-30-0	Sigma
2-hydroxypropyl–β-cyclodextrins	$(C_6H_9O_5)_7 \cdot (C_3H_7O)_{4.5}$	128446-35-5	Seebio
Octa-*O*-acetyl sucrose	$C_{28}H_{38}O_{19}$	116015-75-6	UC-Chemistry*
Octa-*O*-methyl sucrose	$C_{15}H_{26}O_{12}$	126-14-7	UC-Chemistry*

*Materials manufactured at the organic synthesis laboratory in the Chemistry Department of University of Canterbury by Dr. Andrew Watson.

Seebio Biotech, Inc, Shanghai, China supplied the 2-hydroxypropyl-β-cyclodextrin (2HP-β-CD) powder ($(C_6H_9O_5)_7 \cdot (C_3H_7O)_{4.5}$) with an averaged degree of substitution of 4.5 (CAS # 128446-35-5; molar mass 1541.5 g/mol and molecular substitution per anhydrous glucose unit between 0.57 and 1.29).

3.1.1 Solution preparation

All tested materials were diluted in deionised water (10 µS/cm, pH 6.9) prepared using the following general procedure:

1. Slow solvent aggregation to a previously known amount of solute.
2. Gradual heating of the aqueous solutions on a water bath until full solvation was achieved (50˚C to 75˚C).
3. Subsequent storage of the concentrated solutions into plastic tight sealed containers.

The supersaturated solutions were prepared by increasing the dissolution temperature to 75 ± 2°C for short periods of time, and then promptly storing the solutions at lower temperatures (50°C ± 2°C) in air-tight sealed containers to avoid precipitation. All solutions were prepared, processed and characterised in triplicate. All sealed solution containers were stored inside the Marford photoelastic stress freeze cabinet at 50°C ± 2°C. Subsequently, all of the physical properties of the solutions were measured at 50°C ± 2°C to avoid further precipitation of the saccharides. Density was measured on a Mettler-Toledo (XPE) analytical microbalance.

All solution processing was carried out at 50°C ± 2°C to minimise the thermal variability of the materials physical-chemical properties. A detailed description of the synthesis of octa-*O*-acetyl sucrose and octa-*O*-methyl sucrose (provided by the Department of Chemistry at the University of Canterbury) is presented in Chapter 4.

3.2 Electrospinning

For the laboratory scale production, a modified Electrospinz ES1™ machine was used throughout the experimentation (Figure 3.1). A syringe pump (NE-500, New Era Pump Systems Inc., NY, USA) was used to deliver the electrospinning solution to the spinneret (metal hypodermic syringe needle, internal diameter of 0.3 mm) at a flow rate of 0.3 µl/min, instead of a gravity-assisted flow system.

All solutions were suplied to the spinneret at a temperature of 50°C ± 2°C, using a custom-built heating coil jacket for the glass syringe, since the solutions were considerably too viscous to be delivered to the spinneret at room temperature (20°C).

The modified electrospinning apparatus ES1™ was enclosed in a grounded Faraday cage at a temperature and relative humidity of 35°C ± 1°C and 38 ± 3 %, respectively. Ambient conditions inside the Faraday cage were recorded using a hygrometer and a multienvironment and wireless sensor. Electrospinning of the various solutions was performed using an applied voltage of +15 kV and a spinneret-to-collector distance of 15 cm, resulting in an electric field strength (E) of 1 ± 0.02 kV/cm.

A Glassman high voltage power supply (EQ series with reversible polarity) was used instead of the provided EMCO power supply of the ES1™ machine. The polarity of the applied voltage was not found to influence the electrospinnability of any of the tested solutions, indicating that the test solutions have a polarity-independent charge-carrying capability. Electrospun specimens were collected using a grounded aluminum foil substrate and subsequently stored in a temperature-controlled desiccator at low ambient humidity prior to characterisation by microscopy.

Figure 3.1 - Electrospinz ES1™ lab scale electrospinning machine.

For the industrial scale production of some of the materials, the Komodo™ "sonic" electrospinning system, at the Revolution Fibres production site in Auckland, was used for prototype and product development (Figure 3.2). This machine was co-developed between research partners, as part of this PhD research project, to scale up production rates needed to

achieve the required nanofibre volume for the manufacturing of mānuka honey pollution products.

The Komodo™ is a unique electrospinning machine, awarded with the New Zealand engineering excellence award in 2012, and is the only machine in the world using sonic electrospinning as the preferred electrode configuration method for the industrial scale production of nanofibre. All processing parameters and solution formulation recipes used on this machine are IP sensitive and cannot be disclosed in this thesis or elsewhere in publishable literature.

Figure 3.2 – Revolution Fibres – Komodo™, industrial scale electrospinning machine.

3.3 Characterisation methods

3.3.1 Physical-chemical properties of the solutions

The average values of pH, electrical conductivity and surface tension of the solutions were measured in triplicate at a temperature of 50°C ± 2°C. The pH of the solutions was measured

using a pH meter (Seven Easy, Mettler-Toledo GmbH, Greifensee, Switzerland), with a claimed precision of ± 0.02. The surface tension was measured using an optical goniometer (KSV CAM200, KSV Instruments Ltd., Finland). The electrical conductivity of the solutions was measured using a conductivity meter (EDT Instruments, RE387TX, Dover, United Kingdom), with a claimed precision of ± 0.5 %.

3.3.2 Process imaging

A high-speed motion camera (MotionPro® X3) with sensitivity of 1280 × 1024 pixels was used for capturing photographic images of the jet during flight. The fibre in flight was illuminated by six 12 V/50 W halogen lamps to provide consistent lighting conditions during video capture.

3.3.3 Rheometry

The rheological behaviour of tested materials was measured using an Anton Paar MCR series rheometer (Anton Paar GmbH, Graz, Austria). All experiments were performed at a temperature of 50°C ± 1°C with a cone and plate configuration having a 50 mm diameter and 2° angle between the surface of the cone and plate.

Unavoidable least pre-shear calibration forces were automatically exerted by default settings on tested solutions, immediately after the highly viscous solutions were deposited on the rheometer plate, prior to testing.

The rheological properties were measured in rotational mode as a function of the shear rate (0.1–1000 s^{-1}), and in oscillatory mode with a strain of 0.1 % as function of the angular frequency (0.1–1000 s^{-1}).

A strain of 0.1 % was determined to be within the linear viscoelastic range of the solutions as determined from a strain sweep. Zero-shear viscosities were given by fitting the complex viscosity data from the oscillatory tests using the Cox/Merz relation at an averaged viscosity of 0.1s^{-1}. Both storage and loss moduli were measured in angular (oscillatory) mode.

3.3.4 Scanning electron microscopy

The microstructures of the electrospun samples were examined with scanning electron microscopy (SEM, JEOL JCM-5000 NeoScope Tokyo, Japan). Specimens were observed by secondary electron imaging without the use of a gold or carbon sputtered coating, at an accelerating voltage of 10 kV in high vacuum mode.

3.3.5 High performance liquid chromatography (HPLC)

Sample preparation was carried out by dissolving a weighed amount of syrup in 1 mL of reverse osmosis-purified water. After centrifugation at 14000 rpm for 10 min, the supernatant was placed in a HPLC vial. Retention times and response factors generated by calibration standards of known sugars were used to identify and calculate concentrations of the unknown components.

The concentrations were compared against three different points of the calibration curves for each sugar, and the results obtained had a coefficient of determination (r^2) close to unity (0.999). HPLC analysis was carried out using a Waters 2690 Pump, auto-sampler and Econosphere 5 micron amino column at 30°C. An isocratic mobile phase of 75.0 % acetonitrile: water was used. Eluted sugars were detected using a Waters 2414 refractive index detector at 40°C.

3.3.6 Fourier transform infrared spectroscopy (FTIR)

Fourier transform infrared spectroscopy was used to determine the chemical composition of the glucose syrup, liquid and solid samples using a Perkin Elmer spectrometer (Spectrum one FTIR).

Frequencies from 450 to 4000 cm^{-1} were used to produce transmittance (%T) and reflectance (%R) spectra of the liquid and solid samples, respectively. In the case of the solid samples, direct measurement of the electrospun material was preferred over forming typical KBr pellets

to increase the clarity of the spectra. For liquid samples, standard NaCl (salt) plates coated with the tested glucose syrup solution were used (Chapter 6).

3.3.7 Non-dimensional numbers equations

The relaxation time for each solution was approximated by the relaxation modulus based on the tube model (Figures A1.1 – A1.21). Calculated values for each solution are shown on Table A1.1. The following non-dimensional numbers were solved to determine the visco-elasto-capillary parameters.

- Deborah number (intrinsic) $De_{intrinsic}$ = relaxation time of the material (λ) / Rayleigh time scale for inertia capillary break-up [density (ρ)* length scale (L^3)/surface tension ($\varkappa$)]$^{(1/2)}$
- Reynolds number Re = [velocity (v)* axial length (L) *density (ρ)] / viscosity (η)
- Weissenberg number Wi = velocity(v)*relaxation time (λ)/ length scale (L)
- Capillary number Ca = zero-shear viscosity (η)* jet speed (V) / surface tension of the fluid ($\varkappa$)
- Weber number We = Ca*Re
- Ohnesorge number Oh = Ca/Re
- Elasticity number El = (Wi/De)/Re
- Elasto-capillary number Ec = De/Oh

Values for the relaxation times of tested solutions, using currently available rheological techniques, varied from 9s for F/+SAT solution to 0.04 s for GS/+SAT solution. Graphs of the experimental data fitting using a simplified version of the tube model e.g., $\lambda = k(G')/k'(G'')$ are presented in the Appendix of this thesis.

CHAPTER 4

SACCHARIDE ELECTROSPINNABILITY

4.1 Introduction

Carbohydrates having at least one glucose molecule ($C_6H_{12}O_6$) within their structure, are commonly referred as saccharides and usually divided into four categories: monosaccharides, disaccharides, oligosaccharides, and polysaccharides. Saccharide-based materials are the energy storage medium for many living organisms and the most basic structural component of many biomaterials [250, 251].

The results presented in this chapter show for the first time that a heterogeneous mixture containing mono-, di- and tri- saccharides can form continuous filaments during electrospinning, and can exhibit the same behaviour as polymeric solutions while being electrospun; namely the formation of a stable jet followed by whipping instability. In this chapter, the electrospinnability of aqueous solutions of reducing (glucose, fructose) and nonreducing (sucrose) saccharide solutions is investigated.

Both pure component solutions and mixtures of the saccharide solutions were examined to determine the effect of composition and concentration on the electrospinnability of saccharides. The saccharide concentration in aqueous solution was either undersaturated (-SAT), saturated (SAT), or supersaturated (+SAT). The electrospinnability of the saccharide solutions was then compared with the chain entanglement and visco-elasto-capillary theories, typically used to model the electrospinnability of polymers.

Also, the significance of noncovalent interactions in the electrospinnability of modified sucrose solutions (e.g., octa-*O*-acetyl sucrose and octa-*O*-methyl sucrose) was investigated as a function of the acetylation and methylation of sucrose. Both, octa-*O*-acetyl sucrose and octa-*O*-methyl sucrose are only capable of acting as H-bond acceptors (e.g. from solvent molecules such as water), since neither compound has any hydroxyl groups. Therefore neither octa-*O*-acetyl sucrose nor octa-*O*-methyl sucrose can participate in intermolecular reciprocal hydrogen-bonding interactions with other molecules of the solute.

However, it is still not clear how electrospinnability relates to the hydrogen donor and hydrogen acceptor interactions, Debye's length, permanent and/or induced dipole-dipole, and other complex electrodynamic interactions caused by the high voltages that drive the electrospinning process.

4.2 Experimental procedures

4.2.1 Materials and solution preparation

Various undersaturated, saturated and supersaturated solutions composed of pure, binary and ternary combinations of D-glucose ($C_6H_{12}O_6$, > 99.5 %), D-fructose ($C_6H_{12}O_6$, > 99%), and D-sucrose ($C_{12}H_{22}O_{11}$, > 99.5 %), were prepared for electrospinning.

The naming of the various solution compositions was abbreviated as follows: glucose (G), fructose (F), sucrose (S), glucose-fructose-sucrose (GFS), glucose-fructose (GF) and glucose-sucrose (GS). Additionally, the samples were labelled according to the concentration regime: undersaturated (-SAT), saturated (SAT) and supersaturated (+SAT). For example, FS/+SAT indicates a supersaturated solution with equal amounts of both fructose and sucrose.

4.2.2 Rheometry

The dynamic viscosity (μ) of the saccharide solutions was measured in both oscillatory and flow tests with shear rates ($\dot{\gamma}$) or varying frequency from 0.1 to 1000 s^{-1}. A strain of 0.1 % was determined to be within the linear viscoelastic range of the solutions as determined from a strain sweep measured at a frequency of 1.5 Hz.

The zero-shear viscosity was determined from the complex viscosity data obtained by oscillatory tests using the standard Cox–Merz relation at an average shear rate of 0.1 s^{-1}. The storage (G') and loss (G'') moduli were measured in oscillatory mode over an angular frequency (ω) range of 0.1-1000 s^{-1}.

However, shear viscosity and storage moduli (G') data, is only reported for saccharide /+SAT solutions, as lower concentrations did not show a marked difference on the measured rheological properties.

4.3 Experimental results and discussion

4.3.1 Electrospinnability of saccharide solutions

Electrospinnability for tested materials was evaluated based on the foremost continuous and abundant filament formation, notwithstanding droplet formation and beaded filament structure. F/+SAT and S/+SAT and solutions and their combinations exhibited the best electrospinnability results, in comparison with glucose containing solutions (Figures 4.1 and 4.2).

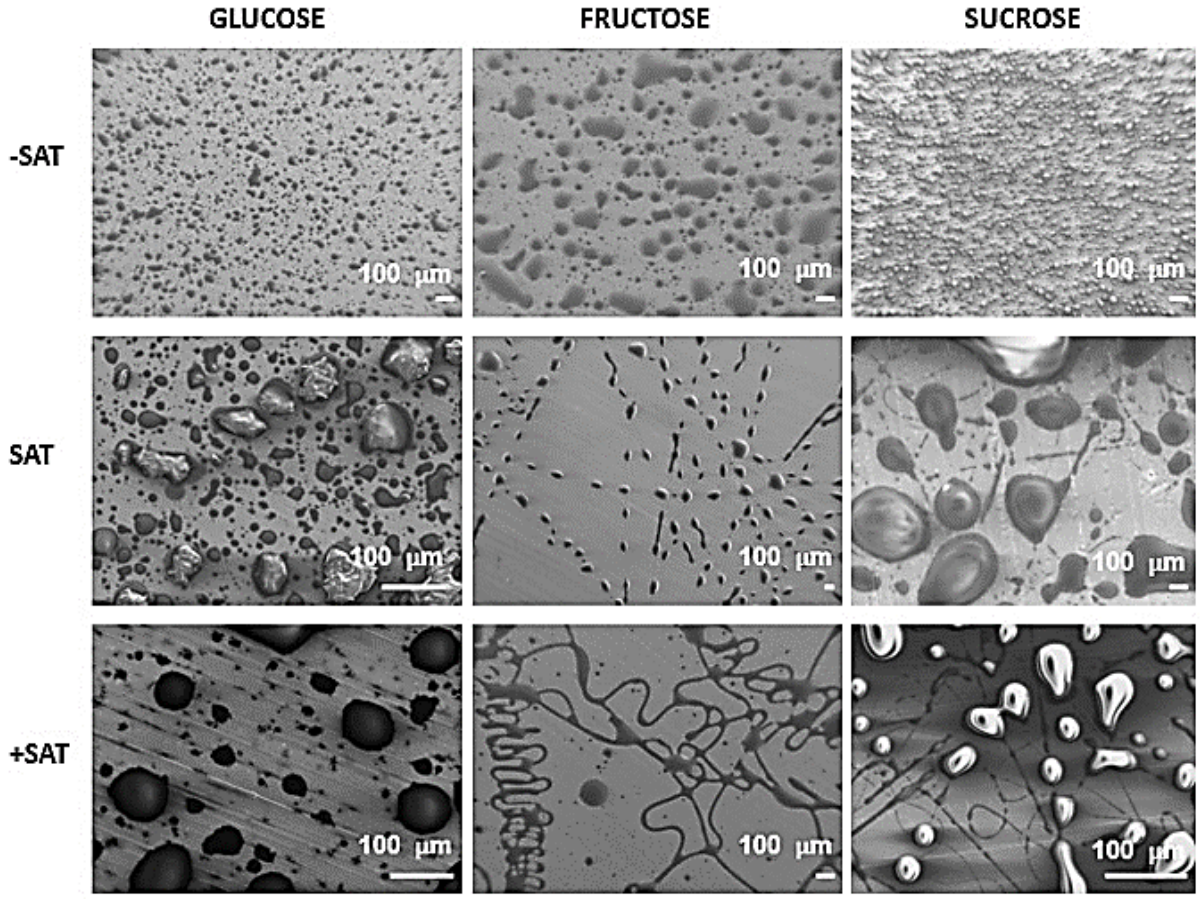

Figure 4.1- Scanning electron micrographs of submicron droplets and filaments of the pure saccharide solutions produced by electrospinning at 50˚C.

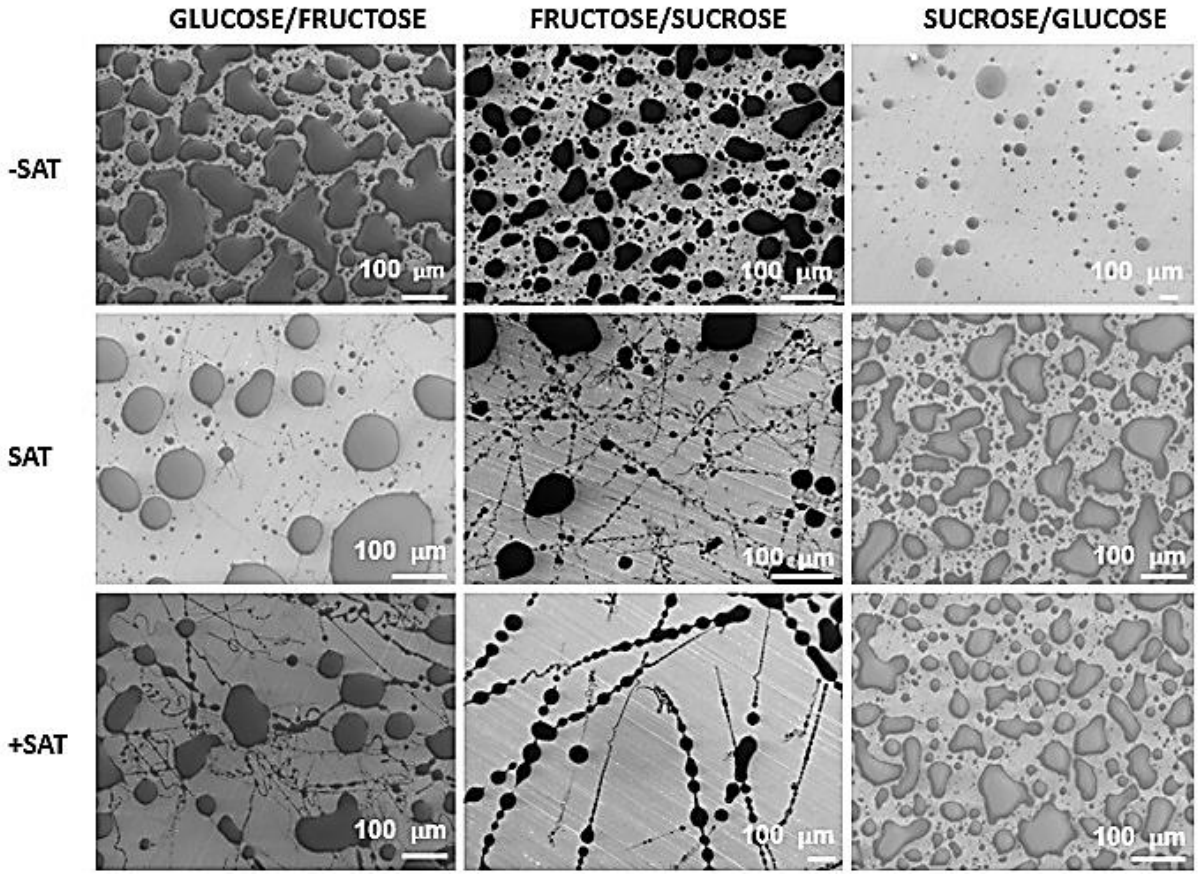

Figure 4.2 - Scanning electron micrographs of submicron droplets and filaments of the binary saccharide solutions produced by electrospinning at 50˚C.

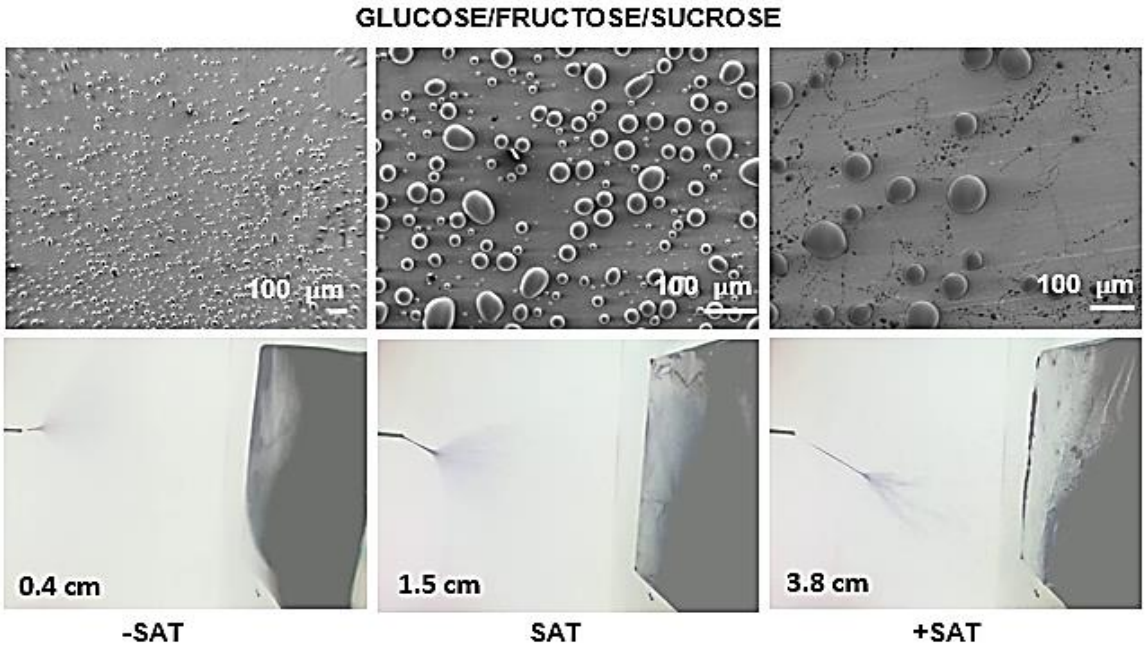

Figure 4.3 - Scanning electron micrographs and high-speed photographs of submicron droplets, filaments and jets of the ternary saccharide solutions produced by electrospinning at 50˚C.

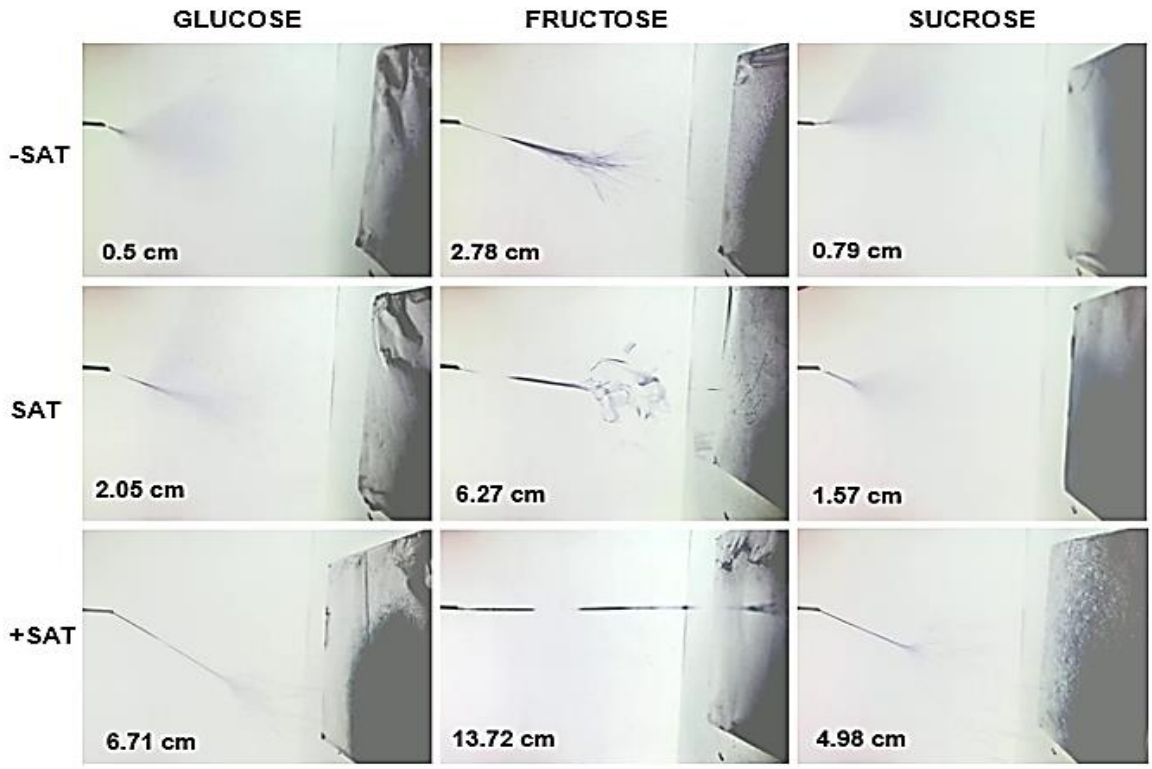

Figure 4.4 - High-speed photographs of the pure saccharide jets produced by electrospinning at 50˚C.

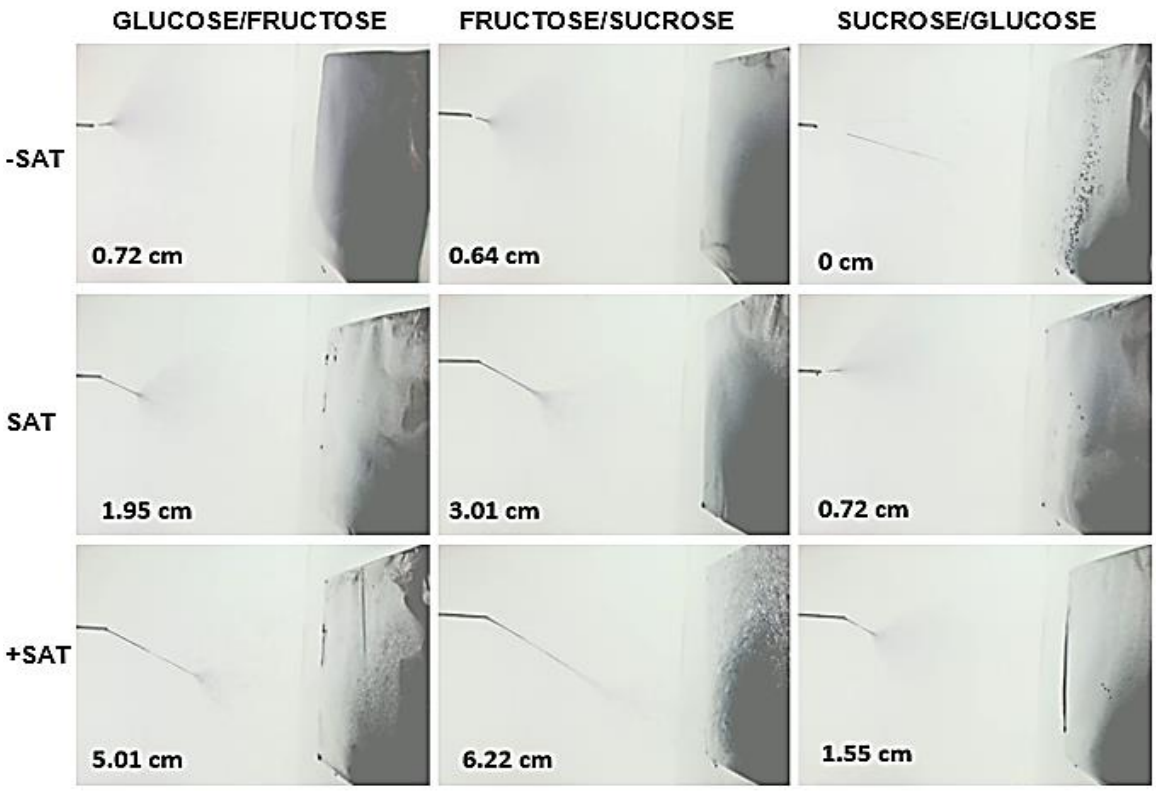

Figure 4.5 - High-speed photographs of the binary saccharide jets produced by electrospinning at 50˚C.

However, both G/SAT and F/+SAT solutions showed filament formation (Figure 4.2). Likewise, the ternary combination of glucose, sucrose and fructose /+SAT solution also showed filament formation (Figure 4.3). In contrast, both glucose and sucrose /SAT and /+SAT solutions did not showed any filament formation (Figures 4.1 and 4.2).

Both stable jet formation and chaotic whipping instability were observed for most sucrose-containing solutions at supersaturated concentrations (Figures 4.3–4.5). However, no stable jet formation was observed for SG/-SAT (Figure 4.5). In particular, F/+SAT showed the longest straight jet and the best electrospinnability behaviour for the pure saccharide solutions, as evidenced by their continuous filament formation (Figure 4.1 and 4.4).

4.3.2 Physical-chemical properties of solutions

The highest density (1.61 g/mL), electrical conductivity (4.39×10^{-4} S/m), and surface tension (12.109 N/m) was found for FS/+SAT, GFS/-SAT, and GS/+SAT, respectively. In contrast, the lowest density (1.36 g/mL), conductivity (0.03×10^{-4} S/m), and surface tension (7.687 N/m) was found for G/-SAT, F/+SAT, and G/-SAT, respectively. Higher densities related to greater electrospinnability (Figure 4.6).

In contrast, lower conductivities at higher concentrations promoted filament formation (Figure 4.8). However, no obvious relationship between surface tension and electrospinnability was observed (Figure 4.7). The average standard deviations for the density, conductivity and surface tension were 0.0617 g/mL, for 0. 228 10^{-4} S/m and 0.4457 N/m, respectively. Circled areas on all graphs (Figures 4.6–4.10) exhibited the highest electrospinnability, taken as the formation of the longest continuous filaments with stable jet formation.

In contrast to the expectation that relatively higher conductivities correspond to higher ionic mobility, hence increased electrospinnability, samples with lower conductivities electrospun best (Figure 4.8) [193]. Moreover, electrospinnable solutions corresponded to higher pH values of tested solutions, e.g., F/+SAT (5.8) and S/+SAT (5.0), GF/+SAT (4.8) and FS/+SAT (4.3). Although pH for tested saccharide solutions was rather acidic, this phenomenon is in agreement with other literature reporting low pH values for caramelised syrups [171].

Lower conductivity values could suggest that charge during electrospinning may not be solely transported by ionic diffusion. Likewise, an increase in jet length (Figures 4.3–4.5) was observed to correlate with the formation of continuous filaments (Figure 4.1–4.3).

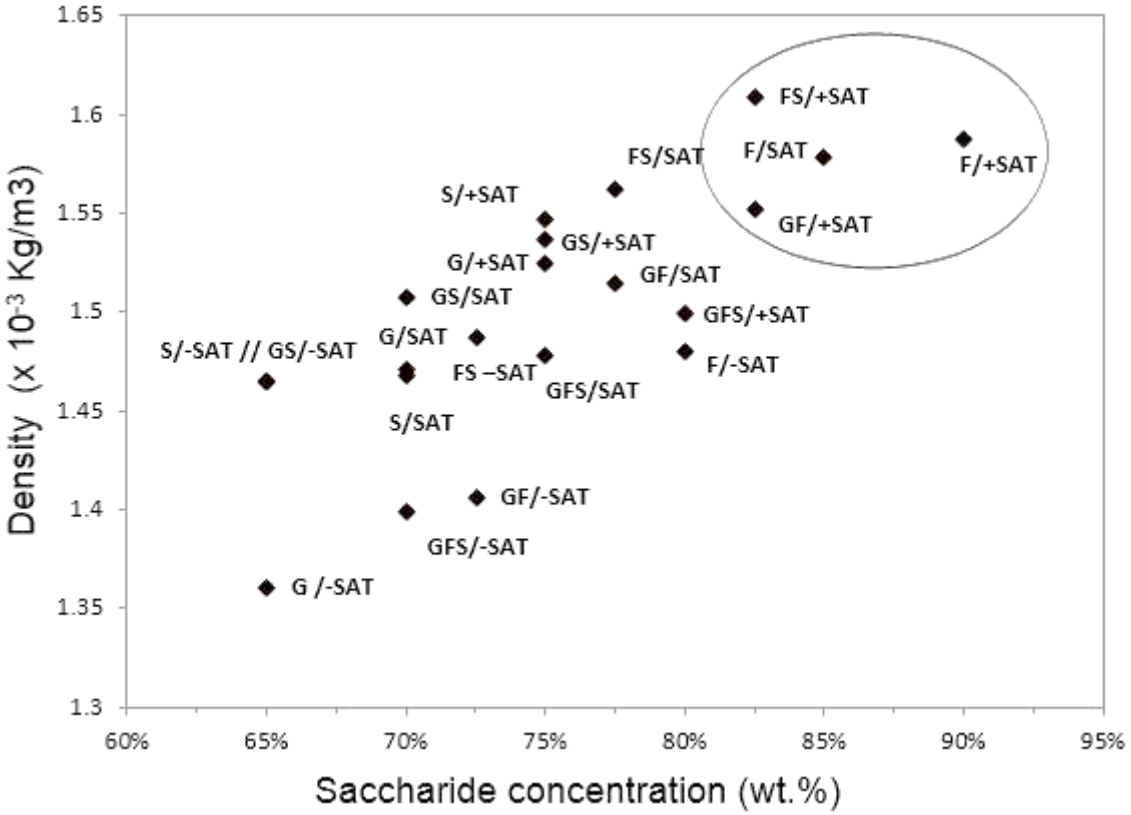

Figure 4.6 - The density of the aqueous saccharide solutions as a function of the saccharide concentration at 50˚C. Circles indicates those solutions with improved electrospinnability (greater filament formation).

Surface tension, conductivity and viscoelasticity are important factors in the electrospinnability of any given material. However, in the case of most biopolymers and supramolecular polymers, such properties find their origin in secondary chemical forces, rather than in covalently physical bonding mechanisms [172-175]. For example, hydrogen bonding can have a significant effect on capillary-driven processes, such as in the cases of microfluidics and electrospinning [176-180].

Longer relaxation times of some supramolecular polymer solutions are also associated with higher electro-visco-elasticities, resulting in improved electrospinnability [71, 110]. Often, such viscoelastic behaviour could be explained by the sticky reptation model of associating networks.

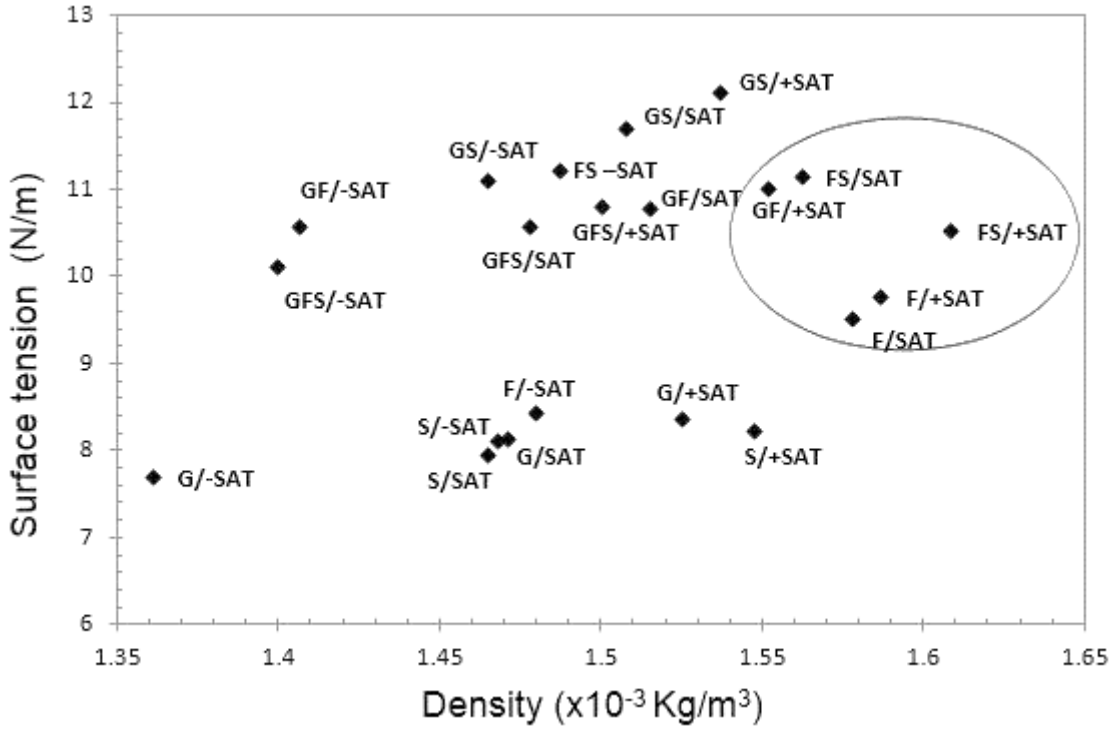

Figure 4.7 - Surface tension as a function of density at 50˚C. Circle indicates those solutions with improved electrospinnability (greater filament formation).

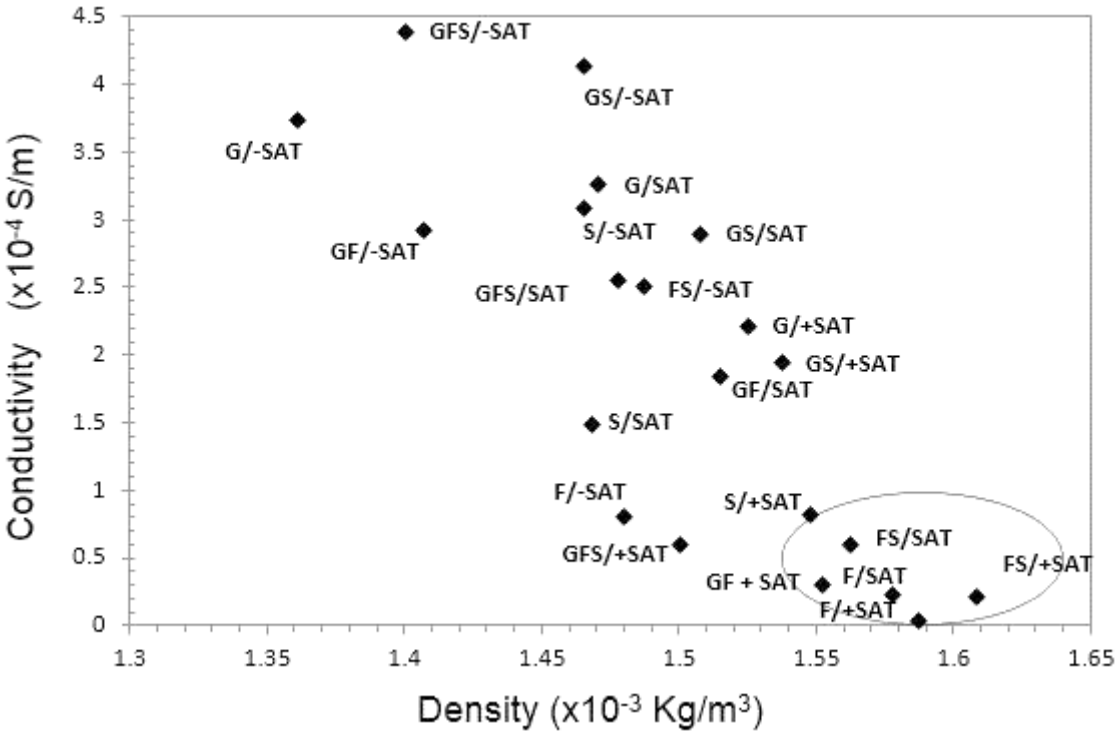

Figure 4.8 - Conductivity as a function of density at 50 C. Circle indicates those solutions with improved electrospinnability (e.g., higher filament formation).

The sticky reptation model proposes that reversible (short-term) bonds in supramolecular polymers, such as hydrogen bonds, can act as "sticky points" for the so-called "associative supramolecular networks", and so dictate the long-term stress and strain dynamics of the bulk solution [185].

In other words, concentrated saccharide solutions could behave as an interconnected network or gel, for time scales shorter than the lifetime of these reversible bonds (e.g., hydrogen bonding) [185]. Moreover, it is known that increased jet length or electrospun filaments may indicate a polymer solution with a higher elasticity [54, 81, 113, 181-183].

The associated electrospinnability for viscoelastic polymer systems is also found on nonpolymeric systems, as supported by the relationship between higher zero-shear viscosities, longer stable jet lengths (elasticity) and electrospinnability of tested saccharide solutions (Figures 4.9 and 4.10).

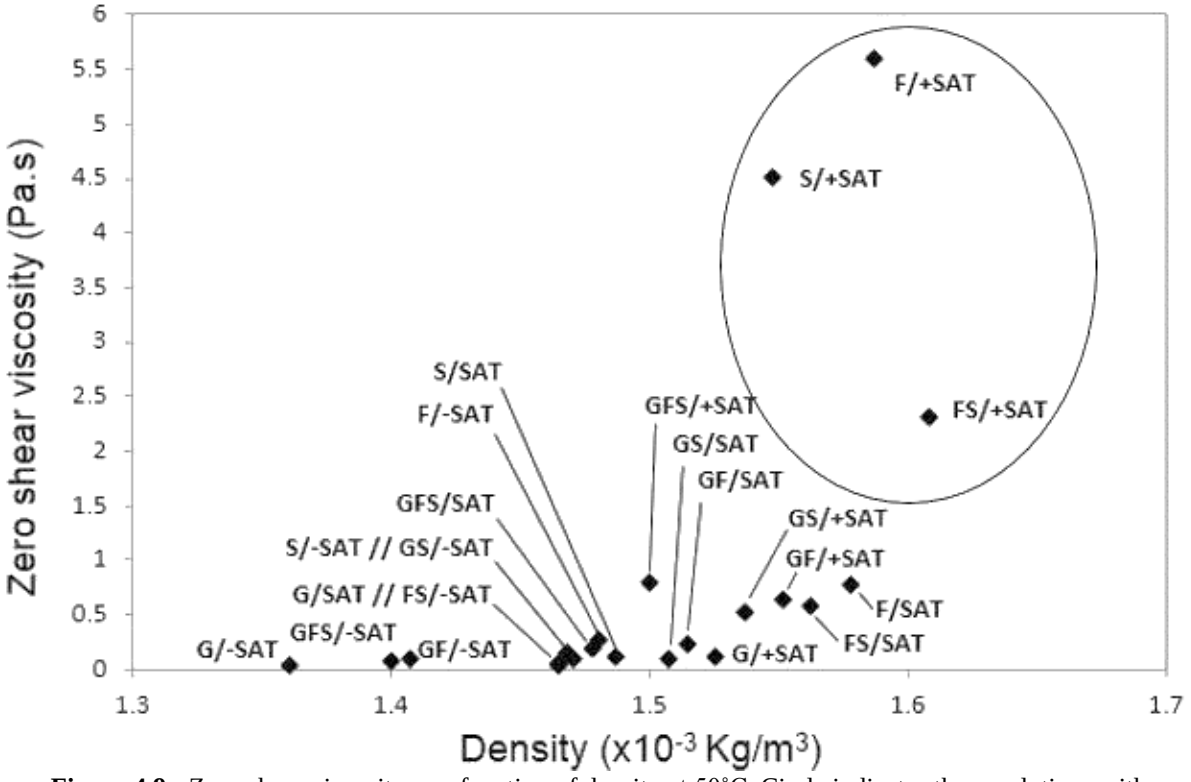

Figure 4.9 - Zero-shear viscosity as a function of density at 50˚C. Circle indicates those solutions with improved electrospinnability (greater filament formation).

Furthermore, the elasticity of supramolecular polymers while in solution may be related to electrospinnability through gelation or colloid aggregation via hydrogen bonding networks

[110, 184, 185]. Moreover, viscoelasticity also may play an important role in the electrospinnability of cyclodextrins [163, 166]. For example, Uyar et al. proposes that hydrogen bonding promotes the self-assembly of CD molecules into aggregates, resulting in solutions of higher elasticity and electrospinnability [166].

Similarly, sucrose aqueous solutions can strongly bind water molecules in its hydration sphere, orientating water molecules even at long distances, as in hydrocolloids clusters [114-116, 186].

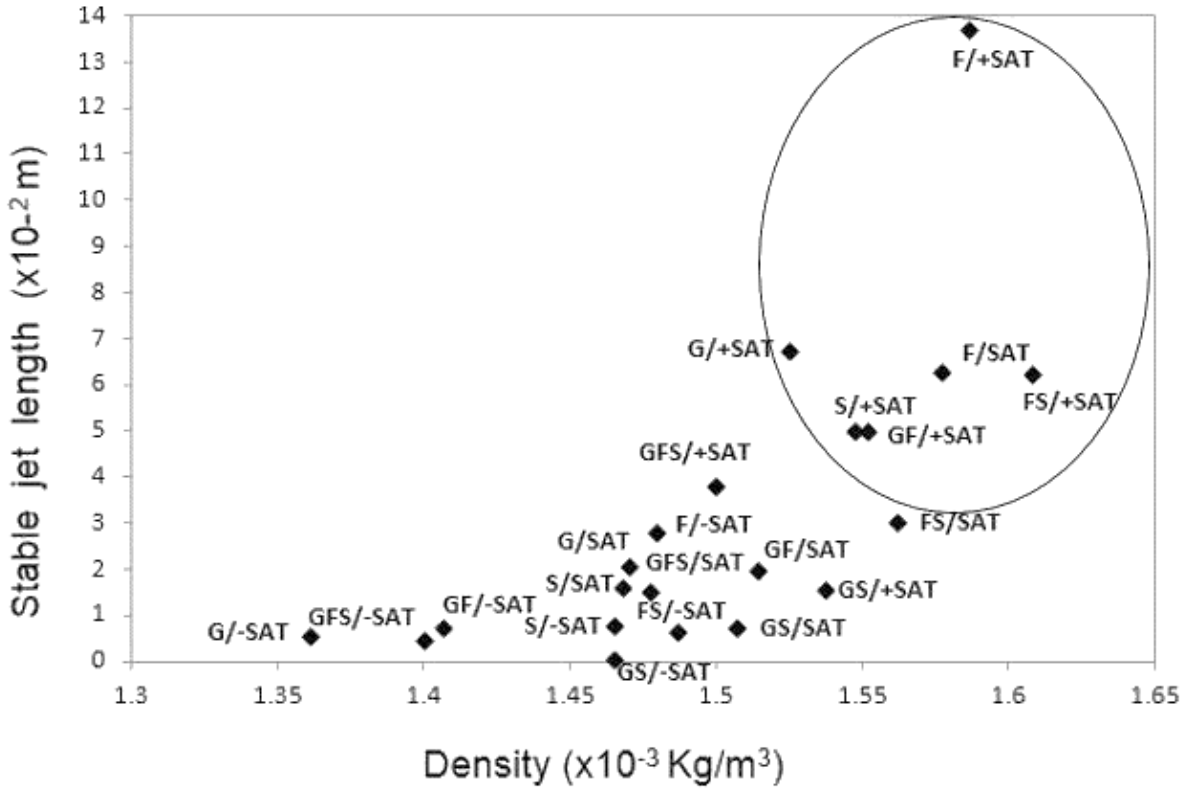

Figure 4.10 - Stable jet length as a function of density at 50˚C. Circle indicates those solutions with improved electrospinnability (greater filament formation).

4.3.3 Viscoelasticity of saccharide solutions

Viscosity values measured for saccharide solutions were relatively lower when compared with typical polymeric materials usually measured at 20˚C, since the associated dynamic shear viscosities for tested saccharide solutions did not exceed 10 Pa·s at 50˚C (Figure 4.11). Moreover, in contrast to the expectation that diluted saccharide solutions behave as Newtonian fluids, most of the fructose- and sucrose-containing concentrated solutions behaved as non-Newtonian fluids (Figure 4.11).

Similarly, Quintas et al. found that nucleation and crystal growth of metastable supersaturated sucrose aqueous solutions during shear stress do not correlate with the expected Newtonian behaviour predicted by the Arrhenius model [187].

However, no conclusive experimental evidence has been reported on the correlation between the nucleation processes of concentrated sucrose aqueous solutions during shear stresses and the viscoelasticity of the solution. Hence, the chemical bonding dynamics (nucleation) relating to the associated colloid aggregation (van der Waals) and self-assembly processes (hydrogen bonding) that influence the electrospinnability of concentrated saccharide solutions are still too complex to validate experimentally [117, 166, 171].

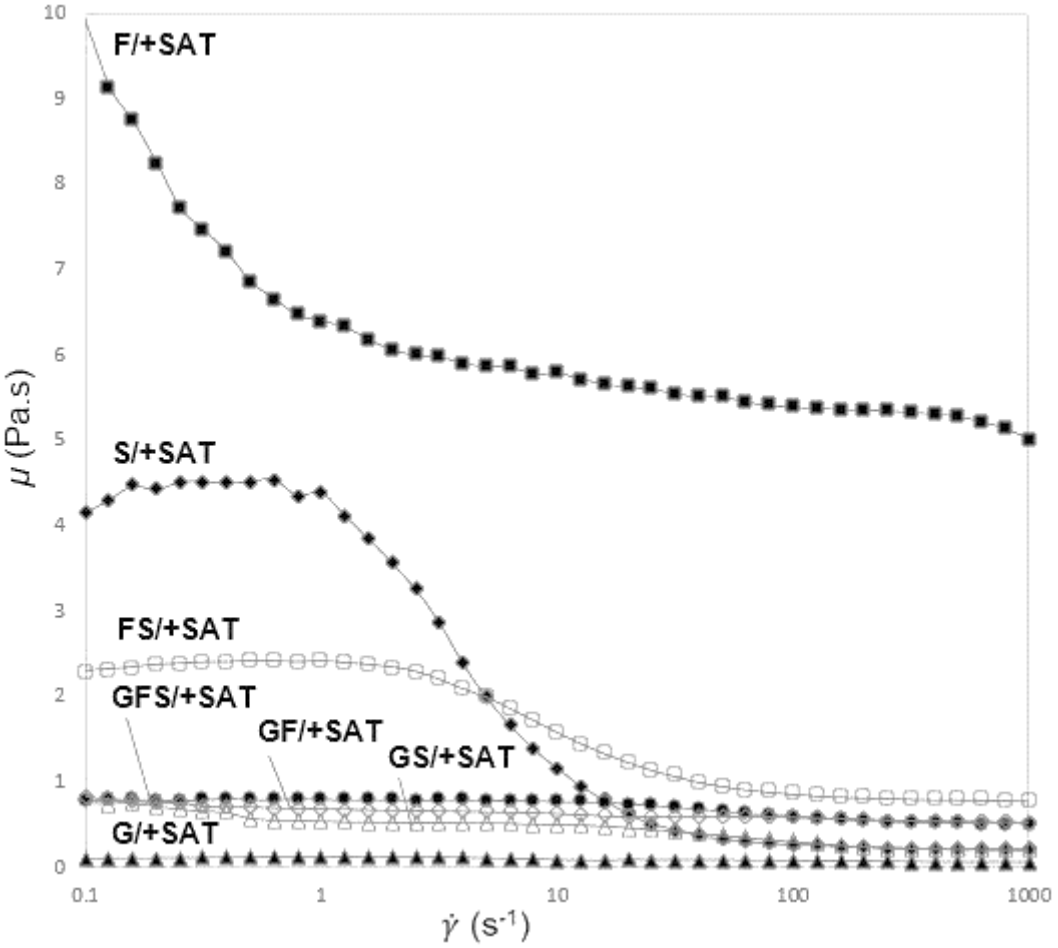

Figure 4.11 - Shear rate ($\dot{\gamma}$) to dynamic viscosity (μ) relationship for single, binary and ternary combination of saccharide at 50˚C.

The non-Newtonian behaviour of the nonreducing sugars is especially noticeable for the sucrose and fructose-sucrose supersaturated solutions, as evidenced by the shear thinning

behaviour of FS/+SAT (Figure 4.11). Also, all tested samples were more viscous than elastic due to the G' values always being lower than their respective G'' (Appendix A1). However, S/+SAT showed the highest G' at higher angular frequencies while F/+SAT showed the lowest G' at all angular frequencies (Figure 4.12). Likewise, binary mixtures of sucrose solutions showed higher G' at all angular frequencies, while GF/+SAT showed the lowest G' of all solutions (Figure 4.12). Moreover, F/+SAT, which exhibited the longest stable jet length (Figure 4.4), also showed the second lowest G' of all the solutions.

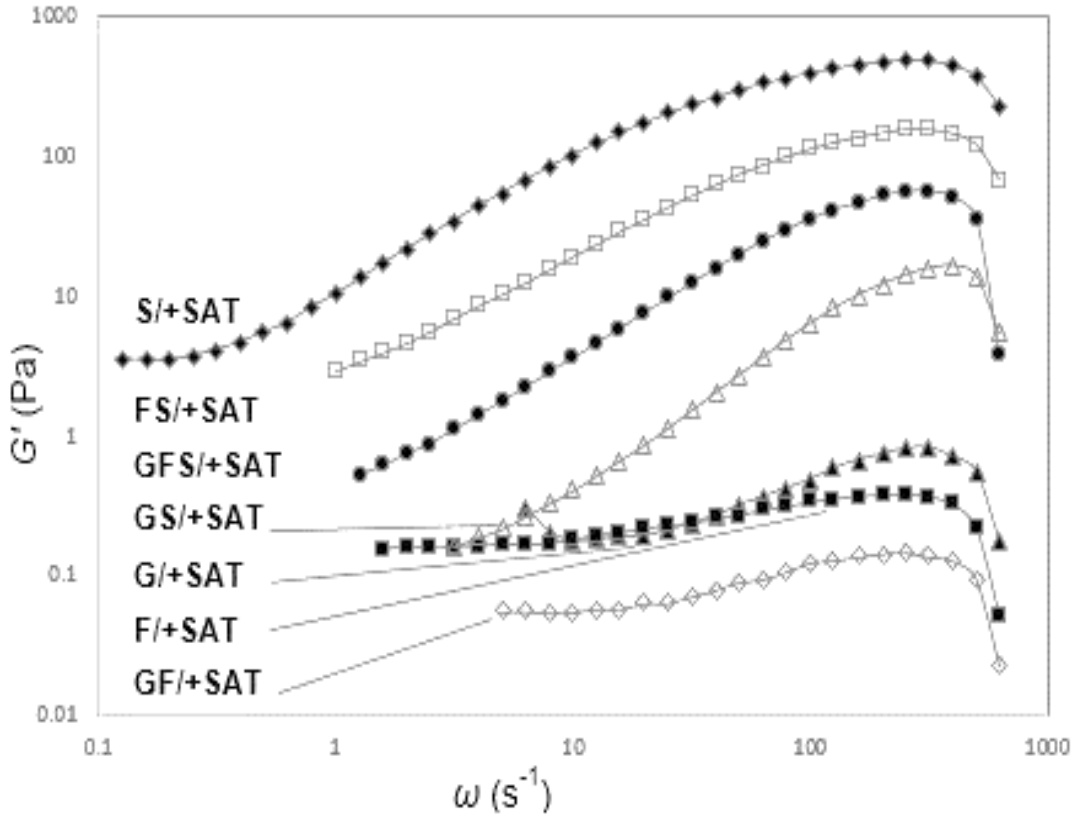

Figure 4.12 - Angular frequency to storage modulus (G') relationship for single, binary and ternary combination of saccharide at 50˚C.

The apparent complex viscoelastic behaviour may be associated with the nonlinear additivity of hydrogen bonding and van der Waals forces when subjected to external electric fields [71, 72]. For example, electron-dynamic interactions like Lifshitz–van der Waals interactions that arise from permanent dipole-dipole interactions (Keesom interaction), dipole-induced dipole (dispersion) interactions (London forces), and dipole-induced dipole (induction) interactions (Debye forces) can promote an asymmetric electronic configuration of the molecules within the solution.

The orientation of the charged solvent (ionised water) molecules may in turn be associated with a high surface density of electron-donors (reducing sugars), often related to a net repulsive Lifshitz–van der Waals interactions between molecules [71, 72].

However, no conclusive evidence has been found on the relationship between Lifshitz–van der Waals interactions and electrospinnability of food-grade polysaccharide [128]. Also, no conclusive evidence has been reported on the relationship between van der Waals interactions and higher Trouton ratios (e.g., extensional to shear viscosity ratio), or on the significance of elasticity (e.g., storage modulus > loss modulus) in the electrospinnability of supramolecular materials. Moreover, neither chain entanglement nor elasto-visco capillary theories consider chemical bonding properties in their models [79, 109].

4.3.4 Electrospinnability models

4.3.4.1 Chain entanglement theory

The stable formation of polymer fibres during electrospinning requires greater than two entanglements per chain to provide sufficient molecular cohesion, according to the chain entanglement theory. The critical overlap concentration (c^*) may be calculated using Equation 4.1, where M is the molecular mass, N_a is the Avogadro number, and $\langle r^2 \rangle^{3/2}$ is the root-mean-square end-to-end distance.

$$c^* \approx \frac{3M}{4\pi * [(r^2)^{3/2}] * N_a} \qquad \text{Equation 4.1}$$

Macromolecules with low molecular mass and many peripheral hydroxyl groups (e.g., high hydrophilicity) cannot be described by an end-to-end distance, due to fluctuations in their hydration shells [180]. Consequently, the use of the hydrodynamic radius (R_h) offers a more accurate representation of molecular dimensions (van der Waals radii) than the root-mean-square end-to-end distance, as given by Equation 4.2.

$$R_h = \sum_i^n 2\left(\frac{r/n}{\sqrt{2\pi}}\right) \qquad \text{Equation 4.2}$$

Using open source software Avogadro 2.0 as the computational method to model the van der Waals molecular ratio for each saccharide molecule, the Merck Molecular Force Field (MMFF)

for sucrose, glucose, and fructose, through a standard geometry optimisation was calculated. Subsequently, an approximate hydrodynamic radius (R_h) of the glucose, fructose and sucrose molecules was determined by averaging the linear distances between each carbon and peripheral hydrogen and oxygen atom (Figure 4.13) [180-183]. The critical overlap concentration (c^*) was then calculated using Equation 4.1, and values are shown in Table 4.1).

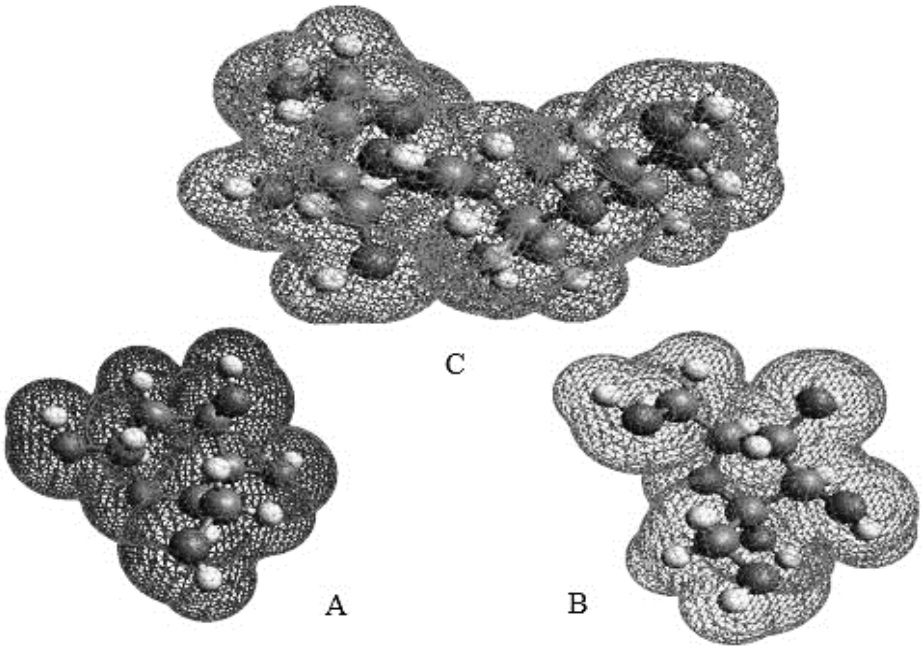

Figure 4.13 - Molecular models showing their van der Waals molecular ratios for glucose (A), fructose (B) and sucrose (C).

Based on the presented evidence, critical concentration or chain entanglement theory applied to electrospinning does not predict the electrospinnability of tested saccharide solutions. The required critical entangled (C*e*) concentrations ($Ce \sim 10 \times c^*$) predicted by the model is one order of magnitude higher than the critical overlap concentration (c^*) found for the tested saccharide solutions (Table 3.1).

In other words, the electrospinnability of nonpolymeric systems can be achieved with less than $2 \times c^*$ (where $Ce = 10 \times c^*$), contrasting with the chain entanglement electrospinnability condition of $2 \times Ce$.

Table 4.1: Critical overlap concentration values for all solutions based on the hydrodynamic radius (R_h)

Parameter	Solution						
	G	F	S	GFS	GF	GS	FS
M (g/mol)	180. 2	180. 2	342. 3	210. 6	180. 2	236. 9	228. 8
R_h (Å)	2. 5	3. 1	6. 2	3. 9	2. 8	4. 4	4. 7
c* (wt. %)	291. 1	151. 2	36. 8	90. 2	203. 7	72. 9	56. 1

4.3.4.2 Visco-elasto-capillary theory

Numerous models from polymer physics, rheology and fluid dynamics have been developed to explain the behaviour of non-Newtonian polymer jets [54, 81, 113]. Some of these models have been applied to electrospinning and incorporate the electro-capillary effects as well as the viscoelastic properties of the material. Inertia-less flows of elastic fluids with free-flowing surface can be represented by the combined importance of elastic and capillary effects compared with viscous stresses.

Electrospinnability predicted by these models depends on the growth of a visco-elasto-capillary wave, similar to the Rayleigh instability that scales with λ^{-1}, where λ is the characteristic polymer relaxation time [81, 188]. This corresponds to the elasto-capillary number (Ec = Wi/Ca); an increase in this number results in a strong stabilisation of the jet. Thus, the Deborah number must be greater than 1 for stable fibre formation [188]. Therefore, the following conditions must be true, Oh > 1 (viscosity) and De > 1 (elasticity), in order for a continuous non-beaded filament to be formed. The relationship between visco-elasto-capillary theory and jet formation is summarised in Figure 2.6

Surface tension drives thinning and viscosity or elasticity resist necking in a capillary thinning process such as electrospinning [79]. Therefore, a higher De and Re are needed for electrospinnability, since both imply a higher or longer relaxation time of the overall system with respect to the capillary perturbation wavelength [54, 81, 113, 188]. Moreover, the longest Rouse relaxation time for polymers is usually in the range of 1 to 3 s. Relaxation processes that occur on smaller time scales than 10–100 ms cannot be unambiguously resolved [188].

During electrospinning, molecular relaxation is usually increased with the strength of the external electric field. This effect cannot be attributed to the electro-rheological effect alone, but also to the polarisation current induced in the solution.

Depending on the chemical potential gradients within the system, and their associated secondary bonding mechanisms, (van der Waals, hydrogen bonding), a particular relaxation time for the solution could be then associated with the fluid jet under electrical stresses. However, the Rouse model only predicts adequately the long-time diffusion for chains shorter than the critical entanglement length.

Moreover, relaxation times for many biopolymers and supramolecular polymers with relatively small chains and a high degree of OH^- groups and/or permanent dipoles cannot usually be determined by the Rouse model. Similarly, the Rouse model holds for only up to a certain crossover time or frequency for short chain molecules in solutions over the chain entanglement concentration (e.g., colloidal aggregates).

Aggregates of small molecules measured over the higher frequencies might only move within a "tube" formed by the surrounding aggregates (hydration shells), as described by the reptation model. Hence, a simplified version of the tube model e.g., $\lambda = k(G')/k'(G'')$, was used instead of the Rouse model, for predicting the longest relaxation times of the solutions (see Figures A1.1 – A1.21).

However, even the simplified version of the tube model did not accurately fit the predicted values over the whole range of frequencies, due to the high standard deviations at lower concentrations. Approximate values were then used to estimate the intrinsic Deborah number, and consequently calculate the non-dimensional numbers required by the elasto-visco-capillary theory, as proposed by McKinley et al., and as described on Table A.1.1 of Appendix 1.

Based on the intrinsic Deborah and elasto-capillary number relationship, the visco-elasto-capillary theory provides a better description than the chain entanglement model of the behaviour exhibited by saccharide solutions used in the present work (Figure 3.15). This further supports a correlation between increased electrospinnability and higher Deborah and elasto-capillary numbers for the tested saccharide solutions.

However, visco-elasto-capillary theory does not offer an explanation as to how bounded water and aqueous phase separation (aggregate formation) relates to hydrogen bonding interactions and jet charge-transport mechanisms [189, 191, 192]. Nonetheless, visco-elasto-capillary theory suggests that longer relaxation times or the capacity to remain electrically stressed for longer periods of time, correlated to a higher electroviscoelasticity, resulting in improved electrospinnability.

Modified sucrose solutions (e.g., octa-*O*-acetyl sucrose and octa-*O*-methyl sucrose), with different hydrogen bonding capacities and molecular polarities, were electrospun to further investigate secondary bonding and electrospinning process relationships.

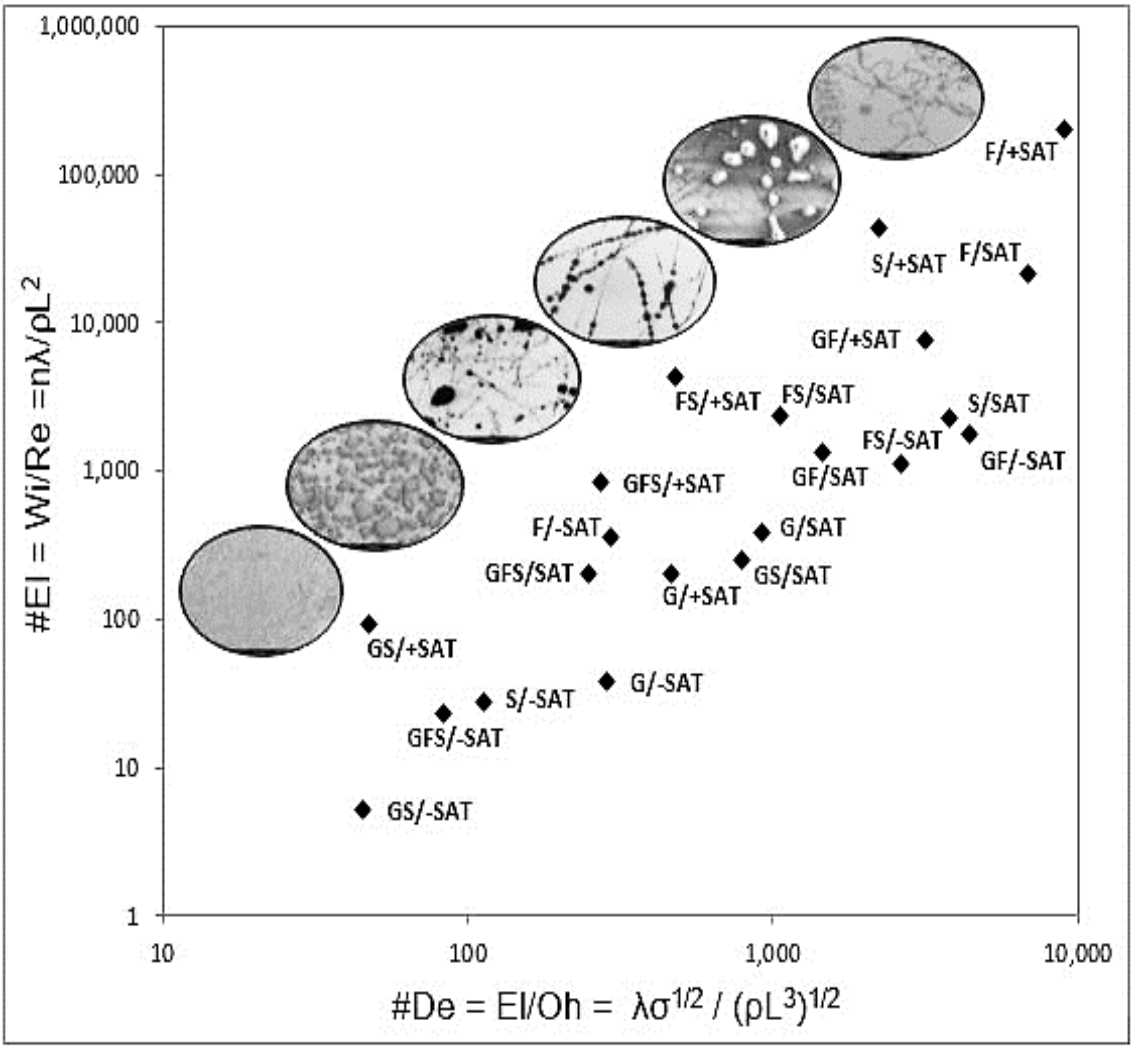

Figure 4.14 - Logarithmic scale of the elasto-capillary numbers plotted against the intrinsic Deborah numbers for all saccharide solutions, at all concentrations at 50˚C.

4.4 Electrospinning of octa-acetyl/-methyl sucrose

The significance of intermolecular forces on the electrospinnability of modified sucrose derivatives (e.g. octa-*O*-acetyl sucrose and octa-*O*-methyl sucrose) using an aqueous solution of sucrose as the control, was investigated. Octa-*O*-acetyl sucrose has been used as enzymatic catalysis additive for selective hydrolysis in some lipases [256, 257]. In comparison, octa-*O*-methyl sucrose is commonly used as non-crosslinking agent for polymer synthesis [258].

In this study, octa-*O*-acetyl sucrose and octa-*O*-methyl sucrose were used as test materials for evaluating the significance of hydrogen bonding and van der Waals forces in the electrospinnability of saccharide solutions. Neither compound has the capacity to donate hydrogen with nearby solvent molecules. Whereas, sucrose has the capacity to accept and donate hydrogen to other solvent molecules like water.

Moreover, octa-*O*-methyl sucrose ($C_{20}H_{38}O_{11,}$ 454.51 gr/mol) is 33% more massive than sucrose ($C_{12}H_{22}O_{11}$, 342.11 gr/mol), while octa-*O*-acetyl sucrose ($C_{28}H_{38}O_{19}$, 678.60 gr/mol) has 98% more mass. Likewise, the hydrogen bond acceptor sites (oxygens) for octa-*O*-methyl sucrose (eleven) are equivalent to the number of oxygens in sucrose (eleven) but 40% less than octa-*O*-acetyl sucrose (nineteen). However, the rotatable bond sites of octa-*O*-methyl sucrose (thirteen), are less than the rotatable bond sites octa-*O*-acetyl (twenty-one) but more than the rotatable bond sites of sucrose (five), Figures 4.15 and 4.16.

The electrospinnability of sucrose solutions (Figures 4.1 and 4.2), supports the argument that reciprocal intermolecular H-bonding between solute and solvent molecules is required for the electrospinnability of supramolecular materials. However, the fact that octa-*O*-acetyl sucrose is more polar than octa-*O*-methyl sucrose yet neither has the capacity for reciprocal intermolecular H-bonding, offers the possibility to test the significance of van der Waals forces (dipolar moment dynamics) in the electrospinnability of saccharide materials (Table 4.2).

The hydrogen bond accepting capabilities and the high molecular polarity of the tested compounds was certainly an important requirement for the electrospinnability of the sugar-materials used in this study. Nonetheless, a clear relationship between the hydrogen bonding capability and polarity of the compounds to their relative electrospinnability, is not yet clear despite presented experimental evidence.

4.4.1 Materials and solutions synthesis and properties

D-sucrose ($C_{12}H_{22}O_{11}$, > 99.5 %, CAS # 57-50-1) was used as supplied (Sigma-Aldrich, Germany) without further purification. Octa-*O*-acetyl sucrose (Figure 4.16) was synthesised by stirring sucrose (51.35 g, 150 mmol) in pyridine (146 mL, 12 eq) under N_2. The vessel was then cooled with a water/ice bath before acetic anhydride (136 mL, 10 eq) was added slowly.

The reaction was then left to warm at room temperature overnight. The next day, the reaction was concentrated under vacuum before pre-absorbing onto silica gel. The material was then purified by flash column chromatography (b. p. 40-60 °C) with an eluent; Et_2O-Acetone/petroleum (2:1) and ether (R_f = 0. 55). The product (95.99 g, 94% yield) was isolated as a colorless crystalline solid after co-evaporation with Et_2O.

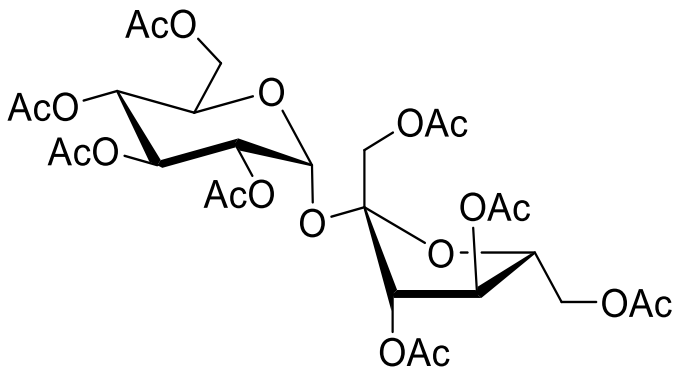

Figure 4.15 - Octa-*O*-acetyl sucrose.

Octa-*O*-methyl sucrose (Figure 4.16) was synthesised by stirring sucrose (41.08 g, 120 mmol) in a mixture of DMSO (650 mL) and 50% w/v NaOH (130 mL, 1.7 eq). Once the sugar had formed a gel, iodomethane (90 mL, 1.5 eq) was then added before the reaction was then left to stir overnight.

The next day water (2.4 L) was added, and the mixture was extracted with Et_2O (3 x 2.4 L). The combined organic layers were then dried ($MgSO_4$), filtered, and concentrated under vacuum. The residue was then purified by flash column chromatography (b. p. 40-60 °C) with an eluent composed of; Et_2O-Acetone/petroleum (1:1) and ether (R_f = 0. 13) give octa-*O*-methyl sucrose (13.40 g, 25% yield) as a yellow oil.

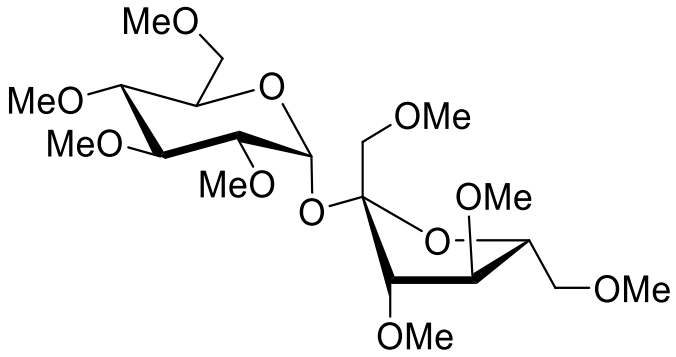

Figure 4.16 - Octa-*O*-methyl sucrose.

Concentrations of 75 wt. % sucrose, octa-*O*-methyl sucrose and octa-*O*-acetyl sucrose in deionised water for all three solutions were used. The aqueous solutions were prepared by using a water bath at a temperature of 50 ± 2 °C until complete solute dissolution was achieved. Subsequently, samples were stored at 50 ± 2 °C to avoid precipitation of the concentrated sugars.

The n-octanol / water partition coefficients (cLogP) for sucrose (-3.7), octa-acetyl sucrose (-0.9) and octa-methyl sucrose (-1.2) were approximated (+/- 0.5) using Chemdraw (Table 4.2). The solution of octa-*O*-acetyl sucrose had the highest pH value and the lowest conductivities of all the solutions investigated (Table 4.2). In contrast, the solution of octa-*O*-methyl sucrose had the lowest pH value and the lowest surface tension value of all the solutions. Sucrose (the control) had the highest surface tension and conductivity of all the samples. However, octa-*O*-acetyl sucrose showed the best electrospinnability (continuous filament formation) of all the samples tested (Figure 4.17).

Table 4.2 - Physical-chemical properties of modified sucrose solutions and control.

Material	pH	Conductivity ($x10^{-4}$ S/m)	Surface tension (N/m)	Density (kg/m^3)	Partition coefficient	Hydrogen bonding capacity
Octa-*O*-acetyl sucrose	6.75	0.01	4.52	1.21×10^3	-0.9	Acceptor
Octa-*O*-methyl sucrose	4.88	0.15	2.78	1.03×10^3	-1.2	Acceptor
Sucrose	5.07	0.82	8.21	1.55×10^3	-3.7	Acceptor / Donor

4.4.2 Electrospinnability of solutions.

Octa-*O*-acetyl sucrose showed an improved electrospinnability as compared with sucrose. In contrast, octa-*O*-methyl sucrose solutions did not present any filament formation during electrospinning; rather electrospraying of droplets was observed. Interestingly, the aqueous sucrose solution presented both filament and droplet formation (*e.g.*, both electrospinning and electrospraying) simultaneously (Figure 4.17).

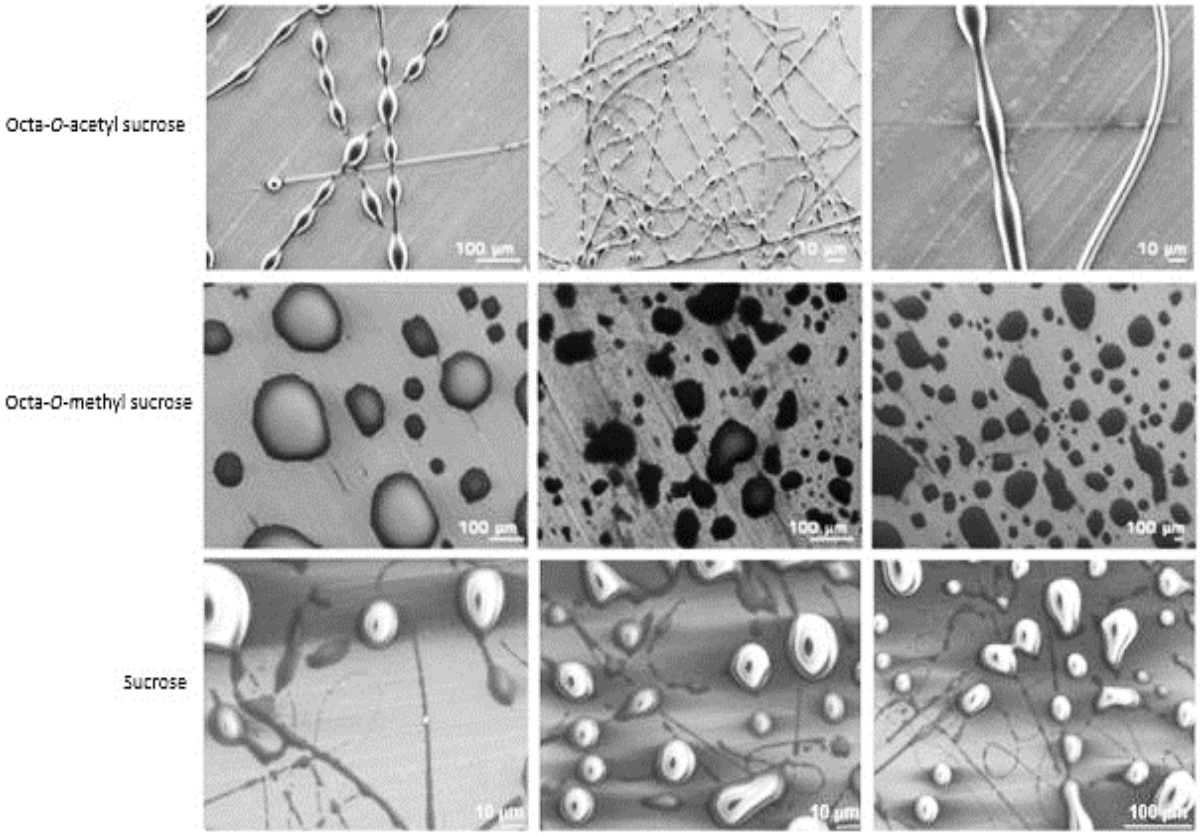

Figure 4.17 – Scanning electron micrographs of octa-*O*-acetyl sucrose and octa-*O*-methyl sucrose in comparison to the control, sucrose; all at 75 w.t % and produced by electrospinning at 50˚C.

The fact that the per-acetylated sucrose solution did electrospin, negates the argument that reciprocal intermolecular H-bonding between solute molecules is absolutely required for electrospinnability. Also, there is a correlation between high pH, low conductivity and a low cLogP (e.g., a high molecular polarity) to the electrospinnability of the octa-*O*-acetyl sucrose. Nonetheless, the fact that sucrose also presented filament formation (to a lesser extent than octa-*O*-acetyl sucrose), suggests that hydrogen bonding, like van der Waals forces, are both required for the electrospinnability of saccharide materials.

However at this point no conclusive evidence relating to the relevance of either hydrogen bonding interactions (solute/solvent and/or solute/solute) and/or permanent or induced dipolar moments in aqueous solutions of octa-*O*-methyl sucrose and octa-*O*-acetyl sucrose, can be directly related to the electrospinnability of the solution. Additionally, it is at this point not clear how electrospinning affects the hydrogen bonding interactions, permanent or induced dipole-dipole interactions, and the resulting Debye length of the solution, produced by the complex electrodynamic interactions caused by the high voltages that drive the electrospinning process.

CHAPTER 5

ELECTROSPINNING OF HYDROXYPROPYL-β-CYCLODEXTRIN (HP-β-CD)

5.1 Introduction

α-, *β*- and *γ*-Cyclodextrins (CDs) are toroidal cyclic oligosaccharides that are composed of 6, 7 and 8 *α*-D-glucopyranoside units, glycosidically linked via the 4-hydroxyl groups of each monosaccharide, respectively [198]. CDs are able to host a wide range of small hydrophobic molecules (or inclusions) within their hydrophobic interior cavity. In contrast, the exterior of the CD molecule is highly hydrophilic, providing the inclusion-CD complexes with water solubility [198].

CDs are often used as carriers for solubilising hormones, vitamins, drugs, and other compounds frequently used in tissue and cell culture and pharmaceutical applications [164, 165, 170, 199]. For example, the complexation of mānuka honey with *α*-cyclodextrin has been reported to have prebiotic effects during digestion, due to the increased antimicrobial activity of the mānuka honey CDs complexes [263]. Also, HP-*β*-CD /Triclosan Inclusion Complexes 160% (w/v) with a 1:1 host-guest complexation, showed improved electrospinnability, except in the case of urea salts addition at concentrations of 20 wt. % [164].

Furthermore, Uyar et al. demonstrated that *α*-, *β*- and *γ*-CDs and their derivatives may be electrospun into continuous fibres, in spite of their low molecular weight (972–1297 g/mol) [166, 200]. Methyl-Beta cyclodextrins (M-*β*-CD) in water and Dimethylformamide (DMF) showed enhanced electrospinnability at higher solvent concentrations of 160% (w/v) for both cases. Interestingly, amorphous structure on the electrospun material was shown across all samples as confirmed by atomic force microscopy (AFM), X-ray powder diffraction (XRD), thermogravimetric analysis (TGA) and differential scanning calorimetry (DSC) [166].

Moreover, it was observed that electrospun hydroxypropyl-*β*-cyclodextrin (HP-*β*-CD) exhibited uniform fibre (e.g., bead-free) formation at concentrations of 160% (w/v), 120% (w/v) and 120% (w/v) in water, DMF and Dimethylacetamide (DMAc), respectively [200].

However, at lower concentrations of HP-*β*-CD in DMF, DMAc and H_2O, HP-*β*-CD solutions could only be electrospun into the form of either beaded structures with little or no fibre formation, bead-on-string structures, or fibres with a ribbon-type morphology [200].

A similar scenario (improved electrospinnability with increased concentration) was shown for the rest of the (HP-γ-CD) and (M-β-CD) solutions tested on either water, DMAc and/or DMF [200]. Furthermore, Uyar et al., proposed that the formation of molecular aggregates of aqueous CDs can be attributed to extensive hydrogen bonding – a critical mechanism allowing the formation of α-, β- and γ-CDs fibres during electrospinning [164-166, 200]. Bounded water on CD-aqueous solutions was reported be as high as 100% for solutions over 60% CDs wt.% concentrations, and as suggested by the authors, electrospinnability by depletion flocculation was the driving mechanism for the observed results [201].

Also, Manasco et al., observed that the electrospinnability of HP-β-CD is reduced in the presence of urea salts [201]. Urea is known to be a chaotropic agent, disrupting hydrogen bonding between water molecules [202]. Urea can also affect the hydrogen bonding between CD molecules and bound water, reducing the size of the CD aggregates [203]. Similarly, Celebiouglu et al., considered the influence of hydrogen bonding on the electrospinnability of aqueous HP-β-CD solutions by adding urea salts to hinder electrospinnability [204].

Nonetheless, discussions regarding the hydrogen bonding maker or breaker capacity of urea for disrupting the tetrahedral configuration of the water stereochemistry, are still not resolved [202, 205]. Argumentation is centred on the capacity of urea to slow down the rotational dynamic of water, by geometrically altering hydrogen bonding networks and water stereochemistry [205].

Also, it has been reported that the hydrogen bonding capacity of aqueous HP-β-CD solutions is affected (as increased CD solubility) by using heavy water as solvent and by the addition of sodium salts, among others additives [203]. Likewise, ethanol-water mixtures have shown to strengthen the hydrogen bonding between respective solvent molecules [206]. Moreover, polar solvents, such as acetone, can also have hydrogen bonding structuring effects on water [207].

Likewise, conductivity, surface tension and pH of aqueous CDs solutions can affect CD-water aggregate formation and consequent electrospinnability [202, 203, 205-207]. Moreover, the influence of pH and noncovalent intermolecular bonding on electrospinnability is also acknowledged in polymeric systems [208-211]. For instance, pH and hydrogen bonding are known to influence the electrospinnability of polymethyl methacrylate and polyvinyl alcohol

[210, 211]. For such polymeric systems, rheological studies have shown that pH and hydrogen bonding directly affect the viscoelastic properties of aqueous and nonpolar solutions.

Likewise, the viscoelasticity of aqueous HP-*β*-CD solutions appears to be dependent on the strength of the hydrogen bonding between CD molecules [201]. For example, aqueous HP-*β*-CD solutions exhibit solid-like behaviour, as indicated by a storage modulus (G′) that exceeds the loss modulus (G″) [201]. However, the relationship between viscoelasticity of CD-aqueous solutions and bounded-water-driven aggregation is not fully understood.

5.2 Experimental procedures

5.2.1 Materials and solutions preparation

The 2-hydroxypropyl-*β*-cyclodextrin (2HP-*β*-CD) material $(C_6H_9O_5)_7(C_3H_7O)_{4.5}$ had molecular substitution per anhydrous glucose unit between 0.57 and 1.29 (Figure 5.1). Aqueous electrospinning solutions were formulated with the intention of either enhancing (Hb-E) or disrupting (Hb-D) the overall hydrogen bonding networks between CD and solvent molecules.

Hence two different solutions were made, a saturated urea solution, aimed at negatively disrupting the hydrogen bonding networks between CD and water molecules (Hb-D), and a diluted sodium bicarbonate ($NaHCO_3$) aqueous solution on a (50:50) acetone/ethanol solvent system, aimed at positively enhancing the overall hydrogen bonding network between CD and water molecules, while promoting solvent evaporation during electrospinning (Hb-E).

The composition of the Hb-E solvent system was 0.5 wt. % sodium bicarbonate in 43.25 wt. % water, with 30 wt. % acetone, 20 wt. % ethanol, and 6.25 wt. % hydrogen peroxide, while Hb-D was prepared as a saturated solution of urea in deionised water. The electrospinning solutions were prepared by dispersing 2HP-*β*-CD (55–70 g/cm^{-3}) in the solvents at a temperature of 50°C ± 2°C.

Subsequently, all solutions were stored at 50°C ± 2°C to avoid precipitation of 2HP-*β*-CD prior to electrospinning. The average values of pH, electrical conductivity and surface tension of the solutions were measured in triplicate at a temperature of 50°C ± 2°C.

5.2.2 Rheometry

The rheological behaviour of the 2HP-*β*-CD solutions was measured using an Anton Paar MCR series rheometer (Anton Paar GmbH, Graz, Austria). All experiments were performed at a temperature of 50°C ± 1°C with a cone and plate configuration having a 50 mm diameter and 2° angle between the surface of the cone and plate.

The rheological properties were measured in rotational mode as a function of the shear rate (0.1–1000 s^{-1}), and in oscillatory mode with a strain of 0.1 % as a function of the angular frequency (0.1–1000 s^{-1}). A strain of 0.1 % was determined to be within the linear viscoelastic range of the solutions as determined from a strain sweep. Zero-shear viscosities were given by fitting the complex viscosity data from the oscillatory tests using the Cox–Merz relation at an averaged viscosity of $0.1s^{-1}$.

Both storage and loss moduli were measured in angular (oscillatory) mode. Unavoidable least pre-shear calibration forces were automatically exerted by default settings on tested solutions, immediately after the highly viscous CD solutions were deposited on the rheometer plate, prior to testing. No accurate relaxation time data were detected from the rheology test, as "hydro-gel" a like behaviour was predominant.

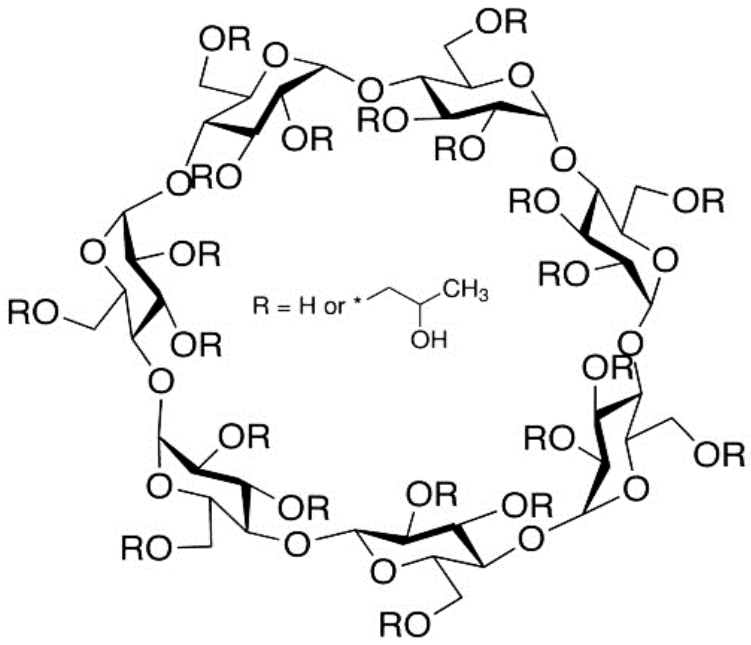

Figure 5.1 - Chemical structure of tested 2-hydroxypropyl-β-cyclodextrin (2HP-β-CD).

5.3 Experimental results and discussion

5.3.1 Physical-chemical properties of 2HP-β-CD solutions

As expected, the 2HP-*β*-CD/Hb-E solutions exhibited both higher pH (Figure 5.2) and conductivity (Figure 5.3) compared with those of the 2HP-*β*-CD/Hb-D or 2HP-*β*-CD/H_2O solutions, due to the presence of bicarbonate salts. In contrast, the surface tension of the 2HP-*β*-CD/Hb-E and 2HP-*β*-CD/H_2O solutions were lower than that of 2HP-*β*-CD/Hb-D (Figure 5.4).

The pH of the 2HP-*β*-CD/Hb-E solutions was higher than all other samples, as expected with the addition of bicarbonate salts. However, all pH values converged to a value of 9.5 with a CD concentration of 70 wt. % (Figure 5.2). Such linear behaviour could be related to the concentration dependency of the hydronium ions' (H_3O^+) mobility while in aqueous solution. In contrast, surface tension for all solutions showed the opposite behaviour, such that surface tension values diverged with increasing concentration of cyclodextrins. For instance, all of the 55 wt. % CD solutions exhibited surface tension values of ~6 to 6.5 N/m, while the value for 75 w.t % CD solutions was 6 to 7.5 N/m (Figure 5.4).

Similarly to pH, such linear effects might be attributable to the concentration dependency of added ionic salts and volatile solvent systems in contact with air. Interestingly, visco-elasto-capillary effects show that an electrospinnable system will tend to minimise its total surface tension to form continuous filaments [79, 82].

For example, 2HP-*β*-CD/Hb-E solutions showed the lowest surface tension values of all samples yet good electrospinnability (Figure 5.4). Furthermore, 2HP-*β*-CD/Hb-E solutions at lower CD concentrations showed a relatively high electrical conductivity (Figure 4.3) although poor electrospinnability (Figure 5.5B).

In contrast, 2HP-*β*-CD/Hb-D solutions did not electrospin into fibres, in spite of a higher conductivity compared to that of the 2HP-*β*-CD/H_2O solutions. The electrospinnability of polymeric systems is known to be related to the increased conductivity of the solution [31, 39, 212-215]. In the present work, a consistent correlation between the conductivity of the CD solutions (Figure 5.3) and resulting solution electrospinnability was not observed (Figure 4.5). Therefore, it appears that the conductivity of tested solutions cannot be directly linked to the electrospinnability of 2HP-*β*-CD (Figure 5.3 and 5.4).

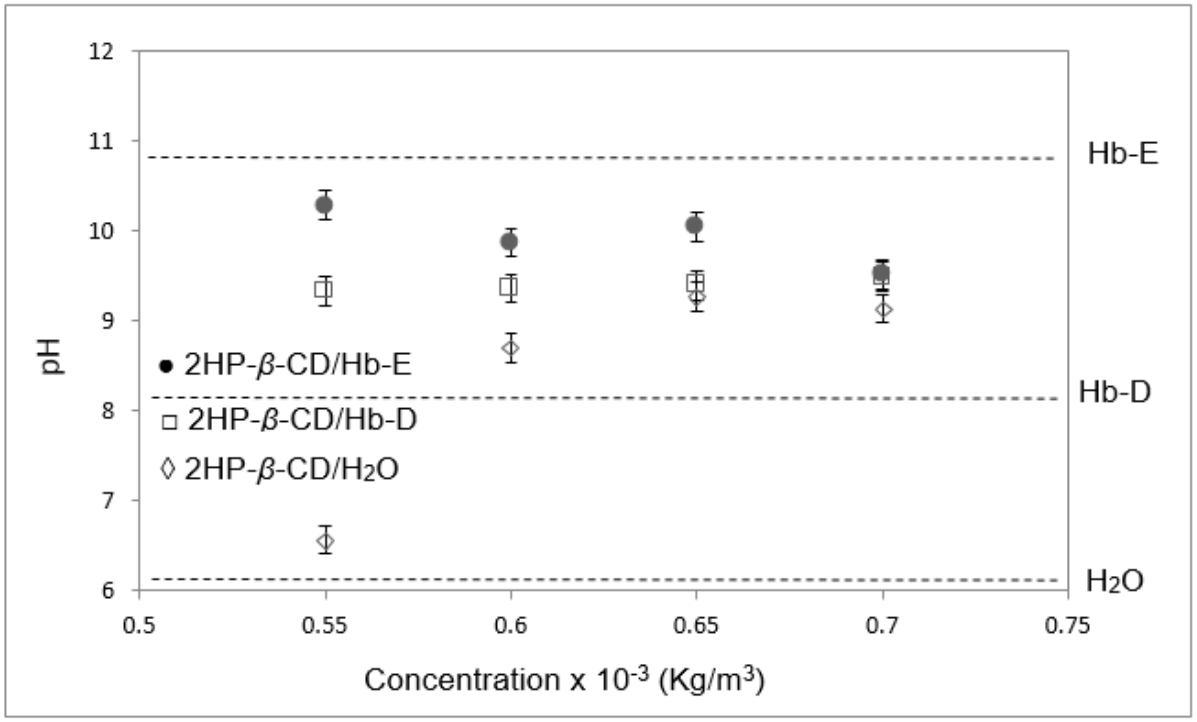

Figure 5.2 - The pH of the 2HP-β-CD solutions as a function of solution type and concentration of 2HP-β-CD (error bars showing an average standard deviation of 0.16).

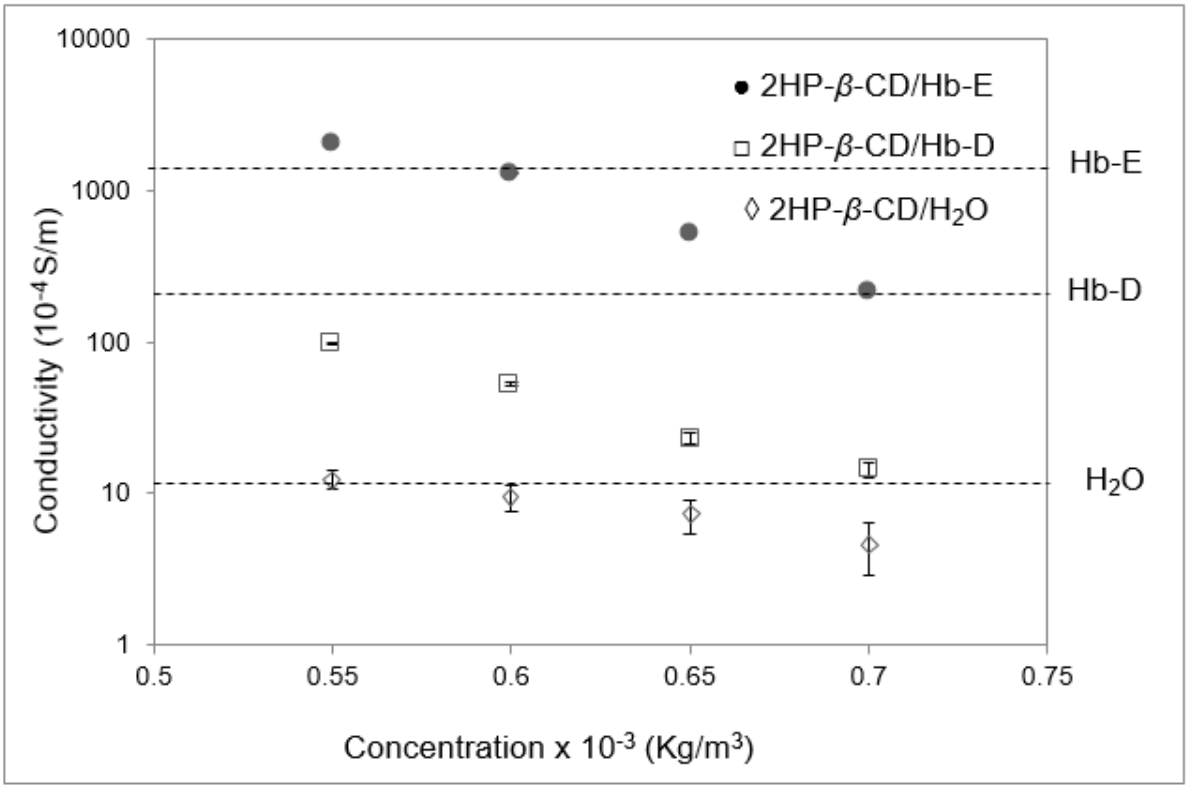

Figure 5.3 - Conductivity of the 2HP-*β*-CD solutions as a function of solution type and concentration of 2HP-*β*-CD (error bars showing an average standard deviation of 0.86).

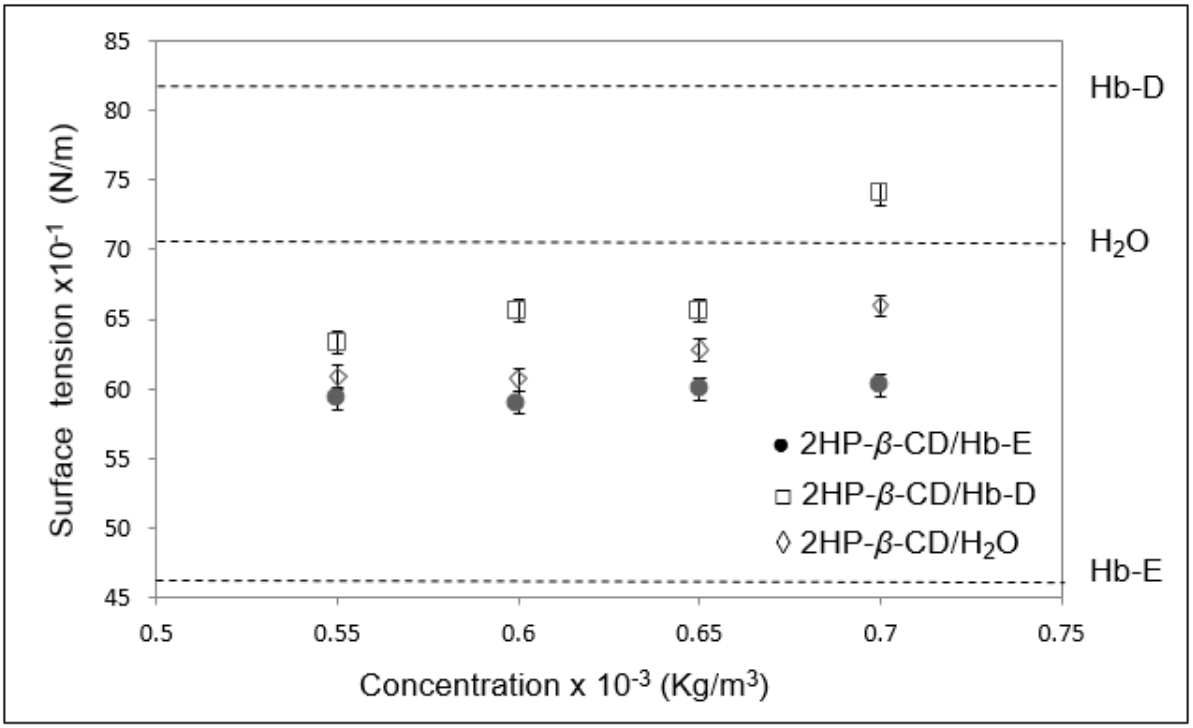

Figure 5.4 - Surface tension of the 2HP-β-CD solutions as a function of solution type and concentration of 2HP-β-CD (error bars showing an average standard deviation of 0.41).

5.3.2. Electrospinnability of 2HP-β-CD solutions

Both stable and chaotic jet formation was observed for all 2HP-*β*-CD/H_2O and 2HP-*β*-CD/Hb-E 60 wt. % solutions. In contrast, electrospraying of droplets occurred for all 2HP-*β*-CD/Hb-D solutions, with no jet formation observed (Figure 5.5C, 5.5F, 5.5I, 5.5L). Consequently, all 2HP-*β*-CD/Hb-D solutions did not present any fibre formation.

The electrospinning of 2HP-*β*-CD/H_2O solutions at concentrations of 55 wt. % and 60 wt. % resulted in electrospraying of droplets and bead-on-string structures, respectively (Figure 5.5A, 5.5D). However, 2HP-*β*-CD/H_2O exhibited beaded morphology and stable fibre formation at concentrations greater than 65 wt. % 2HP-*β*-CD. Interestingly, the electrospinning of 2HP-*β*-CD/Hb-E at concentrations of 60 wt. % and 65 wt. % resulted in fibres that fractured following deposition onto the collector (Figure 5.5E, 5.5F). The presence of fractured fibres may indicate differential shrinkage following deposition, possibly due to a lack of crystallinity within the CD nanofibre, as the amorphous composition of electrospun cyclodextrin nanofibres has been already reported by Celebioglu and Uyar [200, 204].

The experimental data presented in this chapter further supports previous evidence reported by Uyar et al., in respect to the addition of urea salts to aqueous 2HP-β-CD solutions to deter hydrogen bonding within the solvent molecules and subsequent electrospinnability [201- 203].

Hydrodynamic radiuses of 2HP-β-CD molecules reported in literature, spanned from 0.65 nm inner diameter to 1.5 nm outer diameter, per CD molecule [264]. Critical concentration theory values using reported molecular dimensions, does not adequately predict the electrospinnability of tested materials, as concentration over 100 wt. % of solute would be required in order for 2HP-β-CD/H_2O solutions to electrospun.

Also, visco-elasto-capillary theory could not be applied to the electrospinning of CDs in modified solvent systems, due to the complex rheological properties of the solution to calculate the relaxation times of tested solutions during electrospinning (Figures 5.6 and 5.7). Moreover, linear viscoelasticity could not be directly related to the hydrogen bonding within the solutions, since the condition of $G' > G''$ could not be consistently related to the electrospinnability of the solutions as exemplified by 2HP-β-CD/Hb-D (Figure 5.7).

However, the observed viscoelastic behaviour agrees in principle with the visco-elasto-capillary thinning theory of complex fluids; as non-Newtonian fluids with shear thinning viscosity and $G' > G''$ at higher angular frequencies are able to better resist extensional capillary thinning and filament break-up when compared with Newtonian fluids for which $G' < G''$ at low angular frequencies [79, 82, 193]. Interestingly, no electrospinnability was observed for 65 and 70 wt. % 2HP-β-CD/Hb-D solutions, even with $G' > G''$.

Also, 65 and 70 wt. % 2HP-β-CD/Hb-D corresponded to the highest surface tension values for all solutions at such concentrations, as well as showing similar conductivity and pH values in respect to 2HP-β-CD/H_2O solutions at the same concentration range. Therefore, the fact that 60 wt. % 2HP-β-CD/Hb-E shows electrospinnability ($G' > G''$), in contrast to the 2HP-β-CD/H_2O solutions at the same concentrations with $G' > G''$, suggests that the Hb-E solvent system had a positive impact on intermolecular interactions and consequent aggregate formation (electrospinnability) in comparison to water systems.

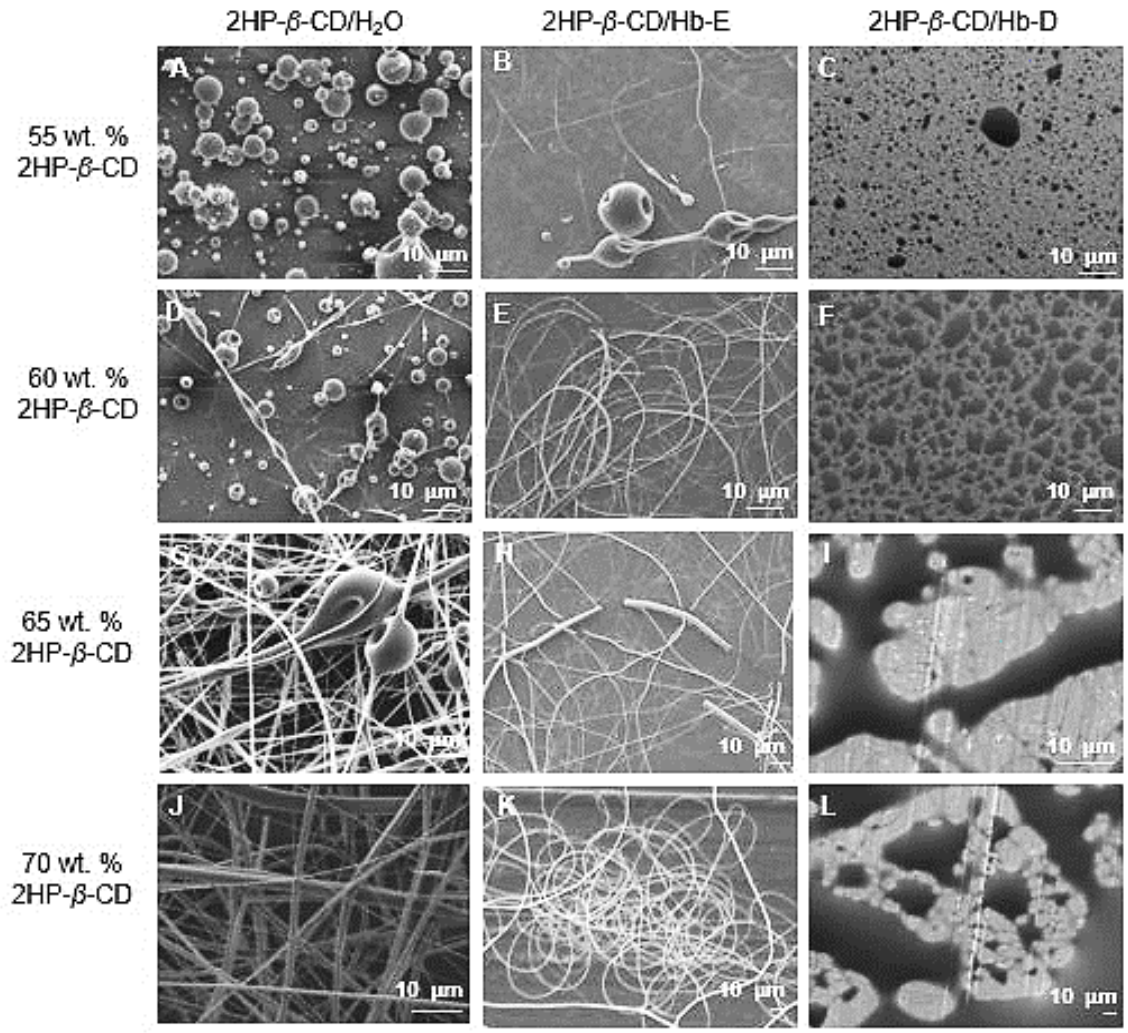

Figure 5.5 - Scanning electron micrographs of as-deposited electrospun 2HP-β-CD samples as a function of CD concentration and solvent type produced by electrospinning at 50˚C.

5.3.3 Viscoelasticity of 2HP-β-CD solutions

Rheological measurements were used to compare the viscoelastic relationships between the electrospinnability of the 2HP-β-CD solutions of varying solvent systems. Shear thinning behaviour was observed as a decrease in the dynamic viscosity (μ) with increasing shear rate ($\dot{\gamma}$). Shear thinning was observed for all solutions during rotational testing (Figures 5.6A, 5.6B and 5.6C). The frequency response of the 2HP-β-CD solutions showed that solutions exhibit predominantly elastic behaviour over the angular frequency (ω) range investigated, as indicated by a storage modulus (G') at least an order of magnitude higher than the loss modulus (G'') (Figures 5.7A, 5.7B and 5.7C). In general, 2HP-β-CD solutions exhibited weakly elastic behaviour above 65 wt. % 2HP-β-CD.

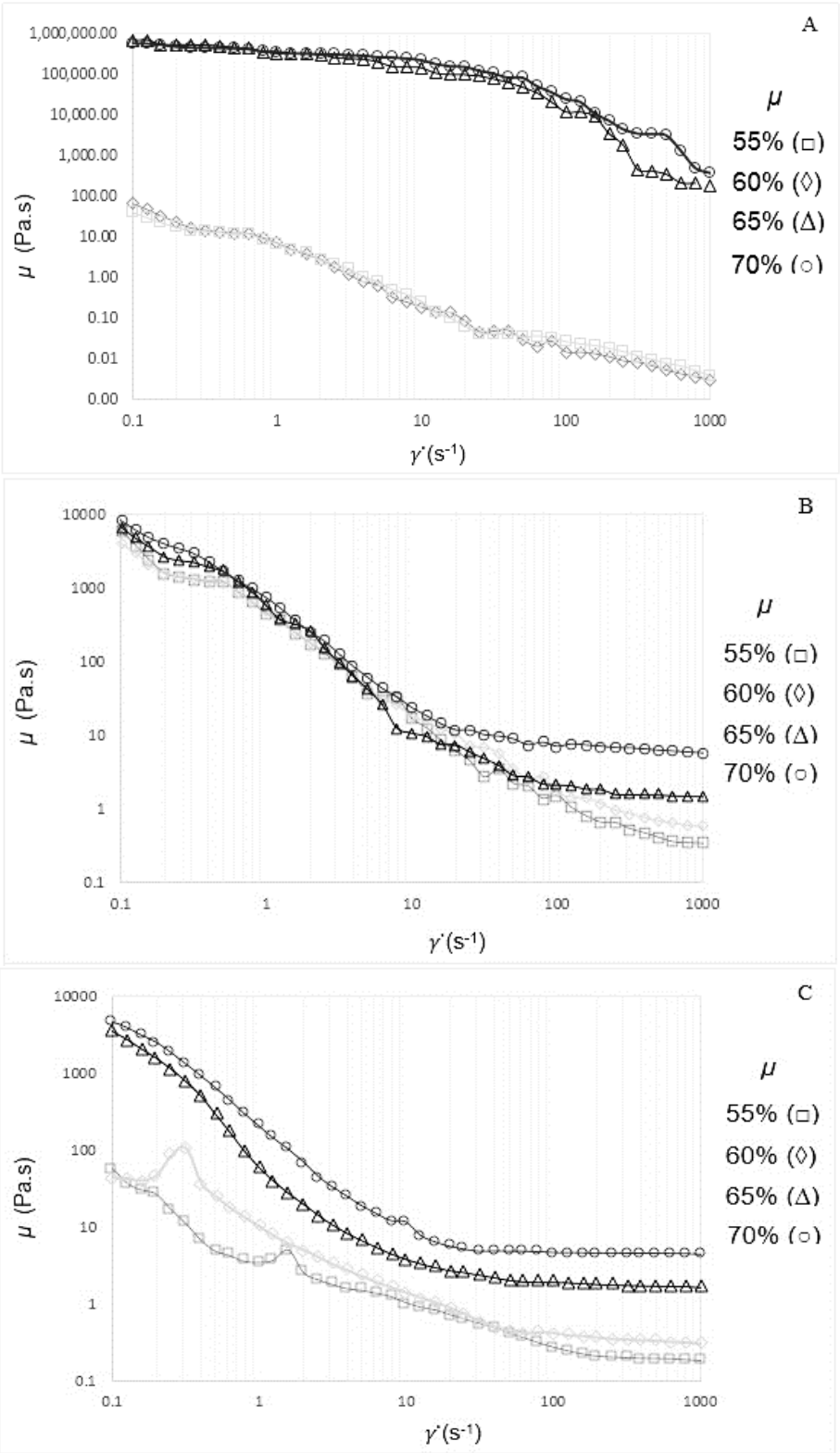

Figure 5.6 - The dynamic viscosity as a function of the shear rate and 2HP-*β*-CD concentration at 50°C; for (A) 2HP-*β*-CD/H_2O, (B) 2HP-*β*-CD/Hb-E and (C) 2HP-*β*-CD/Hb-D

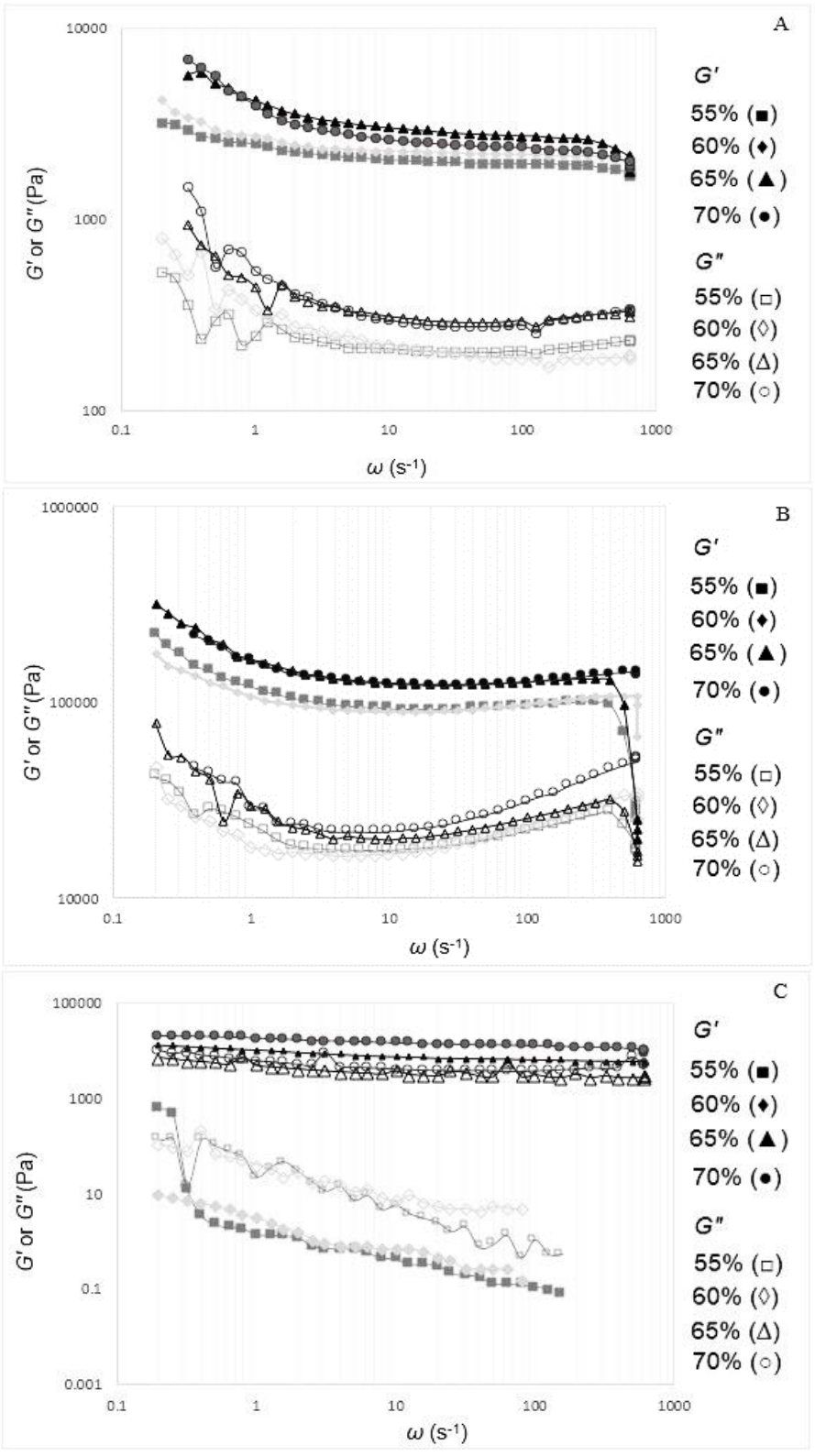

Figure 5.7 - The storage and loss modulus as a function of the angular frequency and 2HP-β-CD concentration at 50°C; for (A) 2HP-β-CD/H2O, (B) 2HP-β-CD/Hb-E and (C) 2HP-β-CD/Hb-D

The storage (G') and loss (G'') modulus of 75% wt. % 2HP-β-CD (10^4–10^6 Pa) was in agreement with that for native β-CD at 150% (w/v) as reported in the literature (Figure 5.7) [204]. In contrast, the viscosity of native β-CD, as reported in the literature [204], ranged between two to three orders of magnitude below that obtained for 2HP-β-CD/H_2O and 2HP-β-CD/Hb-E solutions. Discrepancies with the reported literature values may be attributed to the difference in the molecular weight of the β-CD derivative used in this work (2HP-β-CD) (1460 g/mol) [201].

The difference in the molecular weight could also correspond to the variance in the reported viscosity (Figure 5.6) [201]. Also, a relatively high molecular substitution per anhydrous glucose unit (0.57–1.29) is reported in this work in comparison with data from available literature (0.6–0.9) [204]. Consequently, correlations with present experimental results are not possible due to the lack of published β-CD density and molecular weight values elsewhere in the electrospinning literature [166, 200, 201, 204].

Furthermore, the viscosities of 2HP-β-CD/H_2O at 65 and 70 wt. % CD were five orders of magnitude higher than those for 55 and 60 wt. % 2HP-β-CD (Figure 6.6A). The large difference in viscosity suggests a pronounced increase in intermolecular interactions between the CD molecules above 60 wt. % 2HP-β-CD. Similarly, 2HP-β-CD/H_2O exhibited elastic behaviour where G' is significantly higher than G'' for all CD concentrations (Figure 5.7A).

In contrast, 2HP-β-CD/Hb-D solutions showed lower values of G' and G'' at low concentrations (55–60 wt. % CD) compared with higher CD concentrations for 2HP-β-CD/Hb-D solutions (Figure 5.6).

Moreover, Hb-D based solutions with 65 or 70 wt. % 2HP-β-CD could not be electrospun into fibres even though $G' > G''$. In contrast, 2HP-β-CD/H_2O solutions showing $G' > G''$ could be electrospun into fibres. The 60 wt. % 2HP-β-CD/H_2O solution exhibited poor electrospinnability compared with a 60 wt. % 2HP-β-CD/Hb-E solution that exhibited similar viscoelastic behaviour ($G' > G''$) (Figure 5.5D and 5.5E).

In contrast, electrospinnability was not observed for any 2HP-β-CD/Hb-D solutions, regardless of $G' > G''$ at higher CD concentrations (Figure 5.7). Similarly, 2HP-β-CD/Hb-E samples exhibited $G' > G''$ for all 2HP-β-CD concentrations; however, electrospinnability was not observed for 55 wt. % 2HP-β-CD/Hb-E (Figure 5.7).

Additionally, the development of a plateau in G' over a wide range of angular frequencies suggests that the presence of 2HP-β-CD aggregates resulted in gel-like behaviour for all solutions (Figure 4.7). The nonlinear viscoelastic behaviour observed in the solutions is typically associated with a high number of associating networks, such as those described by the sticky reptation model proposed by Rubinstein et al. [185].

Additionally, a G'-G'' crossover point could not be observed, creating a practical limitation in calculating the molecular relaxation time using rheometry. Thus, Rousse relaxation times of the solutions were not detectable over the range of frequencies investigated.

Likewise, the sticky reptation model of associating networks proposes that rapidly reversible (short-term) bonds in supramolecular polymers, such as hydrogen bonds, can act as sticky points to form associative supramolecular networks that dictate the long-term stress and strain dynamics of the bulk solution [185]. Thus, the solution is capable of behaving as an interconnected network on time scales shorter than the lifetime of the reversible bonds.

Moreover, dielectric or light scattering spectroscopy has shown that the oxygen atoms in a saturated aqueous CD solution could act as "open-close" stickers [167-169], where there are noticeable differences between α-, β- and γ-cyclodextrin (CDs) [216].

Nevertheless, hydrogen bonding donor mechanisms might not necessarily be related to electrospinnability, as shown by the electrospinning of octa-acetyl-sucrose (Chapter 4).

Additionally, the gel-like behaviour of cyclodextrin-based solutions is in agreement with the literature reports on nonlinear viscoelasticity or solid-like behaviour for CD solutions, possibly due to complex intermolecular hydrogen bonding [166, 200-201, 206-208].

Evidence suggests that 2HP-β-CD/Hb-D solutions can still form aggregates with themselves and bounded water in the presence of urea, possibly due to steric effects, as evidenced by their viscoelastic behaviour ($G' > G''$) at higher 2HP-β-CD concentrations.

However, the significance of van der Waals forces versus hydrogen bonding networks during electrospinning, is not yet fully understood (Chapter 4).

Further understanding of the electrospinnability of CDs nanofibres, might have a particular significance for the development of new mānuka honey and CDs complexation nanofibre membranes, with potential applications in the healthcare (antimicrobial facemasks), nutraceutical (cosmetic patches), medical (skin scaffolds), and pharmaceutical (active bandages) industries.

CHAPTER 6

INDUSTRIAL APPLICATION - MĀNUKA HONEY NANOFIBRE MEDIA

6.1 Introduction

Honey, a highly valued food commodity with many prebiotic, antimicrobial and health benefits, is usually composed of 38% fructose, 30% glucose, 1% sucrose/maltose, 9% other sugars, and 22% water, with; containing varying amounts of several suspended solids (oils, flavonoids, polyphenols, etc.) [265].

Honey from native New Zealand mānuka plants (Leptospermum scoparium) is a high value commodity in many parts of the world, especially in Asia (> $1.0 NZD/g). However, the cost of using high-grade mānuka honey (e.g., +26 UMF - Unique Manuka Factor), for producing composite nanofibres with high antimicrobial properties, is considerable.

Antimicrobial effects against a wide range of gram-positive and gram-negative bacteria are well-known properties of mānuka honey. Moreover, the antimicrobial properties of mānuka honey are strongly related to the concentration of methylglyoxal, Leptosperine, Hydroxymethylfurfural, phenolic content and others [265]. For industry standards, the higher the concentration of methylglyoxal, the higher the antimicrobial properties of mānuka honey (e.g., 20+ UMF).

Electrospun composite nanofibres made from chitosan and honey [259], and polycaprolactone and mānuka honey [260] combinations, have shown to enhance the antimicrobial performance of the honey. Also, the addition of mānuka honey oils to platelet-rich plasma has been shown to enhance cellular chemotaxis, mitogenesis, ECM production, and angiogenesis [262].

Also, the electrospinnability of a poly (vinyl alcohol) and methylglyoxal blend (mānuka honey main antimicrobial agent) for antibacterial wound dressing, has been previously reported in literature [261]. However, poly (vinyl alcohol) is not a practical material for neither air filters nor skincare patches, as it is neither mechanically strong for air filtration flows nor has any intrinsic biological activity.

In this chapter, the electrospinnability of food-grade glucose syrup, as carrier bio-material for mānuka oils, was investigated in order to provide affordable honey nanofibre formulations for both air filtration and skincare applications.

However, as food-grade glucose syrup contained added preservatives, the composition of the syrup was investigated by Mass spectrometry and HPLC; in order to determine the purity of the material. Subsequently, the electrospinnability of the specific combination of mono-, di- and trisaccharides components present in the syrup, was further investigated.

In order to provide mechanical and bioactive properties to the nanofibre membranes, a concentrated aqueous mānuka-saccharide solution in combination with proprietary polymer and non-hydrolyzed marine collagen formulations, was used to manufacture the facemasks and skincare patches, respectively (Figure 6.11).

Also, several other IP-sensitive formulations (not reported) containing saccharide materials and mānuka oils (for antimicrobial wound care dressings) were developed by the present author in collaboration with the industrial partner Revolution Fibres Ltd.

6.2 Experimental procedures and results

6.2.1 Glucose syrup properties and composition

A culinary-grade glucose syrup was used as received for the electrospinning experiments (Queen Fine Foods Ltd., Brisbane, Australia). The syrup is a glucose extract derived from maize that contains traces of sulfur dioxide (preservative 220) and sodium sulphite salts (80–150 mg/kg max.).

Hence, the composition of glucose syrup was studied by HPLC and Mass spectrometry, to discard electrospinnability by the presence of polymeric materials. Also, the glucose syrup viscosity was too high for it to flow through the electrospinning capillary, therefore a 75% wt. glucose syrup concentration in 15% wt. water was used (Table 6.1).

Table 6.1 - Physical properties of the glucose syrup at 25°C.

Property	Value
Concentration	75% wt. % syrup/H_2O
Surface tension	98.11 mN/m
Conductivity	1.5 µS/cm
pH	5.5
Density	1.5 g/mL
Zero-shear viscosity	38,600 Pa·s

A possible mechanism for the electrospinnability of the glucose syrup systems could rest upon the ability of mutarotation on the anomeric carbon within the pyranose-glucose ring, which yields the two distinct stereoisomer configurations of glucose (α and β) [114, 219]. This mutarotation process could often produce metastable dihexoses through 1, 6 glycosidic bonds [115, 116, 161].

Saturated solutions of saccharide mixtures could also yield more complex metastable molecular architectures after heat and electrical processing. Furthermore, oligosaccharides and other more complex molecular architectures, possibly reacting with added preservatives could have been produced during the electrospinning of glucose syrup.

However, mass spectrometry (Figure 6.1) and HPLC (Figure 6.2) confirmed that the tested glucose syrup was mainly composed of monosaccharide (glucose and fructose [$C_6H_{12}O_6$]), disaccharide (sucrose and maltose [$C_{12}H_{22}O_{11}$]), and trisaccharide (raffinose [$C_{18}H_{32}O_{16}$]). Evidence of possible chemical modifications (covalent bonding) on the saccharide solutions and saccharide electrospun material remains to be found (Figure 6.1 and 6.2).

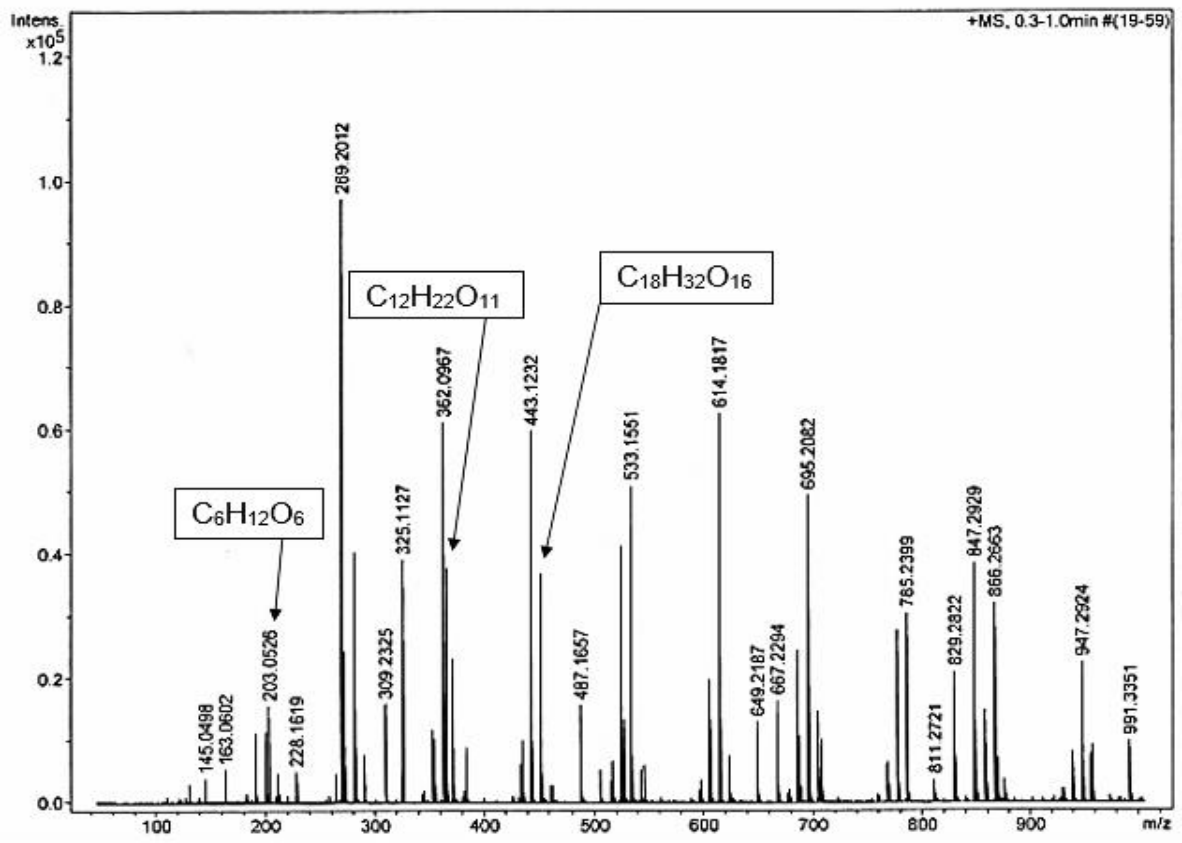

Figure 6.1 - Mass spectrum from MS showing the intensity (y-axis) as a function of the mass-to-charge ratio (x-axis). The presence of the isomers of glucose, sucrose and raffinose are indicated at mass-to-charge ratios of 203.05, 365.1 and 527.16, respectively.

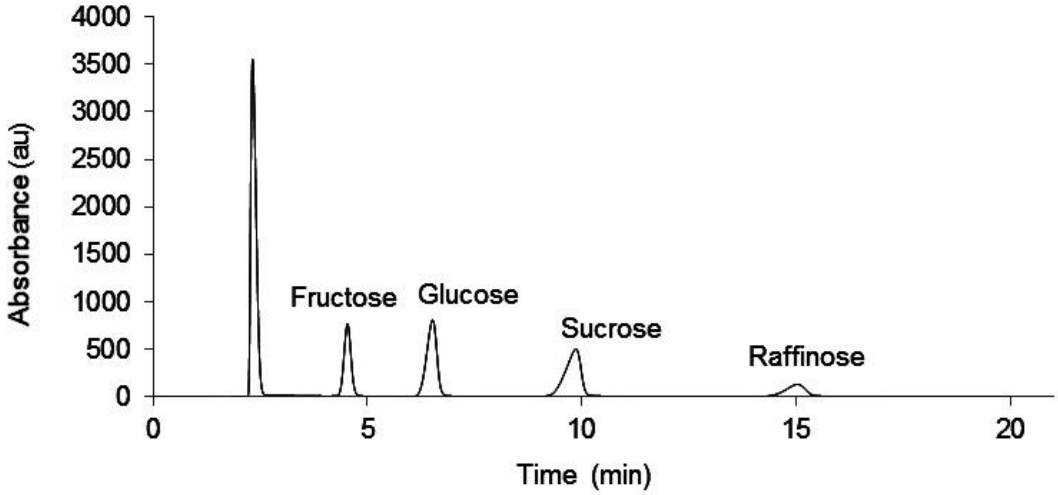

Figure 6.2 - HPLC chromatogram confirming the presence of fructose, glucose, sucrose and raffinose in the glucose syrup. The first peak is the injection peak.

6.2.2 Rheometry

The viscoelastic behaviour of the syrup showed a correlation to the visco-elasto-capillary thinning theory for complex fluids as described by McKinley [82], because the shear thinning response of the viscosity measurements (Figure 6.3A) indicates an initial viscous response of the solution to an increasing shear rate, followed by an elastic thinning response, as indicated by a decreasing shear viscosity (slope) beyond a shear rate of ~0.01 s^{-1} [43, 44].

However, the frequency response of the storage and loss modulus of the syrup shows that this behaviour is mostly elastic [81], since the storage modulus is greater than the loss modulus over the entire frequency range measured (Figure 6.3B). This further supports the evidence that higher Trouton ratios corresponded to better electrospinnability (storage modulus > loss modulus) [128].

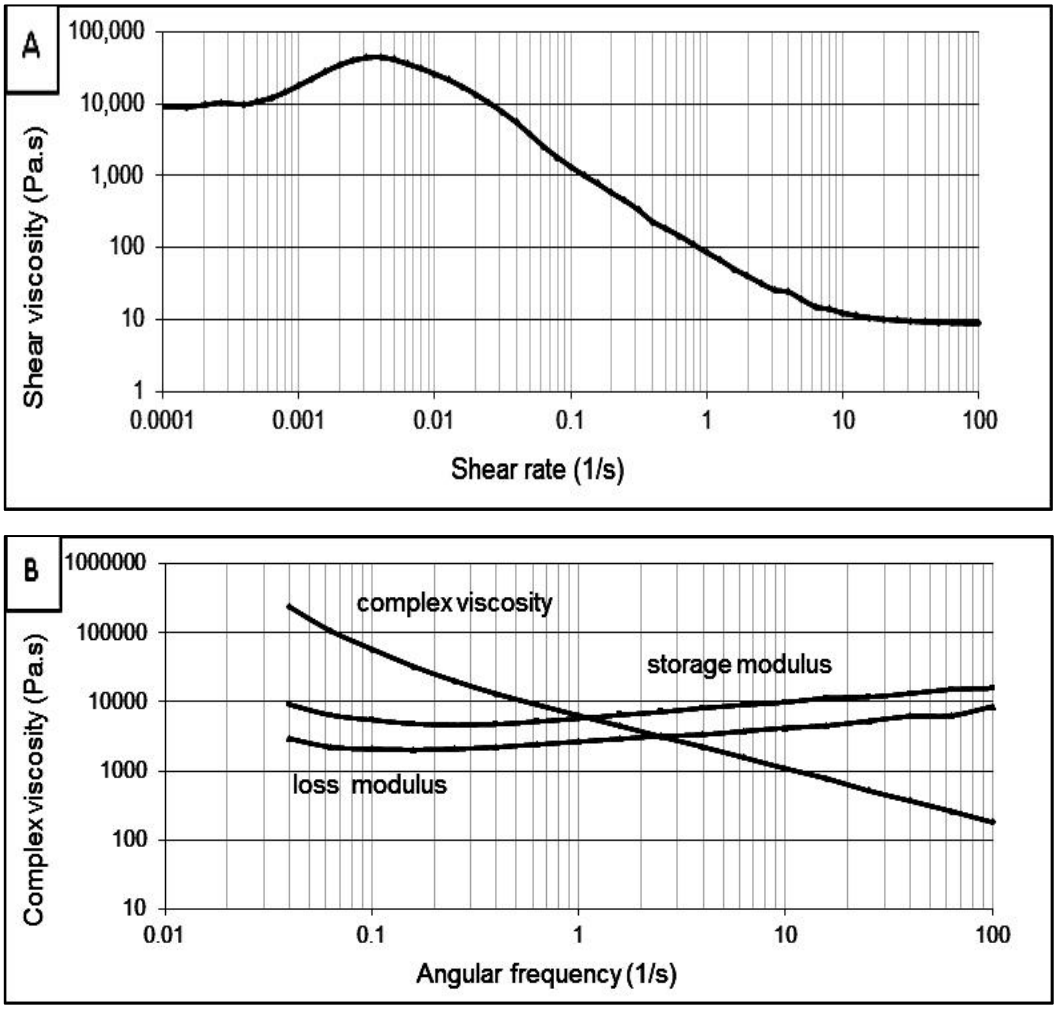

Figure 6.3 - Rheological properties of the glucose syrup: (A) shows the shear viscosity as a function of shear rate, (B) shows the complex viscosity, loss and storage modulus as a function of angular frequency of the glucose syrup.

6.2.3 Glucose syrup electrospinnability

Typical electrospinning behaviour was observed for the glucose syrup, consisting of stable and chaotic jet formation (Figure 6.4). These photographs show the heaviest parts of the electrospun jet as dark beads, within the spinning cone. The polarity of the applied voltage did not influence the electrospinning behaviour of the glucose syrup, hence positive polarity was used throughout the experimentation.

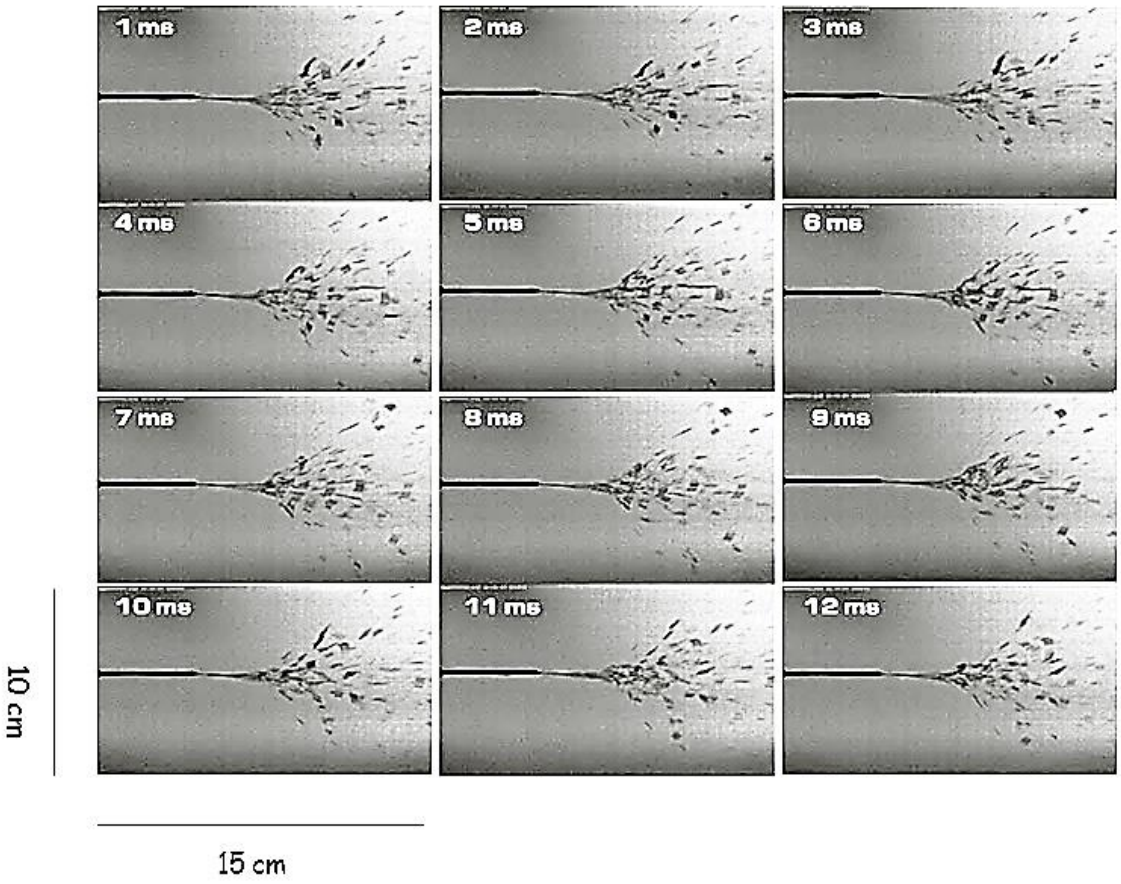

Figure 6.4 - Series of high-speed photographs taken at 1000 fps during the electrospinning of the glucose syrup.

Published results for the results shown in Figure 6.4 and 6.5, demonstrate for the first time that food-grade glucose syrup can form continuous filaments during electrospinning [171]. Also, the highly beaded structures of the filaments (Figure 6.5C and 6.5D) further support the viscoelastic behaviour of the material, as evidenced by rheometry characterisation (Figure 6.3).

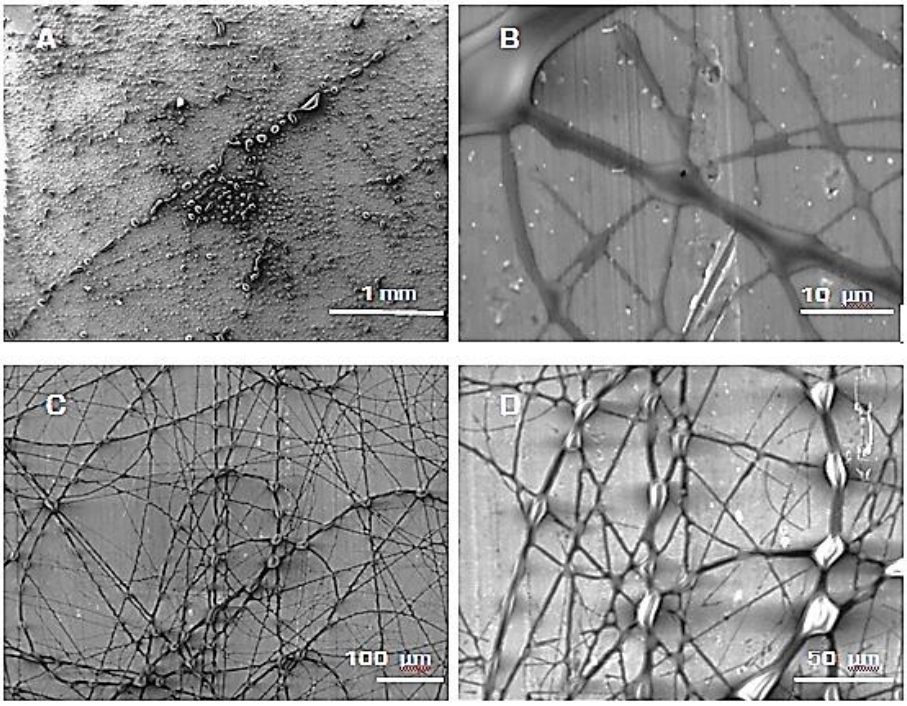

Figure 6.5 - SEM images of electrospun glucose syrup at varying magnifications.

6.2.4 Syrup replica

To further confirm the electrospinnability of the commercially supplied glucose syrup, a duplicate solution was made up by combining the pure components that had been previously identified by HPLC, at similar relative concentrations of each material. Namely, glucose (34 wt. %), fructose (22.5 wt. %), sucrose (32 wt. %), and raffinose (11.5 wt. %) in distilled water, to give a final total solids concentration of 75 wt. %.

The syrup replica solution exhibited similar behaviour to the commercially supplied glucose syrup (e.g., continuous filaments), providing strong evidence that heterogeneous mixtures of mono-, di-, and trisaccharide materials are a viable material for developing sugar-based nanofibre products (Figure 6.6).

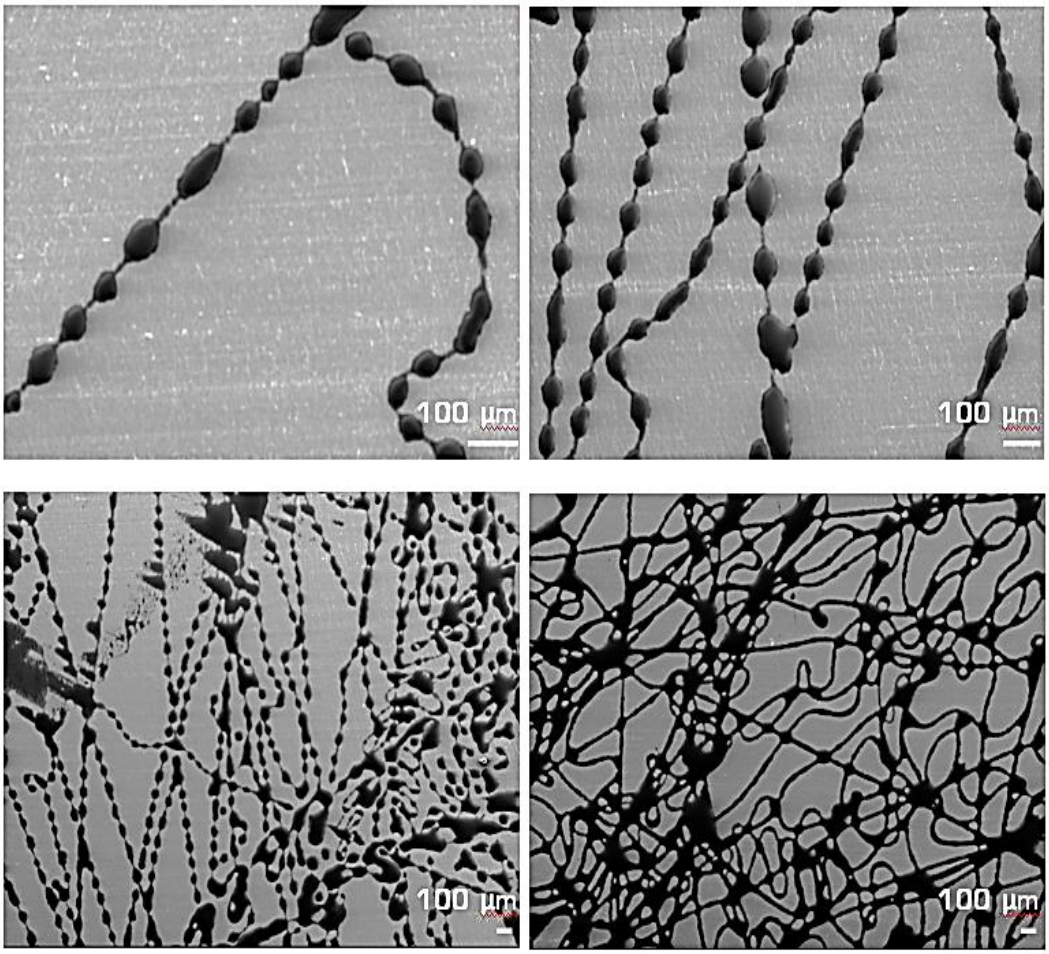

Figure 6.6 – SEM images of electrospun filaments made from the replica of the glucose syrup at 50˚C.

6.3 Mānuka honey nanofibre media

Commercially available mānuka honey did not show electrospinability, mostly due to the high water and suspended solids concentration (>20%). Subsequently, a formulation based on the syrup replica containing mānuka oils, was designed to carry the antimicrobial mānuka bio-actives, as well as to improve nanofibre adhesion between substrate layers. Hence, a mānuka-syrup-collagen and a mānuka-syrup-polymer nanofibre composite, were developed for skincare patches and air filtration facemasks respectively.

Although both prototypes used mānuka oils and glucose syrup (Figure 6.7), the properties of the electrospun nanofibres were completely different (hydrophilic versus hydrophobic), due to the combination with other materials (polymethyl methacrylate - PMMA and marine collagen).

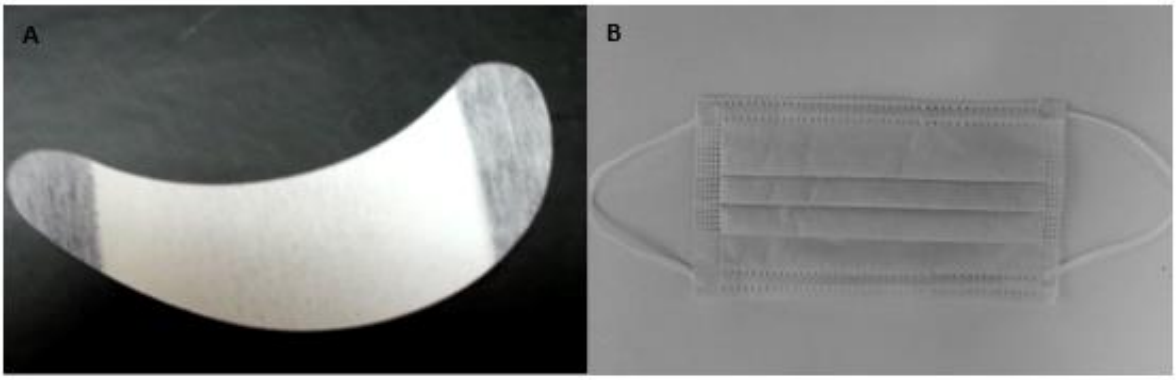

Figure 6.7 – Prototypes of the honey–nanofibre composite media for cosmetic patches (A) and antimicrobial facemasks (B)

6.3.1 Air filtration facemasks

Air filtration markets are becoming an increasingly competitive market, with many new technology developments being commercialised across different air filtration sectors (e.g., antipollution facemasks, air purifiers, HVAC, etc.), especially in China [243, 244, 246]. There are many social and economic circumstances contributing to human health problems, for example low-income urbanites breathe 28% more noxious particulate matter (PM2.5) than residents in high-income areas [245, 247].

High-efficiency microfibre respirators currently available in the market are usually sold at prices ranging from 15 to 35 USD per item, whereas the Chinese minimum wage per day is approximately 23 USD [248, 249]. Furthermore, high breathability (low pressure drop or ΔP) at high-filtration efficiencies is the main design parameter for the development of a commercially successful facemask [243]. Microfibre media can often achieve high efficiencies only at low breathability (high pressure drop) [241, 242, 245-247].

In contrast, nanofibre media can achieve both: high efficiency and high breathability [238, 239-242]. Moreover, the ability to integrate active ingredients (e.g., mānuka oils) into the media is a clear competitive advantage of nanofibre technology versus standard microfibre processing methods [15-17, 240].

The air filtration facemasks prototype developed used several layers of the composite nanofibre material deposited onto a nonwoven polypropylene microfibre substrate, until a density of 1 gram per square meter (1 gsm) was obtained (Figure 6.8).

The composite nanofibre nonwoven medium was then sandwiched between polypropylene substrates and cut to specific roll dimensions. Subsequently, manufactured media was sent to China for processing at an industrial facemask-manufacturing facility (Figure 6.7B).

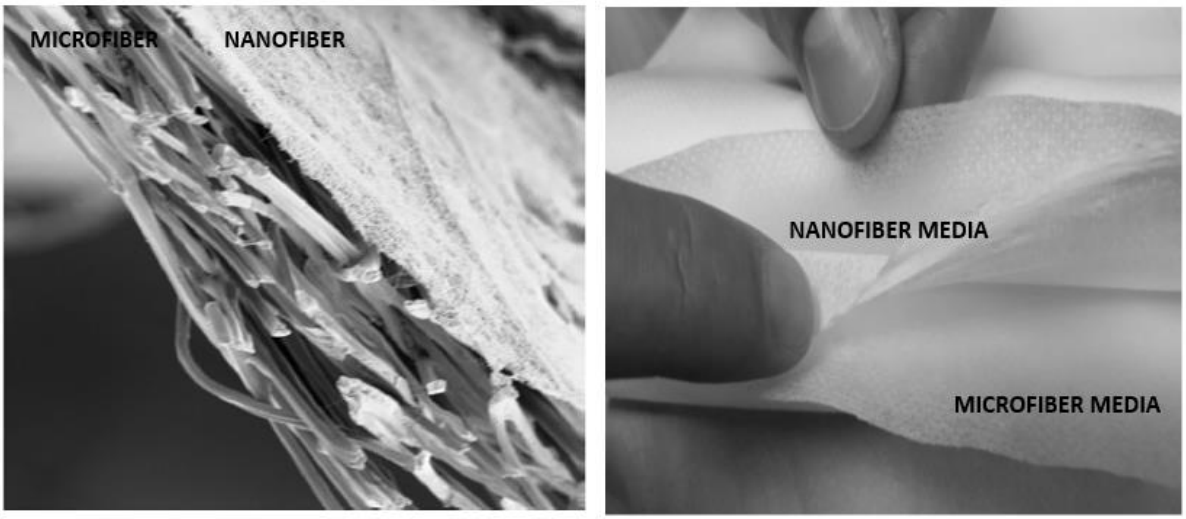

Figure 6.8 – A mānuka–glucose syrup/ polymer composite, electrospun nanofibre layer (1 gsm), sandwiched in between two polypropylene substrates.

6.3.2 Skincare patches

The ActiVLayr™ skin delivery platform is a patented technology (WO/2013/0350720), based on the denatured whole chains of type 1 collagen extracted from NZ hoki fish skins [254]. The type 1 collagen used to produce ActiVLayr™ is highly hydrophilic, because the relatively high content of hydroxyproline in the hoki skins promotes hydrogen bonding networks between the triple helix structure of the collagen [253, 254]. Moreover, this particular source of collagen does not need to be hydrolysed to be processed at room temperature, like most collagens in the market, since the internal triple helix structure is in reversible kinetic-thermal equilibrium at standard ambient conditions [252].

ActiVLayr™ patches are usually commercialised using a wide range of plant and fruit extracts derived from the waste stream of the New Zealand wine and food industries. The ecologically sourced extracts contain a wide range of polyphenols, catechins, vitamins, flavonoids, and others. However, as increasing market demand for mānuka oils, kānuka honey and bee venom products continues to rise in Asia, new formulations based on such materials are highly needed in order for ActiVLayr™ patches to continue to be commercially profitable.

The skincare prototype patch co-developed as part of this thesis used a proprietary combination of saccharides (based on the glucose syrup replica formulation), denatured whole chains of collagen and mānuka oils (Figure 6.9). ActiVLayr™ technology is now available in the market under white label customisation services, and is also under extensive clinical tests, in collaboration with Revolution Fibres.

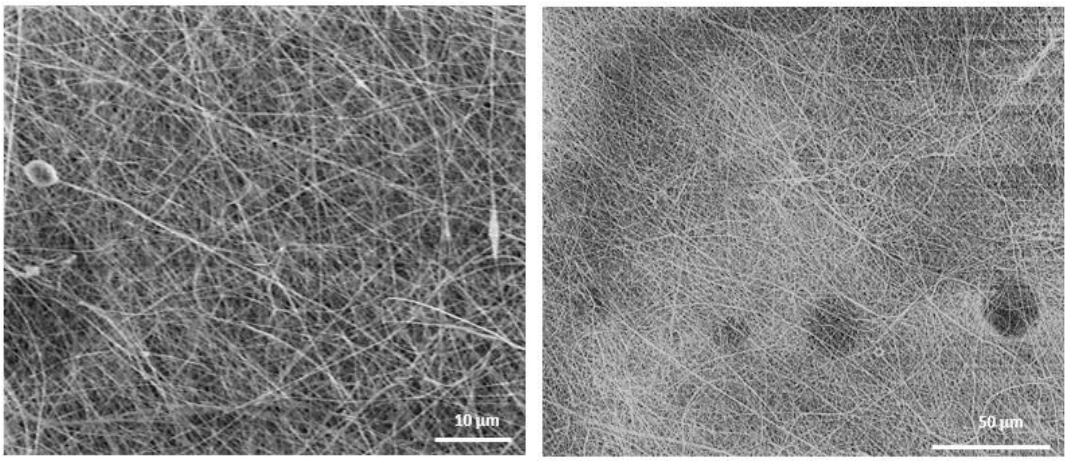

Figure 6.9 – Scanning electron micrograph of the mānuka-syrup-collagen nanofibre composite

CHAPTER 7

GENERAL DISCUSSION

7.1 Introduction

Determining the electrospinnability of a given material is a complex problem that involves the consideration of many different solution and process parameters. As discussed in Chapter 2, electrospinnability is usually approached using simplified mathematical models based on polymer physics, capillary flow and extensional rheology.

However, common theories based on polymer physics and rheology cannot accurately describe the electrospinning behaviour of nonpolymeric systems, such as supramolecular systems with extensive secondary bonding (e.g., saccharide solutions).

Furthermore, the hypothesis that increased saccharide concentration in aqueous solutions would also increase secondary bonding mechanisms between molecules, resulting in increased electrospinnability, was supported by the evidence provided in Chapter 4. Also, evidence on the electrospinnability of octa-*O*-acetyl sucrose offers a new basis for the discussion on the significance of van der Waals interactions during electrospinning.

Moreover, the observation that Hb-D/β-hCD solutions did not electrospun, while Hb-E/β-hCD solutions did electrospun, further supports the hypothesis that secondary bonding mechanisms (e.g., hydrogen bonding) are indeed critical for the electrospinnability of nonpolymeric systems (Chapter 5). Furthermore, extensive secondary bonding interactions in tested β-hCD systems, were the basis of the complex visco-elastic behaviour of the solutions, also a critical factor for their electrospinnability.

The experimental evidence presented in this thesis suggests that complex charge-transport mechanisms, based on the interaction of hydrogen bonding and van der Waals forces alike, are a critical factor for the electrospinnability of saccharides and supramolecular materials.

7.2 CHAIN ENTANGLEMENT THEORY

Chain entanglement theory, describes the electrospinnability of polymeric solutions with concentrations between the critical overlap concentration (c^*) (e.g., semi-dilute, un-entangled) and entanglement concentration (*Ce*) (e.g., semi-dilute, entangled). Electrospinnability thresholds for most polymer systems are generally accepted to be around 2.5 times the entanglement concentration (*Ce*) where C*e* is typically ~10 × c^* [109-111, 154].

However, electrospinnability of sucrose solutions (S/+SAT) occurred at only 2 × *c** whereas the standard chain entanglement condition is 2 × *Ce* (where *Ce* = 10 × *c**). Moreover, the critical overlap concentration predicted by chain entanglement theory for other concentrated saccharide solutions (e.g., glucose and fructose and their mixtures), required *c** values exceeding real solute concentration numbers (e.g., +100 w.t %). Evidence suggesting that the electrospinning of nonpolymeric systems might not be entirely dependent on physical covalent interactions.

For example, sucrose in aqueous solutions strongly binds water molecules within its hydration sphere, orienting water molecules even at large distances as hydrocolloid clusters, a characteristic behaviour of supramolecular materials [175]. Furthermore, self-assembly theories have been proposed by others as a complementary mechanism to chain entanglement, mostly based on depletion flocculation by self-aggregates [164-166, 200, 201].

Moreover, the viscoelastic properties of the tested solutions suggest that increased shear viscosities, as well as high storage modulus (elasticity), are critical factors for electrospinnability of tested materials. However, visco-elasto-capillary theory, similar to chain entanglement theory, is also based on non-Gaussian conformational statistics for relatively long macromolecules, as well as on the physical-chemical scaling concepts of de Gennes commonly used in polymer physics [78, 220].

In other words, neither theory considers reversible bonding (sticky reptation) by hydrogen bonding nor van der Waals forces, as a critical parameter for the unusual relaxation times of the concentrated solutions tested in this thesis.

7.3 Visco-elasto-capillary theory

Visco-elasto-capillary theory sets different boundaries for spinnability, depending on the rheological properties of the solution [54, 82, 79, 188, 193]. Continuous filament formation can be generally described by the Deborah number (De), indicative of elasticity, and by the Ohnesorge number (Oh), indicative of viscosity. In the case of electrospinning, the non-dimensional numbers should fulfil the following electrospinnability condition: $De \geq Oh \geq 1$ [80].

In other words, Rayleigh instabilities would not spread if the extensional deformation (elasticity) caused by the electrical pressure, is faster than the build-up of electrical charges on the jet surface [54, 82, 79, 80, 188, 193]. However, there is a well-known mathematical dependency of the Deborah number (De) on the molecular relaxation time of the material.

Polymer relaxation times are usually calculated by standard rheological methods based on the bulk relaxation time of the macromolecular solution. Relaxation times calculated using standard rheological methods can be imprecise, as such relaxation times can be orders of magnitude longer than the Brownian relaxation times of the bulk state, invariably reflecting collective motions induced by confinement [203].

Moreover, when ultrathin films of even simple nonpolar molecular fluids in a confined physical space are subjected to oscillatory shear, the effective viscosity of the material decays in an apparent power law relationship with respect to the shear rate, implying a considerable distortion of the dynamic structure [221].

Furthermore, such relaxation values would only be accurate when the molecules are at rest and not being electrically stressed, which is not the case for electrospinning. Nonetheless, calculated bulk relaxation times of the solutions by rheological methods can still be used as a reference for the true molecular relaxation times of the materials.

For example, when fitting the storage and loss modulus values using a simplified version of the tube model (Appendix A1), Deborah numbers (De) did correlate well to the electrospinnability of most samples (Figure 4.14).

In general, visco-elasto-capillary theory based on the non-dimensional numbers analysis as proposed by McKinley et al. [15], adequately describe the electrospinnability of the saccharide solutions studied in Chapter 4. Nonetheless, it is still not clear how secondary chemical bonding (e.g., hydrogen bonding and van der Waals forces) and other complex electrodynamic interactions caused by the high voltages that drive the electrospinning process relate to molecular relaxation and electrospinnability.

7.4 VAN DER WAALS ELECTROSPINNABILITY

In a perfect periodic lattice (e.g., metals and ideal conductors), electron waves scatter constructively from the atomic ion cores, resulting in coherent transmission of the stresses, even over rather large distances [180]. However, any imperfections on the lattice, such as anisotropy, surface contamination, and so on, would tend to amplify (constructively or destructively) the electrical or capillary wave propagation, often resulting in lower transmission of the input energy [71, 72, 180].

Likewise, fluid visco-elasticity could also be understood as the sum of the total covalent and noncovalent forces that normally play a role in liquid micro- and macromolecular interactions, as described by the sum of each Gibbs free energy for each individual force [180].

However, the additivity of all intermolecular forces is far from straightforward since different types of force decay with distance at different rates, and according to different laws. For example, van der Waals and hydrogen bonds are much weaker than covalent bonds, with typical energies of 10–50 kJ/mol and bond lengths of 0.3–0.4 nm [180].

Also, van der Waals forces, which can be catalogued into three different subclassifications (Keesom, Debye and London forces), obey similar linking rules. However, in combination, the interactions between these forces can result in completely different behaviours from the predictions expected from the same primary force (van der Waals equations) [180, 175].

For example, the electrospinnability of 2-hydroxypropyl–β cyclodextrins (β-hCD), in both hydrogen bonding enhancing and hydrogen bonding disrupting solvent systems, clearly

showed that electrospinning of supramolecular materials is heavily dependent on intermolecular bonding mechanisms, e.g., hydrogen bonding.

Also, the nonlinear viscoelasticity (gelation) of tested CD solutions further supports the proposition that high-density hydrogen bonding networks might be produced when there is an increment in the degree of hydration (bound water) per CD molecule [167-169].

Furthermore, networks of hydrogen bonds can show the phenomenon of cooperativity, leading to deviations from reciprocal (acceptor/donor) additivity of standard hydrogen bond properties [180]. Moreover, hydrogen bonds could induce dipolar moments through van der Waals mechanisms across the molecular conglomerate, affecting the overall dielectric properties of the material [175, 176, 180].

Additionally, it is well known that hydrogen bonding has a significant effect on capillary-driven processes [162, 189, 191, 192]. Also, hydrogen bonds are involved in proton transfer reactions and may be considered partially activated precursors of such reactions [175, 176, 180].

Similarly, sucrose molecules in aqueous solutions can remain immobile as protons are passing through the concentrated solutions, similarly to a Grotthuss chain mechanism [180]. Moreover, extensive secondary bonding can potentially increase the predicted molecular relaxation times for supramolecular solutions, especially when confined under electrical stresses [71, 72].

However, the electrospinnability of octa-*O*-acetyl sucrose challenges the argument for reciprocal hydrogen bonding electrospinnability. Moreover, such evidence suggests that electrospinnability might be driven by van der Waals forces and to a lesser extent by hydrogen bonding, as suggested by the properties and behaviour of octa-*O*-methyl sucrose.

However, no conclusive proof of either hydrogen bonding interactions (H-donors / H-acceptors) or permanent nor induced dipolar moments, can be categorically correlated to the electrospinnability of octa-*O*-acetyl sucrose. Nonetheless, the apparent hydrogen-accepting capacity and molecular polarity of the tested concentrated solutions were definitely an important requirement for the electrospinnability of tested materials.

In summary, electrospinnability is still an ambiguous phenomenon that can only be described in terms of a series of events finding the right equilibrium conditions for the successful formation of homogenous and continuous nanofibres. Creating a model that can accurately describe the interactions of all of these variables is a complex problem that at this stage has only been partially solved by idealising many of these interactions with limited mathematical assumptions.

CHAPTER 8

CONCLUSIONS

8.1 Summary

New experimental data on the electrospinning of sugars is reported. Relationships between the physical-chemical properties of the solutions and their associated viscoelastic behaviour have been previously discussed. Remarkably, glucose syrup, concentrated saccharide solutions, cyclodextrin mixtures and modified sucrose compounds all showed similar physical-chemical trends associated with their electrospinnability:

- Higher density promoted electrospinnability (Figure 4.6).
- Higher than average surface tension values at higher concentrations also promoted electrospinnability (Figure 4.7, Figure 5.4).
- Lower conductivities at higher concentrations also promoted electrospinnability of tested materials (Figure 4.8, Figure 5.3, Table 4.2).
- Higher pH values also promoted electrospinnability (Figure 5.2, Table 4.2).

Moreover, the electrospinnability of 2-hydroxypropyl–β-cyclodextrin (2HP-β-CD) solutions did show to be strongly linked to the physical-chemical properties of the solvent system based on the following observations:

- Hydrogen bonding disrupting solutions (2HP-β-CD/Hb-D) were not electrospinnable, while the hydrogen bonding promoting solutions (2HP-β-CD/Hb-E) could be electrospun into fibres more easily (at lower concentrations), than the control (2HP-β-CD/H_2O) (Figure 5.5).
- Similarly, only 2HP-β-CD/Hb-E solutions at lower concentrations (60 wt. %) showed electrospinnability (Figure 5.5) despite the relatively high electrical conductivity of 2HP-β-CD/Hb-E solutions in comparison to 2HP-β-CD/H_2O and 2HP-β-CD/Hb-D solutions (Figure 5.3).
- 2HP-β-CD/Hb-E solutions exhibited lower surface tension and higher conductivity, compared with the control and 2HP-β-CD/Hb-D solutions, correlating with improved electrospinnability at lower concentrations (60 wt. %) (Figure 5.4 and 5.5).

Also, the overall effects of the viscoelastic properties of the materials undergoing a capillary thinning process were of significant importance to the electrospinnability of tested materials, as based on the following observations.

- High zero-shear viscosities (Figure 4.9) and longer, stable jet lengths (Figure 4.10) can also be regarded as indicators for the electrospinnability of tested materials.
- Electrospinnability was also promoted by high shear viscosities at lower shear rates, and higher G' at high shear rates ($G' > G''$) (Figures 4.11, 4.12 and 5.6).

In general, visco-elasto-capillary theory was much more suitable for predicting the electrospinnability of saccharide solutions (Figure 4.14), compared with chain entanglement theory (Table 4.1). Likewise, longer relaxation times or the capacity to remain electrically stressed for longer periods of time, correlated to improved electrospinnability (Table A1). Nonetheless, visco-elasto-capillary theory cannot provide an explanation for the relationship between hydrogen donor-acceptor interactions, van der Waals forces, Debye's length and other complex electrodynamic interactions caused by the high voltages that drive the electrospinning process.

8.2 Future work

In summary, the problem of electrospinnability should be evaluated for each given solution-process system, on an individual basis. For example, the following sets of experiments could be developed further to increase our knowledge of the electrospinnability of saccharide and supramolecular materials.

Visco-elasto-capillary properties

- Use extensional rheology to calculate the extensional viscoelastic properties of concentrated solutions. This would be particularly significant for cyclodextrin solutions with very high G' modulus.
- Use dynamic pulsed-field-gradient NMR (PFG-NMR) to measure the molecular size of the saccharides with and without their hydration shell, in order to observe the true radius of gyration and approximate more accurate critical concentration values for all solutions.

Molecular relaxation times

- Use proton diffraction by synchrotron X-ray sources in supersaturated saccharide solutions in order to determine the hydrogen bonding and van der Waals forces dynamics at varying temperatures (e.g., 50˚C).
- Use soft X-ray spectroscopy by small- and wide-angle X-ray scattering (SAXS/WAXS) on an electrospinning jet during flight. This would be particularly significant to evaluate the dynamics of secondary bonding, thermal diffusion and charge transport during the electrospinning process.

Van der Waals interactions

- Execute density functional theory (DFT) and quantum computational chemistry models on concentrated saccharide solutions in order to compare the effects of their van der Waals forces and hydrogen bonding dynamics when subjected to high voltage fields, elevated temperatures and other processing conditions.

The lack of standardised procedures for electrospinning research reflects the increased inconsistency of experimental results and contradictory statistical analysis of the process relationships. In order to further progress the collective scientific knowledge of electrospinnability, it is critical to have access to advanced characterisation equipment and, more importantly, to implement consistent industry standards during experimentation.

REFERENCES

1. Gilbert, William. On the magnet. London, 1600; 1:1-247.
2. Nollet, Abbe. Recherches sur les causes particulieres des phenomenes electrigues. *Les freres Guerin,* 1754; 1:1-509.
3. Zeleny, John. Instability of electrified liquid surfaces. *The physical review,* 1917; 10:1-6.
4. Zeleny John. The discharge of electricity from pointed conductors differing in size. *The physical review*, 1907; 25:305-333.
5. Turner J. G. I. Taylor in his later years. *Annual Review of Fluid Mechanics*, 1997; 29:1-25.
6. Saville D. Electrohydrodynamics: The Taylor–Melcher Leaky dielectric model. *Annual Review of Fluid Mechanics,* 1997; 29:27-64.
7. Lindau L., and Lifshitz E. Electrodynamics as continous media. *Pergamon press,* 1960; 8:1-413
8. Baumgarten P. Electrostatic spinning of acrylic microfibres. Journal of Colloid and Interface Science, 1971; 36:71-79.
9. Larrondo L., and St. John Manley., Electrostatic fibre spinning from polymer melts I, II and III. *Journal of Polymer science,* 1981; 19:909-940.
10. Lord Rayleigh. On the equilibrium of liquid conducting masses charged with electricity. *The london, edinburgh and dublin philosophical magazine and journal of science*, 1882; 1:184-186.
11. Lord Rayleigh. On the instability of jets. *Proceedings of the London mathematical society,* 1878; 1:4-12.
12. Darrell H., and Reneker D. Electrospinning process and applications of electrospun fibres. *Electrostatics*, 1995; 35:151-160.
13. Esfil-Tehno (n.d.) Retrieved June 2015, from http://www.esfiltehno.ee/eng/.
14. Chung H. Young,−Donalson Co., Inc., Book review; "Electrospinning of micro and nanofibres: fundamentals in separation and filtration processes", *Journal of engineered fibres and fabrics*, 2008; 1:1-2.
15. Bhardwaj Nandana. Electrospinning: A fascinating fibre fabrication technique. *Biotechnology/Advances,* 2010; 28:325-347.

16. Ramakrishna S. Electrospun nanofibres as a platform for multifunctional, hierarchically organized nanocomposite. *Composites science and technology*, 2009; 69:1804-1817.
17. Wendorff J. Functional Self-Assembled Nanofibres by Electrospinning. Advances on *Polymer Science*, 2008; 1:107-171.
18. Wendorff J. Nanostructured Fibres via Electrospinning. *Adv Materials*, 2001; 13:70-73.
19. Rutledge G. A Fundamental Investigation of the Formation and Properties of Electrospun Fibres 3, *National Textile Center Annual Report*, 2001; 1:1-9.
20. Rutledge G. A Fundamental Investigation of the Formation and Properties of Electrospun Fibres 2, *National Textile Center Annual Report*, 2000; 1:1-9.
21. Rutledge G. A Fundamental Investigation of the Formation and Properties of Electrospun Fibres. *National Textile Center Annual Report*, 1999; 1:1-10.
22. He J., Wan Y. and Yu J. Scaling law in electrospinning: relationship between electric current and solution flow rate. *Polymer*, 2005:2799-2801.
23. Munir M., Suryamas A., Iskandar F., and Okuyama K. Scaling law on particle-to-fibre formation during electrospinning. *Polymer*, 2009; 50:4935-4943.
24. Wang C., Hsu C., and Lin J. Scaling Laws in Electrospinning of Polystyrene Solutions. *Macromolecules* 2006; 39:7662-7672.
25. Bhattacharyya D., Lin R., and Patra S. Regression analysis of manufacturing electrospun nonwoven nanotextiles. *Journal of material science*, 2010; 45:3938-3946.
26. Yang Y., Li Q., Jia Z., and Guan Z. Experimental Investigation of the Governing Parameters in the Electrospinning of Polyethylene Oxide Solution. *Transactions on Dielectrics and Electrical Insulation*, 2006; 13:580-585.
27. Pattamaprom C., Hongrojjanawiwat W., Koombhongse P., Supaphol P., Jarusuwannapo T., and Rangkupan R. The Influence of Solvent Properties and Functionality on the Electrospinnability of Polystyrene Nanofibres. *Macromol. Mater. Eng.*, 2006; 291:840-847.
28. Heikkila P., and Arlin A. Parameter study of electrospinning of polyamide-6. *European Polymer Journal*, 2008; 44:3067-3079.
29. Lu C., Chen P., Li J., and Zhang Y. Computer simulation of electrospinning. Part I. Effect of solvent in electrospinning. *Polymer*, 2006; 47:915-921.
30. Helgeson M., Grammatikos K., Deitzel J., and Wagner N. Theory and kinematic measurements of the mechanics of stable electrospun polymer jets. *Polymer*, 2008; 49:2924-2936.

31. Thompson C., Chase G., Yarin A., and Reneker D. Effects of parameters on nanofibre diameter determined from electrospinning model. *Polymer*, 2007; 48:6913-6922.
32. T. A. Kowalewski, Blonski S., and Barral S. Experiments and modelling of electrospinning process. *Bulletin of the polish academy of sciences*, 2005; 53:385-394.
33. Li F., Yi X.-Y., and Yin X.-Z. Instability of a viscous coflowing jet in a radial electric field. *Journal of Fluid Mechanics*, 2007; 596:285-311.
34. Li M., Kang S., and Park J. Instability of electrically driven polymer liquid jets. *Mechanical science and technology*, 2006; 20:409-417.
35. He J. Xu L., and Yong Y. Mathematical models for continuous electrospun nanofibres and electrospun nanoporous microspheres. *Polymer Int.*, 2007; 56:1323-1329.
36. Spivak A., Dzenis Y., and Reneker H. Model of steady state jet in the electrospinning process. *Mechanics Research Communications*, 2000; 27:37-42.
37. Kowalewski T., Barral S., and Kowalczyk T. Modeling Electrospinning of Nanofibres, *IPPT-PAN*, 2008; 1:1-14.
38. Naeem F., Xu L., and Wang L. A thermo-electro-hydrodynamic model for vibration-electrospinning process. *Thermal Science*, 2011; 15:1-5.
39. Hohman M. Electrospinning and electrically forced jets II. Applications. Physics of fluids, 2001; 13:2221-2236.
40. Hohman M. Electrospinning and electrically forced jets. I. Stability theory. physics of fluids, 2001; 13:2201-2220.
41. Lukas D., Sarkar A., Martinova L., and Vodsedalkoba D. Physical Principles of Electrospinning - Electrospinning as a Nano-Scale Technology of the Twenty-First Century. *CRC*, 2009; 1:59-140.
42. Basaran O. Small-Scale free surface flows with breakup: Drop formation and emerging applications. 2002; 48:1842-1848.
43. Navier C. Memoire sur les lois du mouvement des fluides. *Mem. Acad. Sci. Inst.* 1822; 6:389-440.
44. Baidakov V., Protsenko S., and Chernykh G. The van der Waals theory of capillarity and computer simulation. *Colloid Journal*, 2001; 64:661-670.
45. Feng J. The stretching of an electrified non-Newtonian jet: A model for electrospinning. *Physics of fluids*, 2002; 14:3912-3926.
46. Barber R. The influence of Knudsen number on the hydrodynamic development length within parallel plate micro-channels. *Advances in fluid mechanics*, 2002; 4:207-216.

47. Giambattista G., Lebowitz J., and Presutti E. Deterministic and Stochastic Hydrodynamic Equations Arising From Simple Microscopic Model Systems. *Mathematics Subject Classification.,* 1991; 1:1-46.
48. Luedtke W., Landman U, Chiu H., Levandier J., Dressler A., Sok S., and Gordon M. Nanojets, Electrospray, and Ion Field Evaporation: Molecular Dynamics Simulations and Laboratory Experiments. *J. Phys. Chem. A,* 2008; 112:9628-9649.
49. Van Honschoten, J., Brunnets N., and Tas N. Capillarity at the nanoscale. *Chemical society reviews,* 2009; 39:1096-1114.
50. Hongbo M. Dynamics of flowing polymer solutions under confinement. *University of Wisconsin- Madision*, 2007; 1:1-144.
51. Adamowicz S. Experimental and ab initio theoretical studies of electron binding to formamide, N-methylformamide, and N,N-dimethylformamide. *Chemical physics*, 1999; 10:4309-4314.
52. Andrade A.L., Science and Technology of Polymer nanofibres. *John Wiley and Sons,* 2008; 1:1-420.
53. Yıldırım O. Dynamics of formation and dripping of drops of deformation-rate-thinning and -thickening liquids from capillary tubes. J. *Non-Newtonian Fluid Mech.,* 2006; 136:17-37.
54. Tirtaatmadja V. Drop formation and breakup of low viscosity elastic fluids: Effects of molecular weight and concentration. *Physics of fluids,* 2006; 18:1-17.
55. Hao G. Droplets formatioin and merging in two-phase flow microfluidics. *Int. J. Mol. Sci.*, 2011; 12:2572-2597.
56. Lopez-Herrera J., Barrero A., Lope A., and Marquez M. Coaxial jets generated from electrified Taylor cones. Scaling laws. *Journal of aerosol science*, 2003; 34:535-552.
57. Taylor G. Electrically Driven Jets. Proceedings of the Royal Society of London A: Mathematical, *Physical and Engineering Sciences,* 1969; 313:453-475.
58. Stanger J., Staiger M, Tucker N., Coles S., Jacobs D., and Kirwan K. An experimental study of the effect of charge density on the Taylor cone. *Solid State Phenomena,* 2009; 151:54-59.
59. Guerrero I., Bocanegra R., Higuera F., and F. de la Mora J. Ion evaporation from Taylor cones of propylene carbonate mixed with ionic liquids. *Journal of Fluid Mechanics,* 2007; 591:437-459.

60. Yarin A., Kommbhongse S., and Reneker H. Taylor cone and jetting from liquid droplets in electrospinning of nanofibres. *Journal of Applied Physics,* 2001; 90:4836-4845.
61. Reznik S., Yarin A., Theron A., and Zussman E.Transient and steady shapes of droplets attached to a surface in a strong electric field. *Journal of Fluid Mechanics,* 2004; 516:349-377.
62. Larsen G., Spretz R., and Velarde-Ortiz, R. Use of coaxial gas jackets to stabilise Taylor cones of volitile solutions and to induce particle-to-fibre transitions. *Advanced Materials,* 2004; 16:166-169.
63. Gañán-Calvo, A. Cone-Jet Analytical Extension of Taylor's Electrostatic Solution and the Asymptotic Universal Scaling Laws in Electrospraying. *Physical review letters,* 1997; 79:217-220.
64. Smith K., Alexander M., and Stark J. Voltage effects on the volumetric flow rate in cone-jet mode electrospraying. *Journal of applied physics,* 2006; 99:1-8.
65. Spasic J., and Hsu J. Interfacial Electroviscoelasticity and Electrophoresis. *CRC Press,* 2010; 1:1-194.
66. Shamai R., Berge B., and Hayes R. Water, electricity and between… On electrowetting and its applications. *Soft Matter,* 2007; 4:38-45.
67. Ott B., and Boerio-Goates J. Chemical Thermodynamics; Advanced Applications. *Oxford,* 2000; 1:1-260.
68. Fong H., and D. Reneker. Beaded nanofibres formed during electrospinning. *Polymer,* 1999; 40:4585-4592.
69. Murray J. Molecular electrostatic potentials. theoretical and computational chemistry. *Elsevier,* 1996; 1:1-664.
70. Stanger J., Wallace A., Larsen N., Staiger M. and Reeves R. The effect of electrode configuration and substrate material on the mass deposition rate of electrospinning. *Journal of Applied Polymer Science,* 2009; 112:1729-1737.
71. Myers D. Surfaces, Interfaces and Colloids; Principles and Applications. *Wiley–VCH,* 1999; 2:1-528.
72. Ninham W., and Lo Nostro P. Molecular forces and self-assembly; in colloid, nano sciences and biology. *Cambridge University Press*, 2010; 1:1-360.
73. Malkin A. Surface Instabilities. *Colloid Journal,* 2007; 70:673-689.
74. Chandrasekhar S. Hydrodynamic and Hydromagnetic Instability. *Oxford, Clarendon Press,* 1961; 1:1-652.

75. Adamson A., and Gast A. Physical Chemistry of Surfaces. *John Wiley and Sons,* 1997; 1:1-808.
76. Wu X., Kostogorova–Beller Y., Goponeko A., Hou H. and Dzenis Y. Rippling of polymer nanofibres. *Physical review letters,* 2008; 78:1-8.
77. Wu X., and Dzenis Y. Wave propagation in nanofibres. *Journal of Applied Physics,* 2006; 100:1-4.
78. De Gennes P., Brochard-Wyart F., and Quere D. Capillarity and Wetting phenomena; drops, bubbles, pearls, waves, *Springer*, 2004; 1:1-292.
79. McKinley G. Dimensionless Groups for understanding free surface flows of complex fluids. *Rheology Bulletin,* 2005; 1:1-8.
80. McKinley G. Iterated stretching and multiple beads-on-a-string phenomena in dilute solutions of highly extensible flexible polymers. *Physics of fluids,* 2005; 17:1-5.
81. Doyle P., Shaqfeh E., McKinley G., and Spiegelberg S. Relaxation of dilute polymer solutions following extensional flow. *Journal of Non-Newtonian Fluid Mechanics,* 1997; 76:79-110.
82. McKinley G. Visco-Elasto-Capillary Thinning and Break up of complex fluids, *MIT – report,* 2005; 1:1-49.
83. Qin X., Jia L., Lu W., Shou D., and Fan J. Stretching of the steady jet in electrospinning: theoretical analysis and experimental verification. *Textile Research Journal,* 2011; 81:388-397.
84. Han T., Yarin A., and Reneker H. Viscoelastic electrospun jets: Initial stresses and elongational rheometry. *Polymer,* 2008; 49:1651-1658.
85. He J., Wu Y., and Zuo W. Critical length of straight jet in electrospinning. *Polymer*, 2005. 46:12637-12640.
86. Feng J. Stretching of a straight electrically charged viscoelastic jet. *Non-Newtonian Fluid Mech.,* 2003; 116:55-70.
87. Filatov Y., and Kirichenko V. Electrospinning of Micro- and Nanofibre: Fundamentals and Applications in Separation and Filtration Processes. *Begell House Inc.,* 2007; 1:1-488.
88. Jeans J. The mathematical theory of electricity and magnetism. *Cambridge University Press,* 1908; 1:1-602.
89. Yarin A., Kommbhongse S., and Reneker H. Bending instability in electrospinning of nanofibres. *Journal of Applied Physics,* 2001; 89:3018-3026.

90. Greiner H. and Wendorff J. Self-Assembled nanomaterials 1; nanofibres. *Advances in polymer science,* 2008; 219:1-175.
91. He Ji-H., Liu Y., Mo Lu-F., Wan Yu-Q., and Xu L. Electrospun nanofibres and their applications. *Rapra,* 2008; 1:1-260.
92. Rutledge G., Hatton T., Singh H., and Wang M. Field-responsive superparamagnetic composite nanofibres by electrospinning. *Polymer,* 2004; 45:5505-5514.
93. Wu Y. Controlling stability of the electrospun fibre by magnetic field. *Chaos, Solitons and Fractals,* 2006; 32:5-7.
94. Clarke D., and Andrew J. Enhanced Ferroelectric Phase Content of Polyvinylidene Difluoride Fibres with the Addition of Magnetic Nanoparticles. *Langmuir,* 2008; 24: 8435-8438.
95. Li P., Liu C., Song Y., Niu X., Liu H., and Fan Y. Aligned Electrospun Nanofibres Induced by Magnetic Field. *Applied Polymer Science,* 2008; 110:3368-3372.
96. Ajao J., Abiona A., Chingome S., and Maaza M. Electric-magnetic field-induced aligned electrospun poly (ethylene oxide) (PEO) nanofibres. *Mater Sci,* 2010; 45:2324-2329.
97. Guggenheim E. Thermodynamics; An advanced treatment for chemists and physicists. *Elsevier,* 1985; 1:1-414.
98. Dayal P. Dynamics and morphology development in electrospinning of polymer solutions. *University of Akron,* 2007; 1:1-200.
99. Eda G., Liu J., and Shivkumar S. Solvent effects on jet evolution during electrospinning of semi-dilute polystyrene solutions. *Polymer,* 2007; 43:1154-1167.
100. Greiner Andreas, Wendorff J., Bognitzki M., Czado W., Frese,T., Schaper A., Hellwig, M., and Steinhart M. Nanostructured Fibres via Electrospinning. *Adv. Mater.,* 2001; 13:70-73.
101. Matkar R. Phase diagrams and kinetics of solid-liquid - phase transitions in crystalline polymer blends. *University of Akron,* 2007; 1:1-217.
102. Garai J. Physical model for vaporization, *University of Park, Florida,* 2006; 1:1-8.
103. Pratyush Dayal, T. Porous fibre formation in polymer–solvent system undergoing solvent evaporation. *Journal of Applied Physics,* 2006. 100:1-6.
104. Xiang-Fa Wu, and Yuris A. Dzenis. Modeling of solvent evaporation from polymer jets in electrospinning. *Appl. Phys. Lett,* 2011; 98:1-3.
105. Ziabicki A. Fundamentals of fibre formation, *John Wiley and Sons,* 1976, 1:1-504.

106. Eichhorn S., Hearle J., Jaffe M., and Kikutani T. Fundamentals and manufactured polymer fibres. *Handbook of textile fibre structure. CRC,* 2009; 1:1-528.
107. Wan Y., Guo Q., and Pan N. Thermo-electro-hydrodynamic model for electrospinning process. *International journal of nonlinear sciences and numerical simulation,* 2004; 5:5-8.
108. Sternling C. and Scriven L. Interfacial turbulence: Hydrodynamic instability and the marangoni effect. *Al.Che. Journal,* 2004; 5:514-523.
109. Shenoy S., Bates W., Frish H., and Wnek G. Role of chain entanglements on fibre formation during electrospinning of polymer solutions: good solvent, non-specific polymer-polymer interaction limit. *Polymer,* 2005; 46:3372-3384.
110. Woerdeman D., Breger Di and Shenoy, S. Role of Chain Entanglements in the Electrospinning of Wheat Protein-Poly(Vinyl Alcohol) Blends. *The Journal of Adhesion,* 2007; 83:785-798.
111. Nie H., He A., Zheng J., Xu S., Li J., and Han, C. Effects of Chain Conformation and Entanglement on the Electrospinning of Pure Alginate. *Biomacromolecule*s, 2008; 9:1362-1365.
112. Teraoka I. Polymer solutions: An introduccion to physical properties. *John Wiley and Sons, Inc.,* 2002; 1:1-349.
113. Monica S., Oliveira R., and McKinley G. Iterated stretching, extensional rheology and formation of beads-on-a-string structures in polymer solutions. *J. Non-Newtonian Fluid Mech.,* 2006; 1:137-148.
114. Pérez, A. Thermodynamic properties of sugars in aqueous solutions: correlation and prediction using a modified UNIQUAC model. *Fluid phase equilibria,* 1996; 123:71-95.
115. Fabri Deborah. Water t2 relaxation in sugar solutions. *Carbohydrate research,* 2005; 340:889-905.
116. Jansson H.Dynamics of sugar solutions as studied by dielectric spectroscopy. *Journal of non–crystalline solids,* 2005; 351:2858-2863.
117. Boddohi S. Engineering Nano assemblies of polysaccharide. *Advanced materials,* 2010; 22:2998–3016.
118. Martino A., Sitinger M., and Risbud M. Chitosan: A versatile biopolymer for orthopaedic tissue-engineering. *Biomaterials,* 2005; 26:5983-5990.
119. Ohkawa K., Cha D., Kim H., Nishida A., and Yamamoto H. Electrospinning of chitosan. *Macromolecular Rapid Communications,* 2004; 25:1600-1605.

120. Duan B., Zhu, Y., Yuan X., Zhang Y., Li X., and Yao K. A nanofibrous composite membrane of PLGA-chitosan/PVA prepared by electrospinning. *European Polymer Journal,* 2006; 42:013-2022.

121. Ignatova M., N. Manolova and I. Rashkov. Novel antibacterial fibres of quaternized chitosan and poly (vinyl pyrrolidone) prepared by electrospinning. *European Polymer Journal,* 2007; 43:1112-1122.

122. Lin T., Fang J., Wang H., Cheng T., and Wang X. Using chitosan as a thickener for electrospinning dilute PVA solutions to improve fibre uniformity. *Nanotechnology,* 2006; 17:3718-3723.

123. Bhattarai N., Edmonson D., Veiseh O., Matsen F., and Zhang M. Electrospun chitosan-based nanofibres and their cellular compatibility. *Biomaterial*s, 2005. 26: p. 6176-6184.

124. Frey M. Electrospinning cellulose and cellulose derivates. *Polymer Reviews,* 2008; 48:378-391.

125. Han S., Youk J., Min K., Kang Y., and Park W. Electrospinning of cellulose acetate nanofibres using a mixed solvent of acetic acid-water: Effects of solvent composition on the fibre diameter. *Materials Letters,* 2008; 62:759-762.

126. Chen L., Bromberg L., Hatton T., and Rutledge G. Electrospun cellulose acetate fibres containing chlorhexidine as a bactericide. *Polymer,* 2008; 49:1266-1275.

127. Liu H. and Hsieh Y. Ultrafine fibrous cellulose membranes from electrospinning of cellulose acetate. *Journal of Polymer Scienc*e, 2002; 40:2119-2129.

128. Stijnman A., Bodnar I. and Tromp R. Electrospinning of food-grade polysaccharide. *Food Hydrocolloid,* 2011; 25:1393-1398.

129. Dong B., Arnoult O., Smith M., and Wnek G. Electrospinning of collagen nanofibre scaffolds from benign solvents. *Macromolecular Rapid Communication*s, 2009; 30:539-542.

130. Chen Z., Mo X., He C., and Wang H. Intermolecular interactions in electrospun collagen-chitosan complex nanofibres. *Carbohydrate Polymers,* 2008; 72:410-418.

131. Hofman K., Tucker N., Stanger J., Staiger M., Marshall S., and Hall B. Effects of the molecular format of collagen on characteristics of electrospun fibres. *Journal of Materials Science*, 2012; 47:1148-1155.

132. Yao C., X.S. Li and T.Y. Song, Electrospinning and crossfinking of Zein nanofibre mats. *Journal of Applied Polymer Science,* 2007; 103:380-385.

133. Selling G., Woods K., Sessa D., and Biswas A. Electrospun zein fibres using glutaraldehyde as the crosslinking reagent: Effect of time and temperature. *Macromolecular Chemistry and Physics*, 2008; 209:1003-1011.

134. Selling G.W., Biswas A., Patel A., Walls D., Dunlap C., and Wei Y. Impact of solvent on electrospinning of zein and analysis of resulting fibres. *Macromolecular Chemistry and Physics*, 2007; 208:1002-1010.

135. Miyoshi T., K. Toyohara and H. Minematsu Preparation of ultrafine fibrous zein membranes via electrospinning. *Polymer International*, 2005; 54:1187-1190.

136. Jiang H., Zhao P., and Zhu K. Fabrication and characterisation of zein-based nanofibrous scaffolds by an electrospinning method. *Macromolecular Bioscience*, 2007; 7:517-525.

137 Woerdeman D., Ye P., Shenoy S., Parnas R., Wnek G., and Trofimova O. Electrospun fibres from wheat protein: Investigation of the interplay between molecular structure and the fluid dynamics of the electrospinning process. *Biomacromolecules*, 2005; 6:707-712.

138. Kowalczyk T., Nowicka A., Elbaum D., and Kowaleski T. Electrospinning of bovine serum albumin. Optimization and the use for production of biosensors. *Biomacromolecules*, 2008; 9:2087-2090.

139. Wnek G., Carr M., Simpson D., and Bowling G. Electrospinning of Nanofibre Fibrinogen Structures. *Nano Letters*, 2003; 3:213-216.

140. Dror Y.,Ziv T., Makarov V., Wolf H., Admon A., and Zussman E. Nanofibres made of globular proteins. *Biomacromolecules*, 2008; 9:2749-2754.

141. Huang Z., Zhang Y., Ramakrishna S., and Tim C. Electrospinning and mechanical characterisation of gelatin nanofibres. *Polymer*, 2004; 45:5361-5368.

142. Zhang Y., Ouyang H., Lim C., Ramakrishna S., and Huang Z. Electrospinning of gelatin fibres and gelatin/PCL composite fibrous scaffolds. *Journal of Biomedical Materials Research*, 2004: 1:156-165.

143. Mo X., Xu C., Kotaki M. and Ramakrishna, S. Electrospun PLA-PCL nanofibre: A biomimetic extracellular matrix for smooth muscle cell and endothelial cell proliferation. *Biomaterials*, 2004; 25:1883-1890.

144. Toskasa G., Hund F., Laourinne E., Cherif C., Smyrniotopolous V., and Roussis V. Nanofibres based on polysaccharide from the green seaweed Ulva Rigida. *Carbohydrate Polymers*, 2011; 84:1093-1102.

145. Boland E. Electrospinning of Biopolymers (Natural and Synthetic) for Tissue Engineering Scaffolds. *Polymer Preprints*, 2003; 44:92-93.
146. Li M., Mondrinos M., Gandhi M., Ko F., Weiss A., and Lelkes P. Electrospun protein fibres as materials for tissue engineering. *Biomaterials*, 2005; 26:5999-6008.
147. Schiffman J., and Schauer C. A review: Electrospinning of biopolymer nanofibres and their applications. *Polymer Reviews*, 2008; 48:317-352.
148. Duling R., Dupaix R., Katsube N., and Lannutti J. Mechanical characterisation of electrospun polycaprolactone (PCL): A potential scaffold for tissue engineering. *Journal of Biomechanical Engineering,* 2008; 130:1-9.
149. Kidoaki S., Kwon I., and Matsuda T. Mesoscopic spatial designs of nano- and microfibre meshes for tissue-engineering matrix and scaffold based on newly devised multilayering and mixing electrospinning techniques. *Biomaterials*, 2005; 26:37-46.
150. Lee K., Jeong L., Kang Y., Lee S., and Park W. Electrospinning of polysaccharide for regenerative medicine. *Advanced Drug Delivery Reviews,* 2010; 61:1020-1032.
151. Manandhar S., Vidhate S and D'Souza N. Water soluble levan polysaccharide biopolymer electrospun fibres. *Carbohydrate Polymers*, 2009; 78:794-798.
152. D. Hermida-Merinoa, Belalb M., Greenlanda B., Woodwarda P., Slarkc A., Davisa F., Mitchellb G., Hamleya I., and Hayesa W. Electrospun supramolecular polymer fibres. *European Polymer Journal,* 2012; 48:1249-1255.
153. Garg H., Cowman M. and Hales C. Carbohydrate chemistry, biology and medical applications. *Oxford - Elsevier,* 2008; 1:1-414.
154. Shenoy S., Bates W., and Wnek G. Correlations between electrospinnability and physical gelation. *Polymer*, 2005; 46:8990-9004.
155. Hu H., Carson G., and Granick S. Relaxation Time of Confined Liquids under Shear. *Physical Review Letters*, 1991; 66:1-4.
156. Reneker D., Yarin A., Fong H., and Koombhongse S. Bending instability of electrically charged liquid jets of polymer solutions in electrospinning. *Journal of Applied Physics,* 2000; 87:4531-4547.
157. Lukáša D., Sarkara A., Martinováa L., Vodsed'álkováa K., Lubasováa D., Chaloupeka J., Pokorný, P., Mikeša P., Chvojkaa J. and Komáreka M. Physical principles of electrospinning: Electrospinning as a nano-scale technology of the twenty-first century. *Textile Progress,* 2009; 41:59-140.
158. Ramakrishna S., Fuhijara K., Teo W., and Lim T. An introduction to electrospinning and nanofibres. *World Scientific Publishing*, 2005; 1:1-382.

159. Reneker D., and Fong H. Polymeric nanofibres. *American Chemical Society,* 2006; 918:1-430

160. Andrade A. Science and technology of polymer nanofibres. *John Wiley and Sons,* 2008; 1:1-420.

161. Arikawa T., Nagai M., and Tanaka K. Characterizing hydration state in solution using terahertz time-domain attenuated total reflection spectroscopy. *Chemical Physics Letters*, 2008; 457:12-17.

162. Desiraju G., and Steiner T. The weak hydrogen bond in structural chemistry and biology. *Monographs on Crystallography*, 2001; 9:1-526.

163. Manasco J. L., Tang C., and Khan S. A. Cyclodextrin fibres via polymer–free electrospinning. *RSC Advances*, 2012; 2:3778-3784.

164. Uyar T., and Celebioglu A. Electrospinning of Polymer–free Nanofibres from Cyclodextrin Inclusion Complexes. *Langmuir*, 2011; 27:6218-6226.

165. Uyar T., and Kayaci F. Solid Inclusion Complexes of Vanillin with Cyclodextrin: Their Formation, Characterisation, and High–Temperature Stability. *Journal of agricultural and food chemistry*, 2011; 59:11772-11778.

166. Uyar T., and Celebioglu A. Cyclodextrin nanofibre by electrospinning. *Chem. Commun.*, 2010; 46:6903-6905.

167. Rossi B., Gomez, L., Fioretto D., Caponi S., and Rossi F. Hydrogen bonding dynamics of cyclodextrin–water solutions by depolarized light scattering. *J. Raman Spectroscopy,* 2011; 42:1479-1483.

168. Madhurima J., and Sanjoy B. Vibrational spectrum of water confined in and around cyclodextrin. *Chemical Physics Letters,* 2011; 509:181-185.

169. Charalampopoulos V., and Papaioannou J. Dipole relaxation and proton transport in polycrystalline γ–cyclodextrin hydrate: A dielectric spectroscopy study. *Solid State Ionics*, 2011; 191:1–11.

170. Challa R., Ahuja A., Ali, J., and Khar R. Cyclodextrin in drug delivery: An updated review. *AAPS Pharm Sci Tech*., 2005; 6:329-357.

171. Lepe P., Tucker N., Simmons L., Watson A., Fairbanks A., and Staiger M. Submicron sized saccharide fibres via electrospinning. *De Gruyter Open – Electrospinning*, 2016; 1:p.1-9.

172. Poland D., and Scheraga H. Energy Parameters in Polypeptides I: Charge distributions and the hydrogen bond. *Biochemistry*, 1967; 6:3791-3800.

173. Yan J., Momany F., Hoffmann H., and Scheraga H. Energy Parameters in Polypeptides II: Semi empirical Molecular Orbital Calculations for model peptides. *Physical chemistry*, 1970; 74:420-433.
174. Yan J., Momany F., Hoffmann H., and Scheraga H. Energy Parameters in Polypeptides III: Semi empirical Molecular Orbital Calculations for Hydrogen–Bonded Model Peptides. *Physical Chemistry*, 1970; 74:2424-2438.
175. Akira H. Supramolecular Polymer Chemistry. *Wiley – VCH*, 2011; 1:1-361.
176. Onsager L. Electrostatic interaction of molecules. *Journal of Physical Chemistry*, 1939; 43:189-196.
177. Wan Y., He J., and Yu J. Allometric scaling and instability in electrospinning. *International journal of nonlinear sciences and numerical simulations*, 2004; 5:243-252.
178. Van Honschoten J., Tas N., and Brunets N. Capillarity at the nanoscale. *Chemical society reviews*, 2009; 39:1096-1114.
179. Wautelet M., Scaling laws in the macro, micro and nanoworlds. *Institute of Physics Publishing*, 2001; 22:601-611.
180. Israelachvili J. Intermolecular and Surface Forces. *Elsevier – Academic Press*, 2011; 3:1-674.
181. Hiemenz P. Polymer chemistry: the basic concepts. *CRC Press*, 1984; 1:1-738.
182. Fujita H. Polymer solutions. Studies on polymer science. *Elsevier – Netherlands*, 1990; 9:1-370.
183. Terakota I. Polymer solutions: An introduction to physical properties. *John Wiley & Sons*, 2002; 1:1-349.
184. Freire J. Relaxation of flexible chains in dilute and non–dilute systems. Dynamic Monte Carlo results for linear and star chains. *Macromolecules, theory simulations*, 1999; 8:321-327.
185. Rubistein M., and Semenov A. Dynamics of Entangled solutions for associating polymers. *Macromolecules*, 2001; 34:1058-1068.
186. Genotelle J., and Mathlouthi M. Role of water in sucrose crystallization. *Carbohydrate polymers*, 1998; 37:335-342.
187. Quintas M., Brandao T., Silva C., and Cunha R. Rheology of supersaturated sucrose solutions. *Journal of Food Engineering*, 2006; 77:844-852.
188. Crest J., and McKinley G. Formation of microfibres and nanofibres by capillary-driven thinning of drying viscoelastic filaments. *MIT report*, 2009; 1:1-43.

189. Arunan E. Categorizing hydrogen bonding and other intermolecular interactions. Pure Applied Chemistry–IUPAC recommendation, 2011; 1:1-5.
190. Everaers D. Computer simulations and scaling concepts in polymer physics. Max Planck-Institut fur Polymerforschung, 2002; 1:1-142.
191. Luzar A. Resolving the hydrogen bond dynamics conundrum. *Journal of chemical physics*, 2000; 113:10663-10675.
192. Boltachev G., and Baidakov V. Extended version o the Van der Waals capillarity theory. *Journal of Chemical Physics*, 2004; 121:8594-8601.
193. Yu J., and Rutledge G. The role of elasticity in the formation of electrospun fibres. *Polymer*, 2006. 47:4789-4797.
194. Jensen S., Tang T.-H., and Csizmadia G. Hydrogen-Bonding Ability of a Methyl Group. *J. Phys. Chem. A.*, 2003; 107:8975-8979.
195. Li Q., Wu G., and Yu Z. The role of methyl groups in the formation of hydrogen bond in DMSO-methanol mixtures. J *Am Chem Soc.*, 2006; 128:1438-1439.
196. Legon A., Wallwork A., and Warner H. Do methyl groups form hydrogen bonds? An answer from the rotational spectrum of ethane—hydrogen cyanide. *Chemical Physics Letters*, 1992; 191:98-101.
197. Komasaa J., Szalewiczc K., and Leszczyński J. Does the methyl group form a hydrogen bond? Ab initio post-Hartree–Fock study on ethane–hydrogen cyanide complex. *Chemical Physics Letters*, 1998; 285:449-454.
198. Del-Valle E. Cyclodextrin and their uses: a review. *Process Biochemistry*, 2004; 39:1033-1046.
199. Okimoto K., Uekama K., and Stella J. The interaction of charged and uncharged drugs with nuetral (HP-Beta-CD) and anionically charged (SBE6-Beta-CD) Beta-Cyclodextrin. *Pharmaceutical Research*, 1996; 13:256-264.
200. Celebioglu A., and Uyar T. Electrospinning of nanofibres from non-polymeric systems: polymer-free nanofibres from cyclodextrin derivatives. *Nanoscale*, 2012; 4:621-631.
201. Manasco J., Tang C., and Khan S. Cyclodextrin fibres via polymer-free electrospinning. *RSC Advances*, 2012; 2:3778-3784.
202. Martin C. Stumpe and Helmut G. Aqueous Urea Solutions: Structure, Energetics, and Urea Aggregation. *Journal of Physical Chemistry*, 2007; 111:6220-6228.
203. Coleman A., and Nicolis I. Aggregation of Cyclodextrins: An explanation of the abnormal solubility of β-Cyclodextrin. *Journal of Inclusion Phenomena and Molecular Recognition in Chemistry*, 1992; 13:139-143.

204. Celebioglu A., and Uyar T. Electrospinning of nanofibres from non-polymeric systems: Electrospun nanofibres from native cyclodextrin. *Journal of Colloid and Interface Science,* 2013; 404:1-7.

205. Carr J., Buchanan L., Schmidt J., Zanni M., and Skinner J. Structure and Dynamics of Urea/Water Mixtures Investigated by Vibrational Spectroscopy and Molecular Dynamics Simulation. *Journal of Physical Chemistry B.*, 2013; 1147:13291-13300.

206. Nose A. and Hojo M. Hydrogen bonding of water-ethanol in alconolic beverages. *Journal of Bioscience and Bio-engineering*, 2006; 112:269-280.

207. Idrissi A., and Jedlovszky P. Hydration free energy difference of acetone, acetamide, and urea. *J. Chem. Phys.*, 2008; 129:291-300.

208. Wang X., Pellerin C., and Bazuin C. Enhancing the electrospinnability of low molecular weight polymers using small effective cross-linkers. *Macromolecules,* 2016; 49:891-899.

209. Wang X., Pellerin C., and Bazuin C. Effect of small molecule hydrogen-bond crosslinker and solvent power on the electrospinnability of poly(4-vinyl pyridine). *Polymer,* 2015; 57:62-69.

210. Son W., Youk J., Lee T., and Park W. Effect of pH on the electrospinning of poly (vinyl alcohol). *Materials Letters,* 2005; 59:1571-1575.

211. McKee M., Elkins C., and Long T. Influence of self-complementary hydrogen bonding on solution rheology/electrospinning relationships. *Polymer*, 2004; 45:8705-8715.

212. Fridrikh S., Brenner M., and Rutledge G. Controlling the fibre diameter during electrospinning. *Physical review letters,* 2003; 90:144502-144506.

213. Subbiah T., Tock R., Parameswaran S., and Ramkumar S. Electrospinning of nanofibres. *Applied polymer science,* 2004; 96:557-569.

214. Reneker D., Yarin A., Fong H., and Koombhongse S. Bending instability of electrically charged liquid jets of polymer solutions in electrospinning. *Journal of Applied Physics,* 2000; 87: 4531-4547.

215. Qin X., Effect of Different Salts on Electrospinning of Polyacrylonitrile (PAN) Polymer Solution. *Journal of Applied Polymer Science,* 2007; 103:3865-3870.

216. Sabadini E., Cosgrovea T. and Egídio F. do C. Solubility of cyclomaltooligosaccharides (cyclodextrins) in H2O and D2O: a comparative study, *Carbohydrate Research,* 2006; 341:270-274.

217. Shikata T., Takahashi R., and Satokawa Y. Hydration and Dynamic Behaviour of Cyclodextrins in Aqueous Solution. *Journal of Physical Chemistry B*, 2007; 111:2239-12247.

218. Jana M., and Bandyopadhyay S. Microscopic Investigation of the Hydration Properties of Cyclodextrin and its Substituted Forms. *Langmuir*, 2009; 25:13084-13091.

219. Sinnott M. L. Carbohydrate chemistry and biochemistry. *Royal Society of Chemistry*, 2007; 1:1-748.

220. De Gennes P. Scaling concepts in polymer physics. *Cornell University Press*, 1979, Ithica; 1:1-321.

221. Deshpande A., and Krishnan, J. Rheology of complex fluids. Springer, 2010, New York.

222. Crespy D., Friedemann K., and Popa A-M. Colloid-Electrospinning: Fabrication of Multicompartment Nanofibers by the electrospinning of Organic or/and Inorganic Disperns and Emulsions. *Macromolecular Rapid Communications*, 2012; 1:978-1995.

223. Angeles M., Cheng H-L., Velankar S. Emulsion electrospining: Composite fibers from drop breakup during electrospinning. *Polym. Adv. Technol,*. 2008; 1:728-733.

224. Xu X., Zhuang X., Chen X., Wang X., Yang L., and Jin X. Preparation of Core-Sheath Composite Nanofibers by Emulsion Electrospinning. *Macromol. Rapid Commun.,* 2006; 27:1637-1642.

225. Agarwal S., and Greiner A. On the way to clean and safe electrospinning-green electrospinning: emusion and suspension electrospinning. *Polym. Adv. Technol.* 2012; 22:372-378.

226. Yarin A. Coaxil electrospining and emulsion electrospinning of core-shell fibers. *Polym. Adv. Technol.,* 2011; 22:310-317.

227. Yan S., Xiaoqiang L., Shuiping L., Xiumei Mo., and Ramakrishna S. Controlled release of dual drugs form emulsion electrospin nanofibrous mats. C*ollids and Surfaces B: Biointerfaces*, 2009; 73:376-381.

228. Xu X., Yang L., Xu X., Wang X.,Chen X., Laing, Q., Zeng J., and Jing, X. Ultrafine medicated fibers electrospun from X/O emulsions. *Journal of Controlled Release*, 2005; 108:33-42.

229. Liao Y., Zhan L., Gao Y., Zhu Z-T., and Fond H. Preparation, characterization, and encapsulation/release stufies of a compoiste nanofiber mat electrospun from an emulcion containing poly(lactic-co-glycolic acid). *Polymer*, 2008; 48:5294-5299.

230. Ray-S. S., Pelot D., Zhou P., Rahman A., Wu X., and Yarin A. Encapsulation f self-healing materilas by coelectrospining, emulsion, electrospinning, solution blowing and intercalation. *J. Mater. Chem.*, 2012; 22:9138-9146.

231. Friedemann K., Tomas C., Kappl M., Landfester K., and Crespy D. Facil and Large-Scale Fabrication of Anisometric Particles from Fibers Synthesized by Colloid-Electrospinning. *Small*, 2012; 1:144-153.

232. Stoiljkovic A., Venkatesh R., Klimov E., Raman V., Wendorff J., and Greiner A. Poly(styrene-co-n-butyl acrylate) Nanofibers with Excellent Stability against Water by Electrospinning from Aqueous Colloidal Dispersions. *Macromolecules*, 2009; 42:6147-6151.

233. Bosman A., Sijbesma R., and Meijer E. Supramolecular polymers at work. *Materials today*, 2004; 1:34-39

234. Greef T., and Meijer E. Supramolecular Polymers. *Aust. J. Chem*. 2010; 63:596-598.

235. Gittins, P., and Twyman, L. Dendrimers and Supramolcular Chemsitry. *Supramolecular Chemistry*, 2003; 15:5-23.

236. Regev O., Vandebril S., Zussman E., and Clasen C. The role of interfacial viscoelasticity in the stabilization of an electrospun jet. *Polymer*, 2000; 51:2611-2620.

237. Pelipenko J., Kristl J., Baumgartner S., and Kocbek P. Interfacial rheology: An overview of measuring techniques and its role in dispersions and electrospiing. *Acta Pharm*., 2012; 62:123-140.

238. Qin W-H., and Wang S-Y. Filtration properties of electrospinning nanofibers. *Journal of Applied Polyer Science*, 2006; 102:1285-1290.

239. Ellision C., Melt blown nanofibers: Fiber diameter distributions and onset of fiber breakup. *Polymer*, 2007; 48:3306-3316.

240. Wang S-X., Yap C., He J., Chen C., and Wong S. Electrospinning: a facile technique for fabricating functional nanofibers for environmental applications. *Nanotechnol Rev*., 2016; 5:51-73.

241. Hung C-H., and Leung W. Filtration of nano-aerosol using nanofiber filter under low peclet number and transitional flow regimne. *Separation and Purification Technology*, 2011; 79:34-42.

242. Sudanrrajan S., Tan K., Lim S., and Ramakrishna S. Electrospun nanofibers for air filtration applications. *Procedia Engineering*, 2014; 75:159-163.

243. China air 2015: Air pollution prevention and control progress in Chinese cities. *Clean Air Asia - Beijing*, 2016; 1:1-80.

244. KPMG. China's connected consumers. *KPMG*, Hong Kong, 2015;1:1-74.
245. Cao J., Xu H., Xu Q., Chen B., and Kan H. Fine particulate matter constituents and cardiopulmonary mortality in a heavily polluted Chinese city. *Environmental Health Perspectives*, 2012; 120:373-378.
246. Quan M., and Junjie Z. Air pollution and defensice expendiures: evidence from particulate-filtering facemasks. *UCSD*, 2014;1:1-47.
247. He Q., Guo W., Zhang G., Yan Y., and Chen L. Characteristics and seasonal variations of carbonaceous species in PM2.5 in Taiyaun, China. *Atmosphere*, 2015; 6:1-13.
248. Fang T., and Lin C. Minimum wages and employment in China. J*ournal of Labor Policy*, 2015; 4:1-30.
249. Loungani Y-H., and Wang G. Minimum wages and firm employment: evidence from China. *International Monetary Fund (IMF)*, 2014;1:1- 47.
250. Davis B., and Fairbanks A. Carbohydrate chemistry. *Oxford Chemistry Primers*, 2002;1:1-100.
251. McMurry J. Fundamentals of Organic chemistry. *Brooks/Cole*, 2002; 5:1-600.
252. Hofman K., and Newberry M. Thermal transition properties of Hoki (Macruronus novaezelandiae) and Ling (Genypterus blacodes) skin collagens: Implications for processing. *Marine drugs*, 2011; 9:1176-1186.
253. Hofman K., Hall B., Cleaver H., and Marshall S. High-throughput quantification of hydroxyproline for determination of collagen. *Analytical Biochemistry*, 2011; 417:289-291.
254. Hofman K., Ion exchange HPLC of a marine collagen. *Journal of Liquid Chromatography and related technologies*, 2009; 17:2512-2529.
255. LeCorre-Bordes D., Jaksons P., Hofman K. Mind the gap: Ensuring laboratory-scale testing of an electropinning product meets commercial-scale needs. J*ournal of Applied Polymer Science*, 2017; 134:44836-44839.
256. Kloosterman M., Weijnen J., De Vries N., Mentech J., Caron I., Descotes G. Schoemaker H., and Meijer E. Octa-*O*-acetyl sucrose: Regioselective deacetylations by lipolytic enzymes. *Journal of Carbohydrate Chemistry*, 1989; 8:1-8.
257. Fernandez-L. G., Palomo J., Cocca J., Mateo, C., Moro P., Terreni M., Fernandez-L. R., and Guisan J. Regio-selective deprotection of peracetylated sugars via lipase hydrolysis. *Tetrahedron*, 2003; 59:5705-5711.

258. Navzer S., Redford F., and Morton L. Use of sucrose-based addtivies as non-crosslinking agents to produce polymers having enhanced thermal stability. *USPTO,* 28 of February 1994; no.5470931.

259. Sarhan W., and Azzazy H. High concentration honey chitosan electrospun nanofibers: Biocompatibility and antibacterial effects. *Carbohydrate Polymers*, 2015; 122:135-143.

260. Minden-B. B., Neuhalfen R., Janowiak B., and Sell S. Preliminary Investigation and characterization of electrospun polycaprolactone and manuka honey scaffolds for dermal repair. *Journal of Engineered Fibers and Fabrics*, 2015; 110:126-138.

261. Bulman S., Goswami P., Tronce G., Russell S., and Carr C. Investigation into the potential use of poly(vinyl alcohol)-methylglyoxal fibers as antibacterial wound dressings. *Journal of Biomaterials Applications,* 2015; 29:1193-1200.

262. Sell S., Wolfe P., Spence A., Rodriguez I., McCool J., Petrella R., Garg K., Ericksen J., and Bowlin G. A. Preliminary study on the potential of manuka honey and platelet-rich plasma in wound healing. *International Journal of Biomaterials,* 2012; 1:1-14.

263. Parkar S., Jobsis C.,Herath T., Stoklosinski H., Klink J., Sansom C., Sims I., and Hedderley D. Metabolic and microbial responses to the complexation of manuka honey with α-cyclodextrin after simulated gastrointestinal digestion and fermentation. *Journal of functional foods*, 2017; 31:266-273.

264. Pavlov G., Korneeva E., Smolina N., and Schubert U. Hydrodynamic properties of cyclodextrin molecules in dilute solutions. *European Biophysics Journal*, 2010; 39:371-379.

265. Alvarez-S. J., Gasparrini M., Forbes-H. T., Mazzoni L., and Giampieri F. The composition and biological activity of honey: a focus on manuka honey. *Foods*, 2014; 3:420-432.

APPENDIX

Visco-elasto-capillary theory analysis

Rouse relaxation times are often inadequate when predicting stress relaxation in processes with large strains in very short times (typical of polymers), since the effective time for the molecules to relax the applied stresses is typically less than 1 ms [188]. However, a simplified version of the tube model e.g., $\lambda = k(G')/k'(G'')$ was used in this study for approaching the longest relaxation times of the solutions, where k is a constant derived from the respective best linear and square fitting of the storage modulus ($G'=k\omega$) and loss modulus ($G''= k\omega^2$) to the angular frequency (ω).

Approximate values were then used to estimate the dimensionless numbers (e.g., Reynolds, Capillary, Weber, Elasticity, Ohnesorge, and Weissenberg) required to find the intrinsic Deborah number as described by the visco-elasto-capillary theory, and as proposed by McKinley et al. [79, 82, 188]. Longer relaxation times of the molecules, or the capacity to remain electrically stressed for longer periods of time, indeed correlated to improved electrospinnability (Figure 4.14).

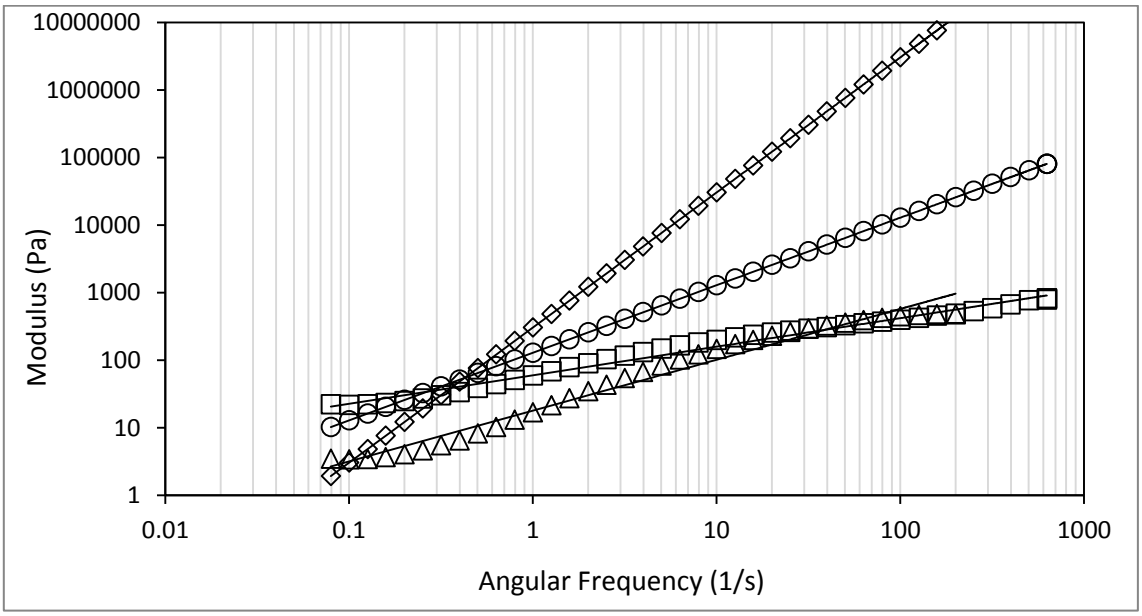

Figure A1.1 - Relaxation modulus to angular frequency relationship for S/+SAT. Real values for the Storage (*G'*) modulus and loss (*G''*) modulus are shown as Δ and □ respectively. Adjusted linear fittings, from the tube model (λ), for *G'* and *G''* are shown as ◊ and ○ respectively.

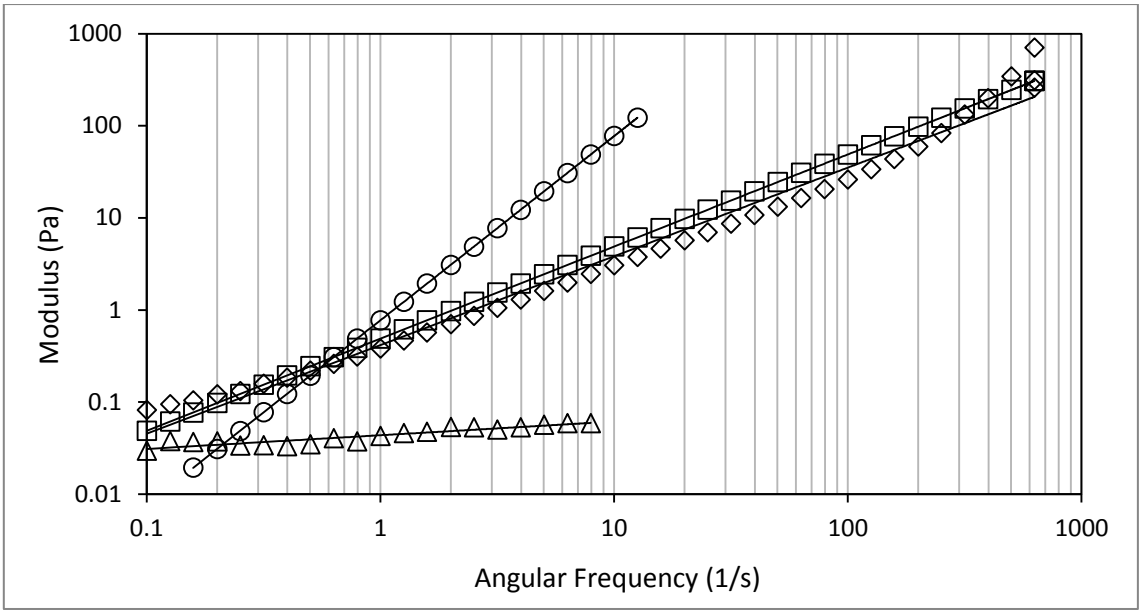

Figure A1.2 - Relaxation modulus to angular frequency relationship for S/SAT. Real values for the Storage (*G'*) modulus and loss (*G"*) modulus are shown as Δ and □ respectively. Adjusted linear fittings, from the tube model (λ), for *G'* and *G"* are shown as ◊ and ○ respectively.

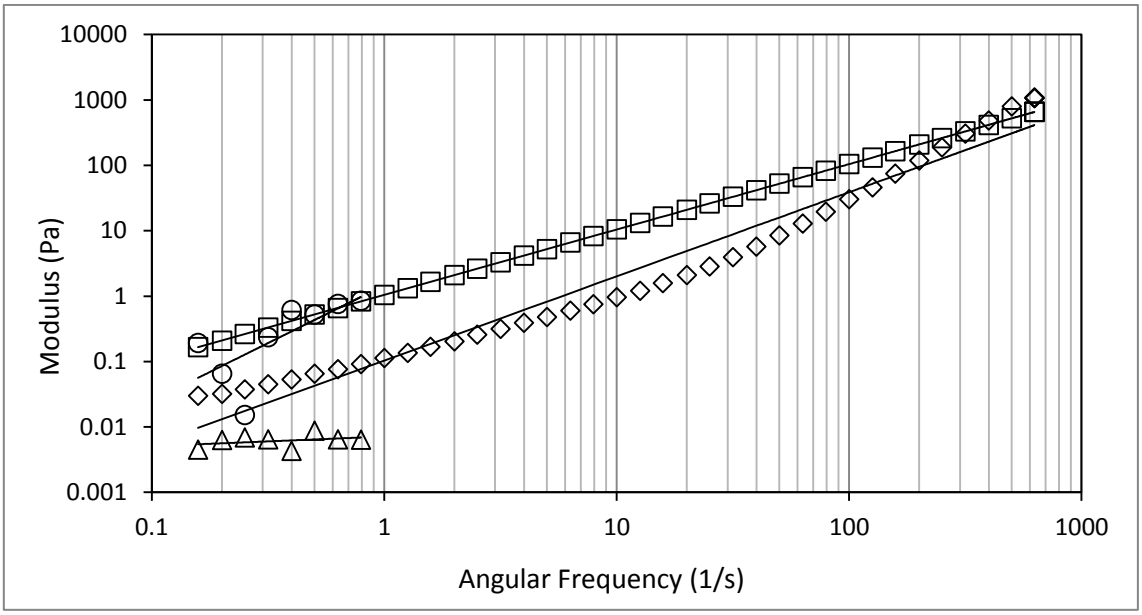

Figure A1.3 - Relaxation modulus to angular frequency relationship for S/-SAT. Real values for the storage (*G'*) modulus and loss (*G"*) modulus are shown as Δ and □ respectively. Adjusted linear fittings, from the tube model (λ), for *G'* and *G"* are shown as ◊ and ○ respectively.

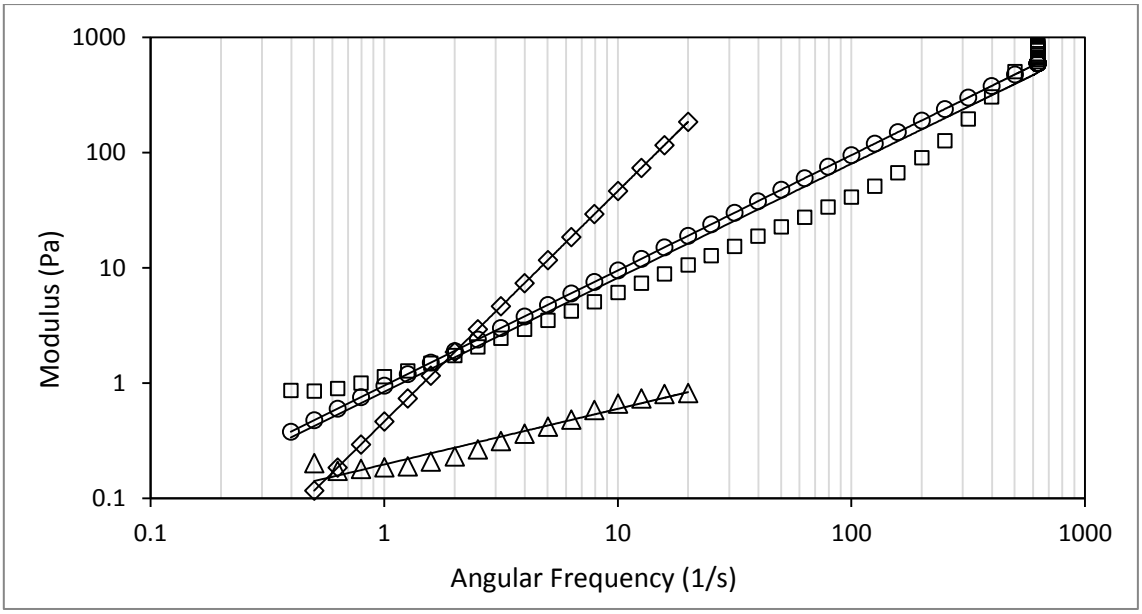

Figure A1.4 - Relaxation modulus to angular frequency relationship for G/+SAT. Real values for the storage (*G'*) modulus and loss (*G"*) modulus are shown as Δ and □ respectively. Adjusted linear fittings, from the tube model (λ), for *G'* and *G"* are shown as ◊ and ○ respectively.

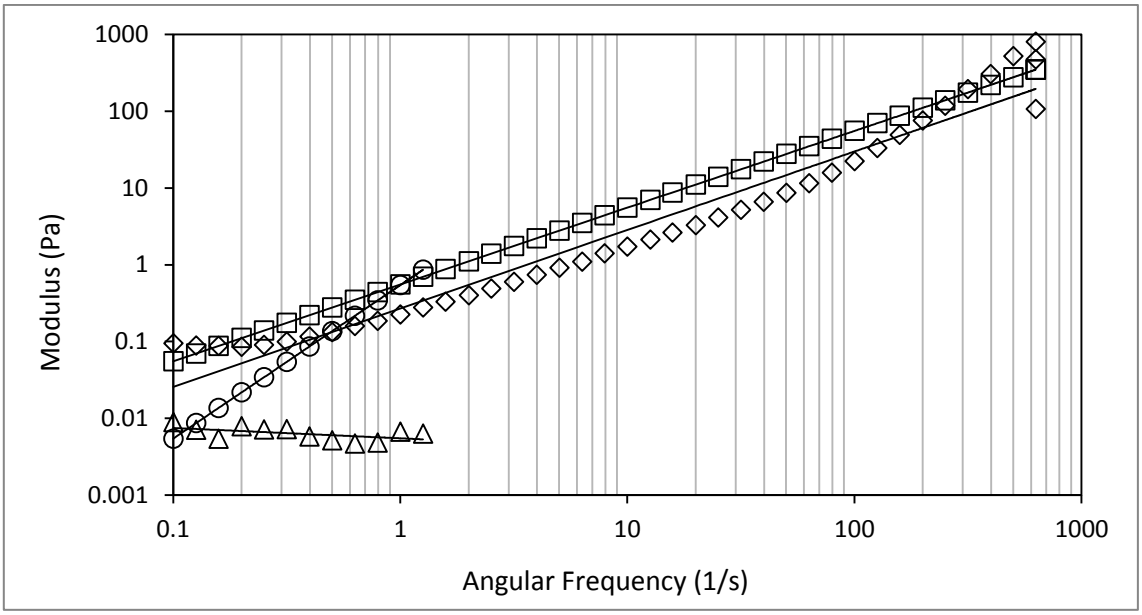

Figure A1.5 - Relaxation modulus to angular frequency relationship for G/SAT. Real values for the storage (*G'*) modulus and loss (*G"*) modulus are shown as Δ and □ respectively. Adjusted linear fittings, from the tube model (λ), for *G'* and *G"* are shown as ◊ and ○ respectively.

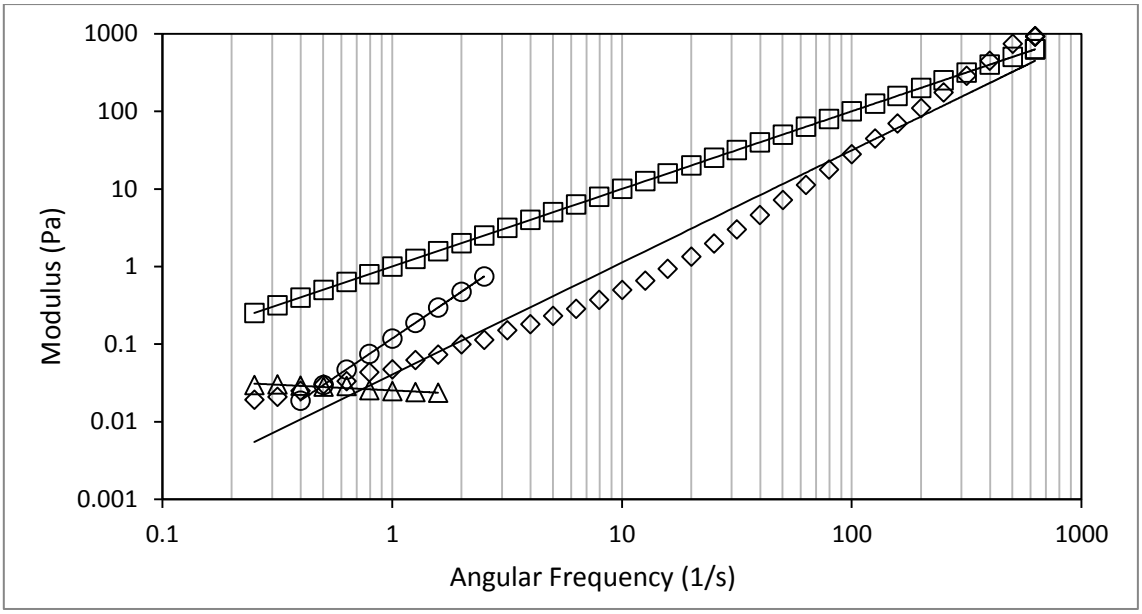

Figure A1.6 - Relaxation modulus to angular frequency relationship for G/-SAT. Real values for the storage (*G'*) modulus and loss (*G"*) modulus are shown as Δ and □ respectively. Adjusted linear fittings, from the tube model (λ), for *G'* and *G"* are shown as ◊ and ○ respectively.

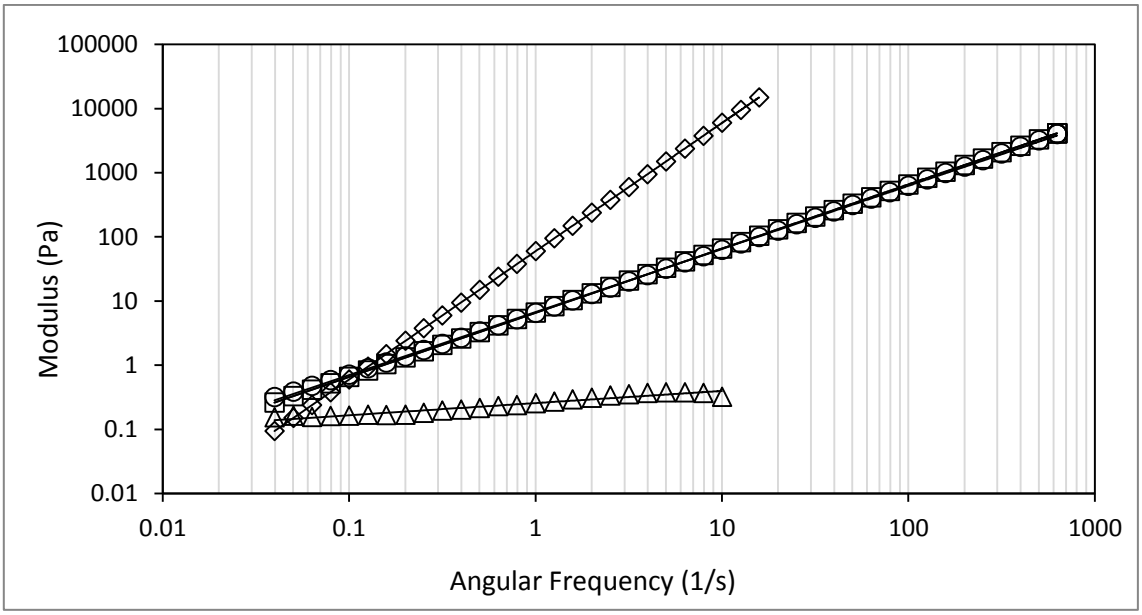

Figure A1.7 - Relaxation modulus to angular frequency relationship for F/+SAT. Real values for the storage (*G'*) modulus and loss (*G"*) modulus are shown as Δ and □ respectively. Adjusted linear fittings, from the tube model (λ), for *G'* and *G"* are shown as ◊ and ○ respectively.

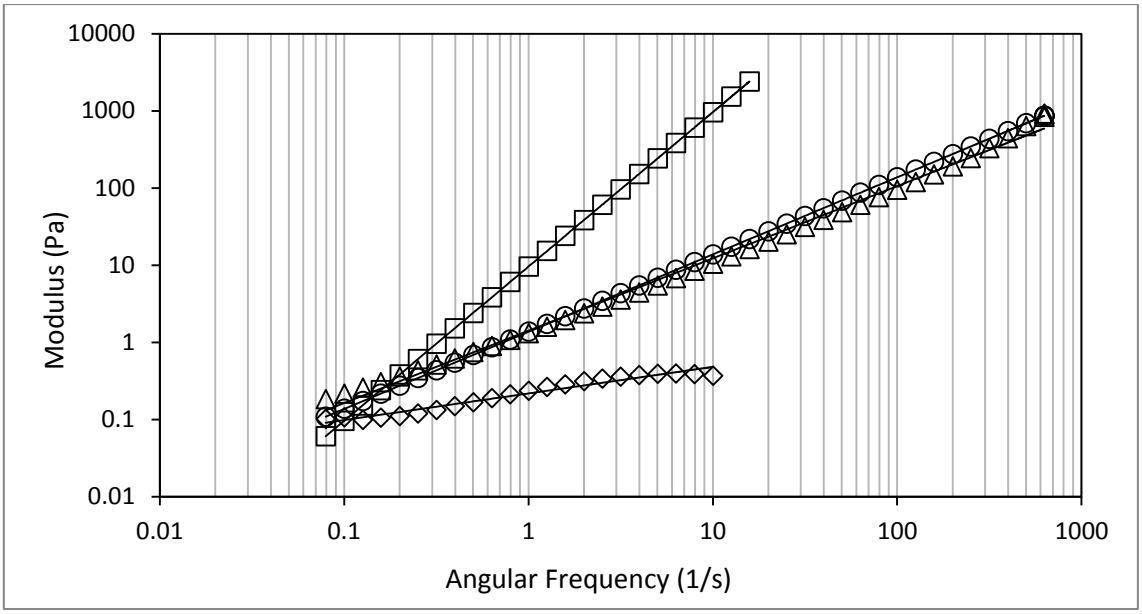

Figure A1.8 - Relaxation modulus to angular frequency relationship for F/SAT. Real values for the storage (*G'*) modulus and loss (*G"*) modulus are shown as Δ and □ respectively. Adjusted linear fittings, from the tube model (λ), for *G'* and *G"* are shown as ◊ and ○ respectively.

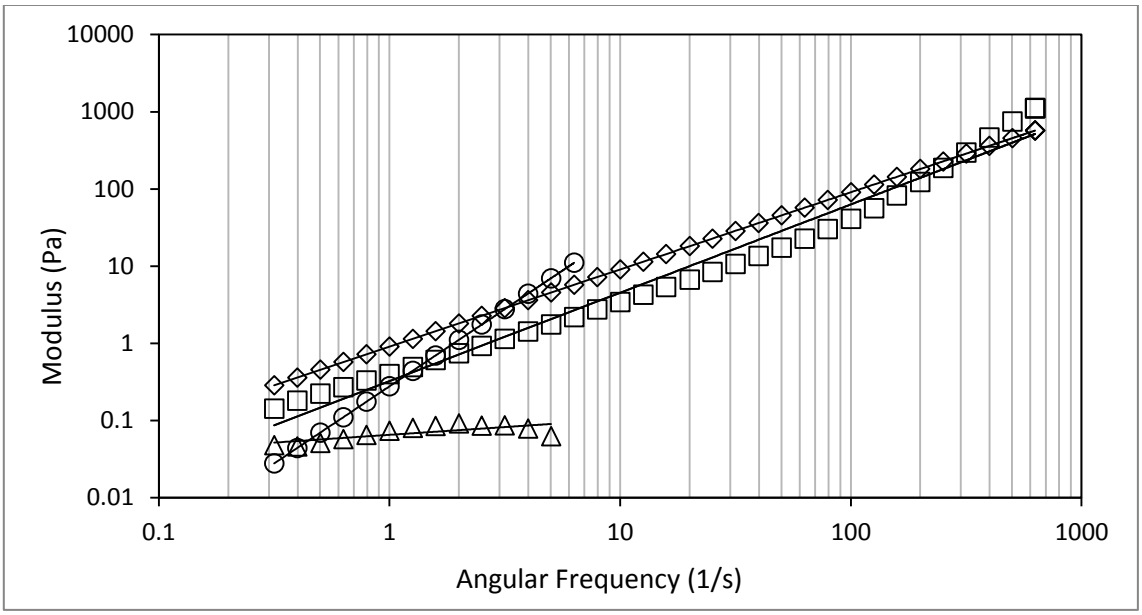

Figure A1.9- Relaxation modulus to angular frequency relationship for F/-SAT. Real values for the storage (*G'*) modulus and loss (*G"*) modulus are shown as Δ and □ respectively. Adjusted linear fittings, from the tube model (λ), for *G'* and *G"* are shown as ◊ and ○ respectively.

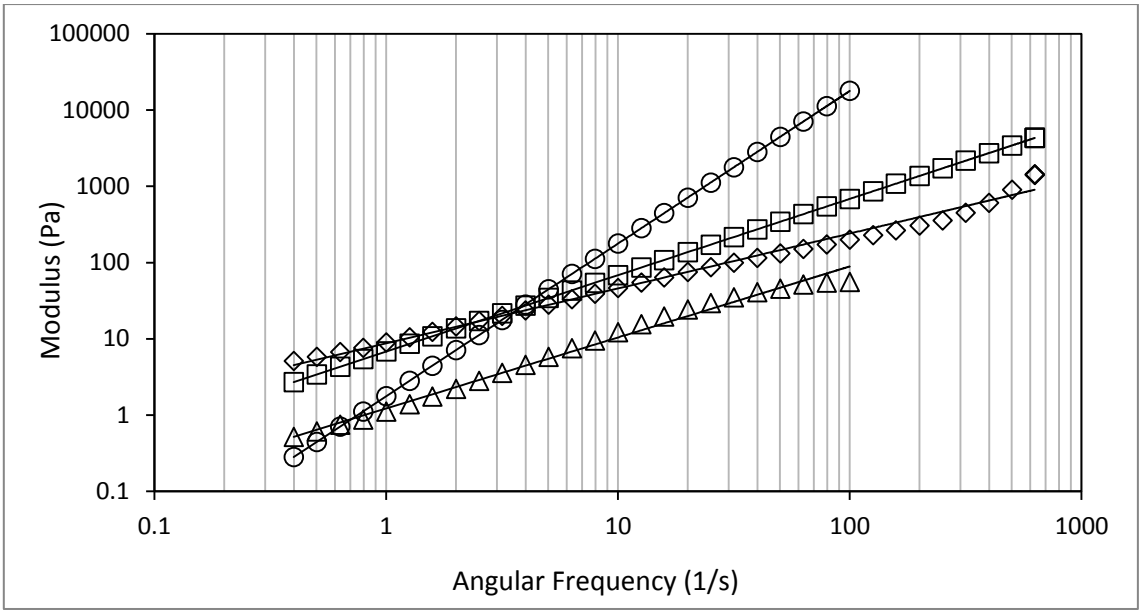

Figure A1.10 - Relaxation modulus to angular frequency relationship for GFS/+SAT. Real values for the storage (*G'*) modulus and loss (*G"*) modulus are shown as Δ and □ respectively. Adjusted linear fittings, from the tube model (λ), for *G'* and *G"* are shown as ◊ and ○ respectively.

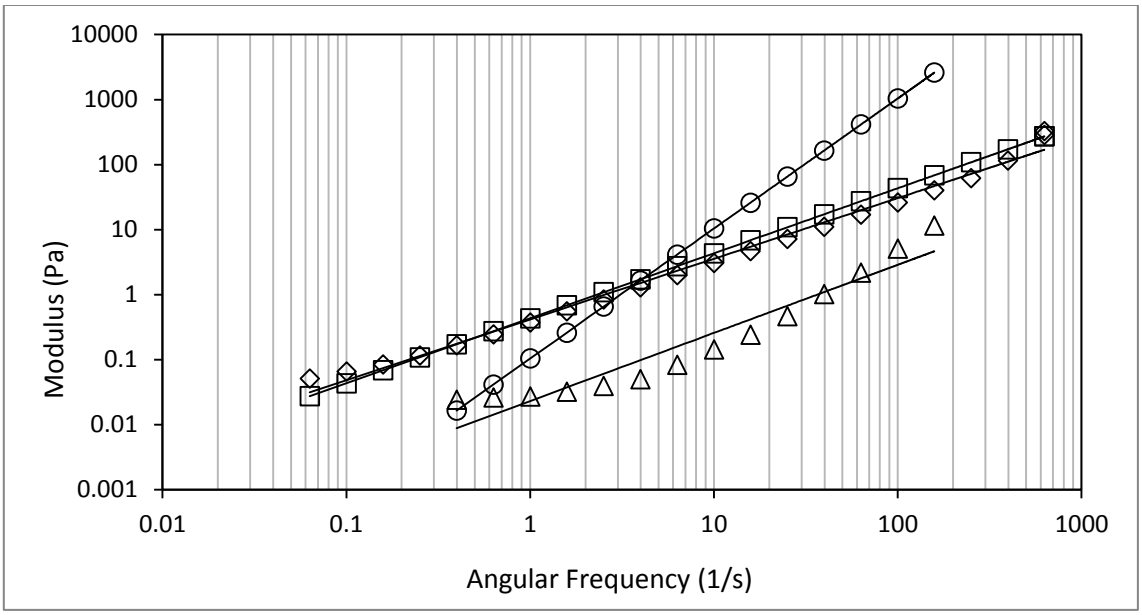

Figure A1.11 - Relaxation modulus to angular frequency relationship for GFS/SAT Real values for the storage (*G'*) modulus and loss (*G"*) modulus are shown as Δ and □ respectively. Adjusted linear fittings, from the tube model (λ), for *G'* and *G"* are shown as ◊ and ○ respectively.

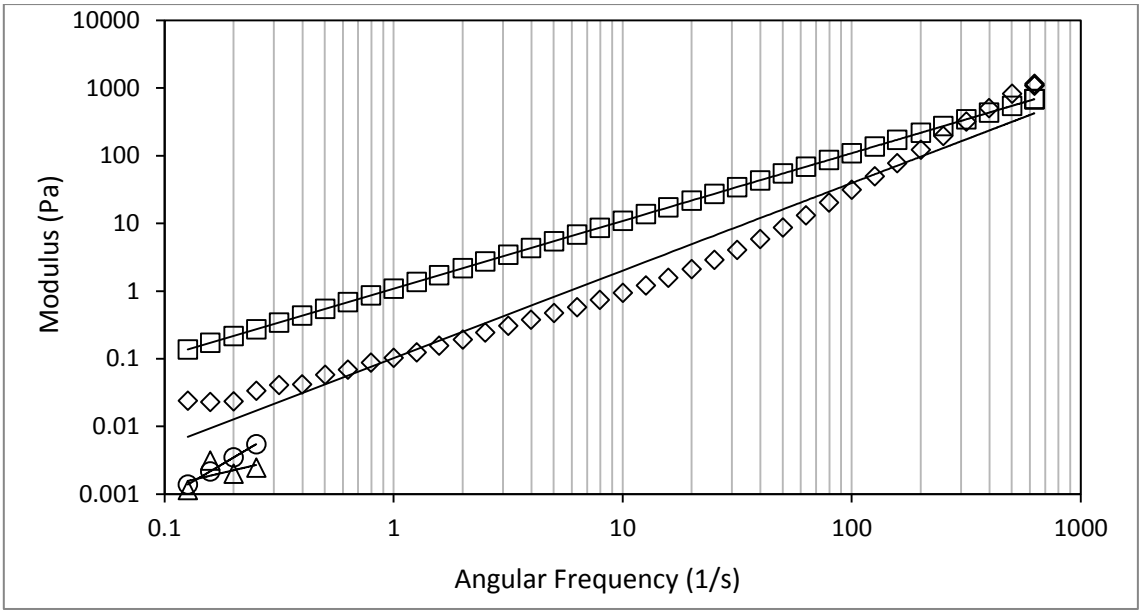

Figure A1.12 - Relaxation modulus to angular frequency relationship for GFS/– SAT Real values for the storage (*G'*) modulus and loss (*G"*) modulus are shown as Δ and □ respectively. Adjusted linear fittings, from the tube model (λ), for *G'* and *G"* are shown as ◊ and ○ respectively.

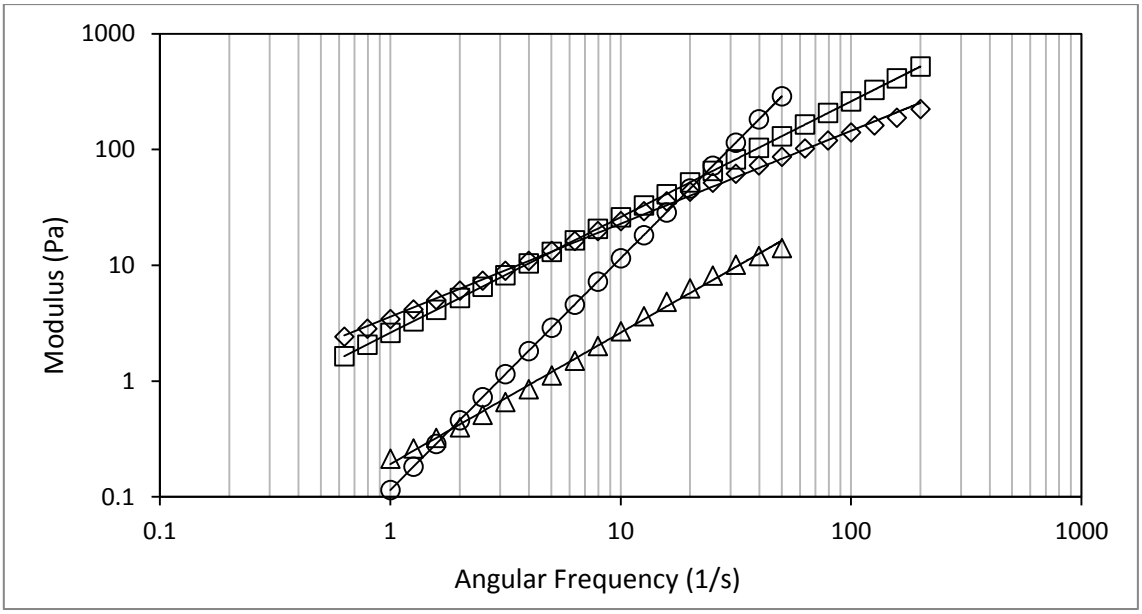

Figure A1.13 - Relaxation modulus to angular frequency relationship for GS/ +SAT Real values for the storage (*G'*) modulus and loss (*G"*) modulus are shown as Δ and □ respectively. Adjusted linear fittings, from the tube model (λ), for *G'* and *G"* are shown as ◊ and ○ respectively.

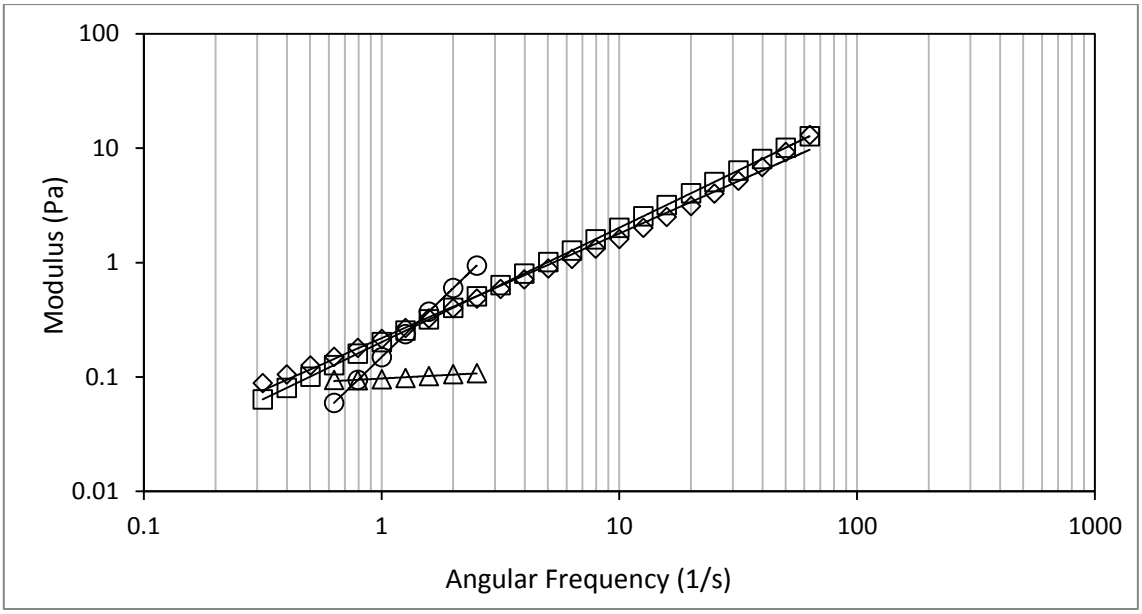

Figure A1.14 - Relaxation modulus to angular frequency relationship for GS/SAT Real values for the storage (*G'*) modulus and loss (*G"*) modulus are shown as Δ and □ respectively. Adjusted linear fittings, from the tube model (λ), for *G'* and *G"* are shown as ◊ and ○ respectively.

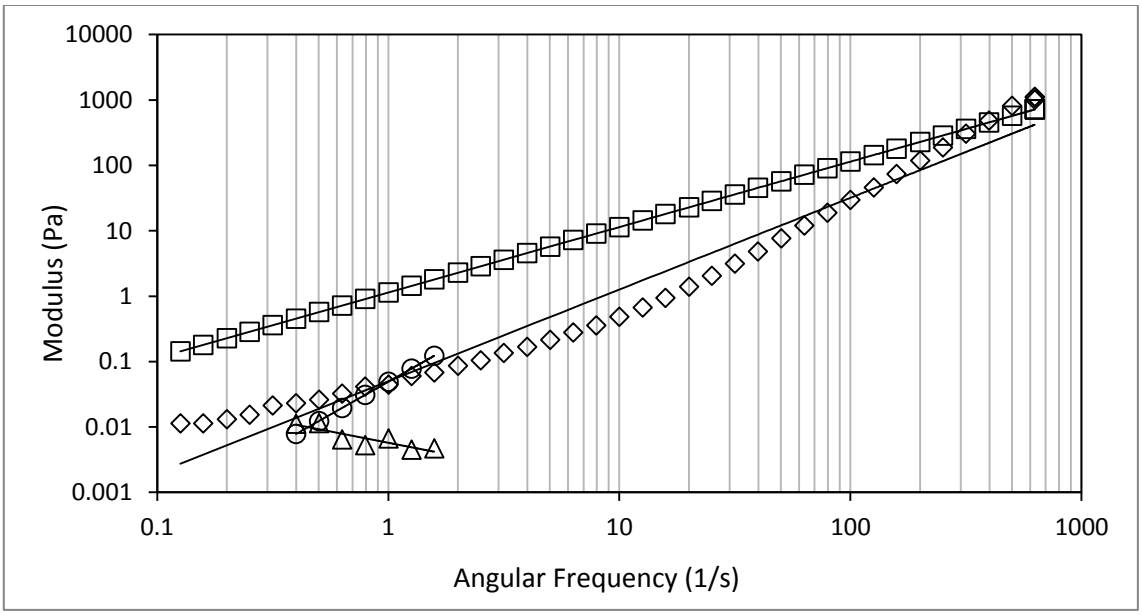

Figure A1.15 - Relaxation modulus to angular frequency relationship for GS/ –SAT Real values for the storage (*G'*) modulus and loss (*G"*) modulus are shown as Δ and □ respectively. Adjusted linear fittings, from the tube model (λ), for *G'* and *G"* are shown as ◊ and ○ respectively.

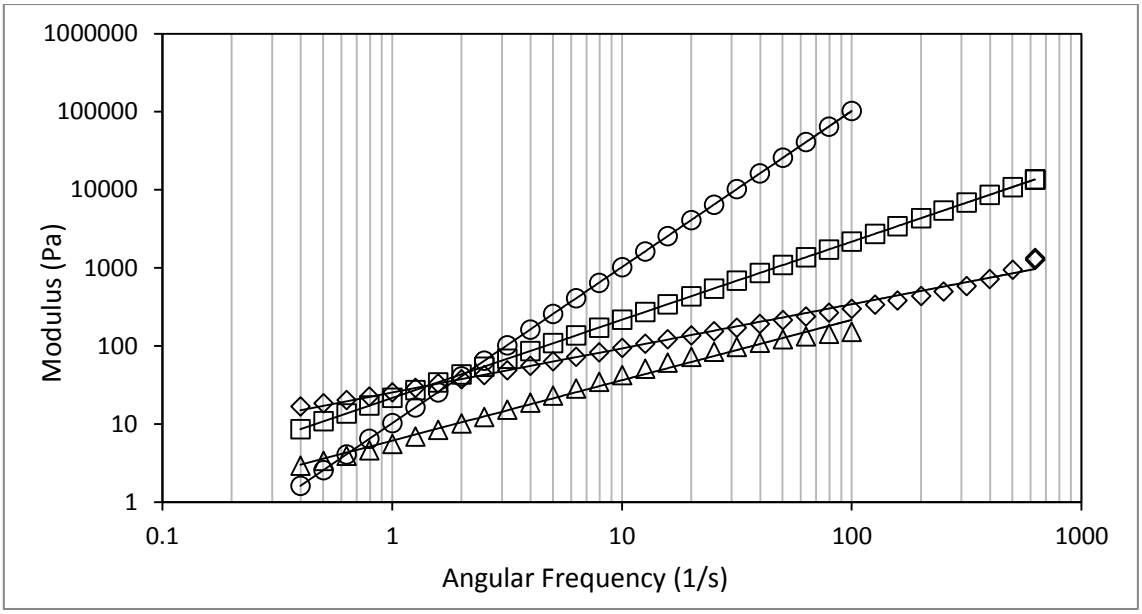

Figure A1.16 - Relaxation modulus to angular frequency relationship for SF/ +SAT Real values for the storage (*G'*) modulus and loss (*G"*) modulus are shown as Δ and □ respectively. Adjusted linear fittings, from the tube model (λ), for *G'* and *G"* are shown as ◊ and ○ respectively.

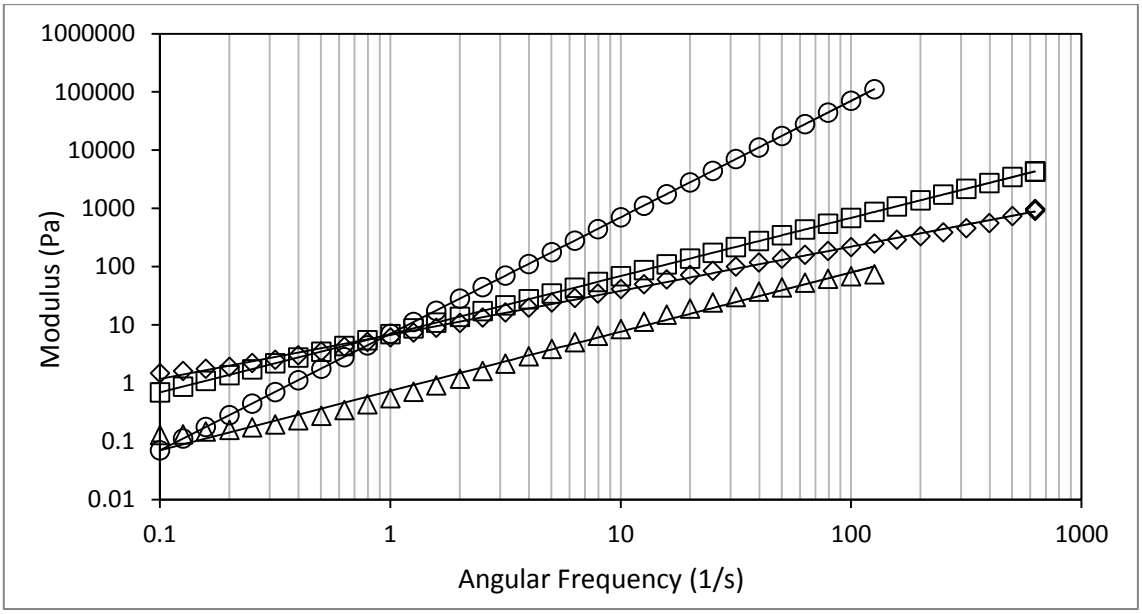

Figure A1.17 - Relaxation modulus to angular frequency relationship for SF /SAT Real values for the storage (*G'*) modulus and loss (*G"*) modulus are shown as Δ and □ respectively. Adjusted linear fittings, from the tube model (λ), for *G'* and *G"* are shown as ◊ and ○ respectively.

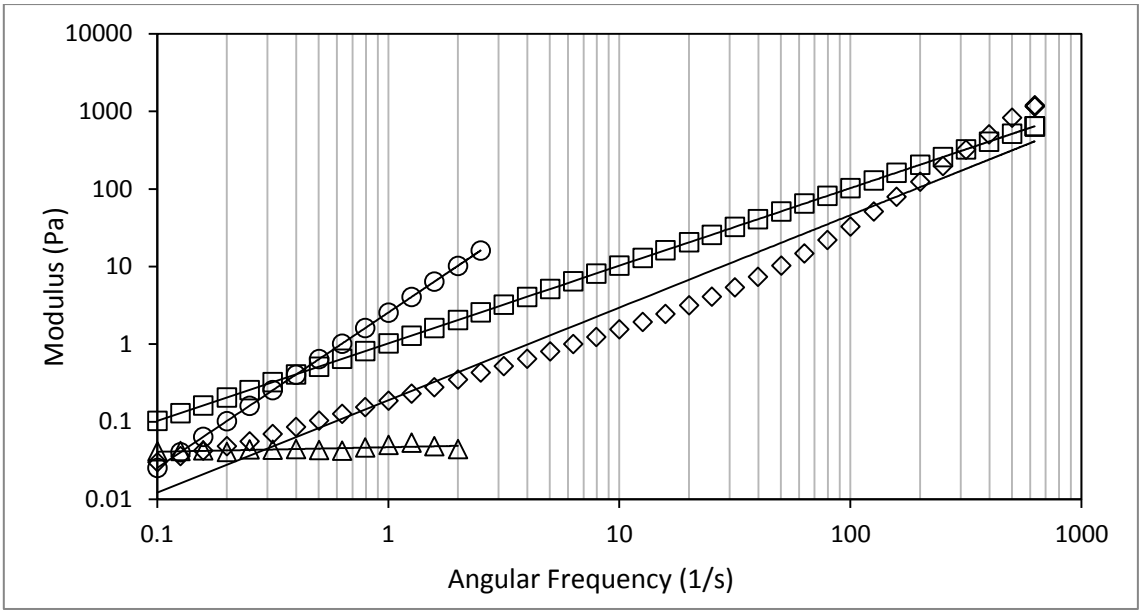

Figure A1.18 - Relaxation modulus to angular frequency relationship for SF/ – SAT Real values for the storage (*G'*) modulus and loss (*G"*) modulus are shown as Δ and □ respectively. Adjusted linear fittings, from the tube model (λ), for *G'* and *G"* are shown as ◊ and ○ respectively.

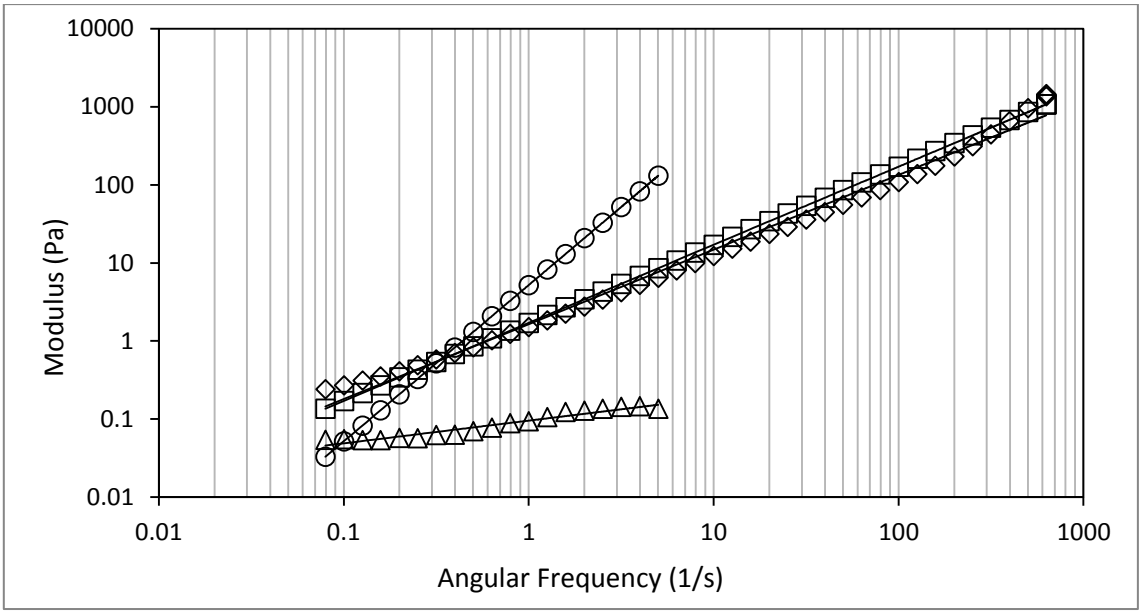

Figure A1.19 - Relaxation modulus to angular frequency relationship for GF/ +SAT Real values for the storage (*G'*) modulus and loss (*G"*) modulus are shown as Δ and □ respectively. Adjusted linear fittings, from the tube model (λ), for *G'* and *G"* are shown as ◊ and ○ respectively.

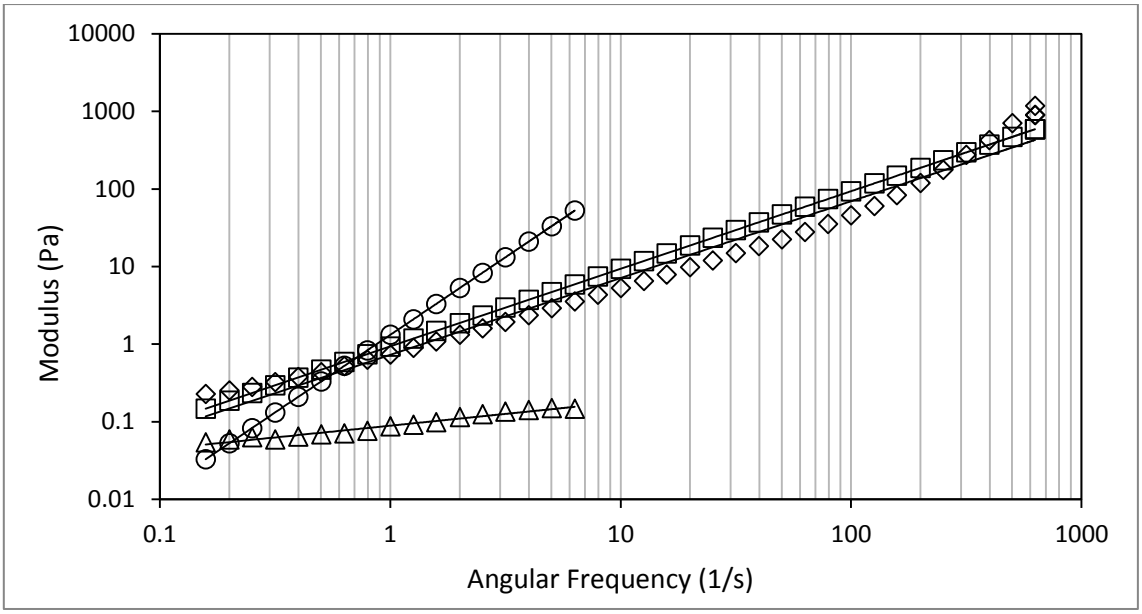

Figure A1.20 - Relaxation modulus to angular frequency relationship for GF/SAT Real values for the storage (*G'*) modulus and loss (*G"*) modulus are shown as Δ and □ respectively. Adjusted linear fittings, from the tube model (λ), for *G'* and *G"* are shown as ◊ and ○ respectively.

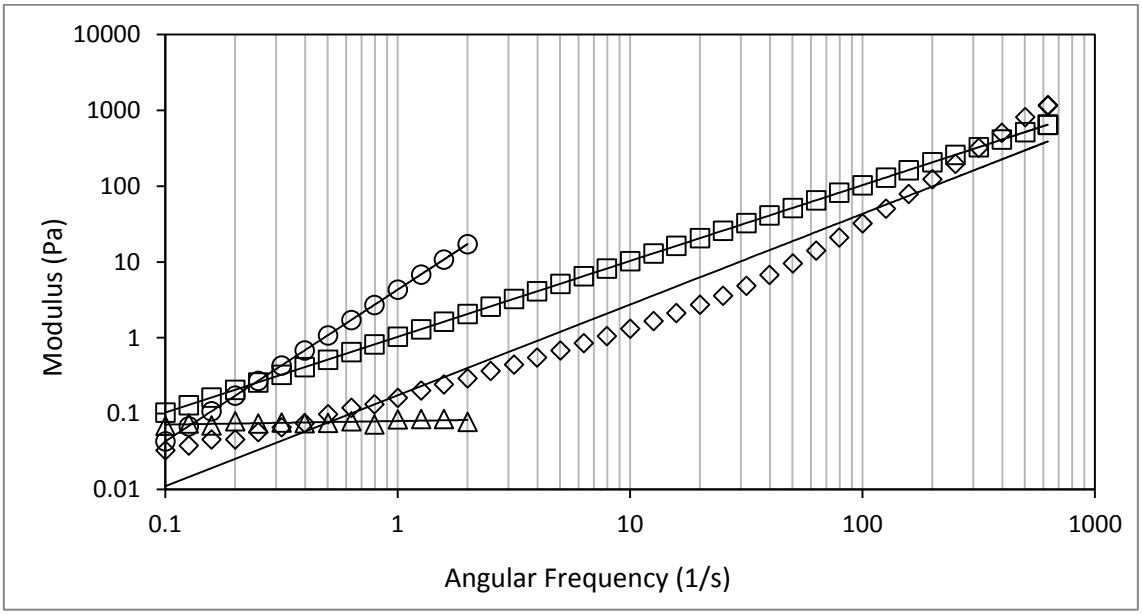

Figure A1.21 - Relaxation modulus to angular frequency relationship for GF/ –SAT. Real values for the storage (*G'*) modulus and loss (*G"*) modulus are shown as Δ and □ respectively. Adjusted linear fittings, from the tube model (λ), for *G'* and *G"* are shown as ◊ and ○ respectively.

Table A.1 List of all non-dimensional numbers calculated for all sample combinations and concentrations.

SAMPLE	Relaxation time (s)	Reynolds #	Weissenberg #	Capillary #	Weber #	Ohnesorge #	Elasticity #	Elastocapillary #	Deborah #
G -SAT	0.29	12.60	483.5	2.37E-07	2.99E-06	53124416.26	38.35	2037359660	285.40
G SAT	0.97	4.83	1835	8.40E-07	4.06E-06	5748942.55	379.75	2183163335	932.86
G +SAT	0.48	4.96	999.5	9.90E-07	4.91E-06	5006338.67	201.47	1008644947	462.73
F -SAT	0.30	2.59	932.7	4.02E-06	1.04E-05	644747.68	359.62	231868658.4	294.34
F SAT	6.98	1.56	33355	1.54E-05	2.42E-05	101574.83	21251.22	2158590135	6843.04
F +SAT	9.08	0.23	46333	0.00011	2.71E-05	1983.13	199821.40	396273819.2	8960.2
S -SAT	0.12	2.73	75.04	1.69E-07	4.62E-07	16183403.94	27.43	444026758.2	113.51
S SAT	3.97	1.56	3577	5.98E-07	9.38E-07	2619835.10	2281.36	5976805326	3784.38
S +SAT	2.36	0.09	4193	3.89E-05	3.80E-06	2507.18	42933.48	107642047.5	2218.53
GFS -SAT	0.07	1.87	43.91	1.42E-07	2.68E-07	13174124.42	23.36	307783603.1	83.11
GFS SAT	0.24	0.99	198.0	6.14E-07	6.09E-07	1615225.13	199.66	322509141.9	249.11
GFS+SAT	0.25	0.69	590.8	6.60E-06	4.59E-06	105522.53	848.24	89508646.64	270.16
GF -SAT	4.18	1.36	2403	2. 05E-07	2.81E-07	6657883.62	1755.20	11685970321	4409.73
GF SAT	1.40	1.14	1550	9.53E-07	1.09E-06	1198555.62	1355.92	1625151626	1458.92
GF +SAT	3.04	0.72	5705	4.37E-06	3.17E-06	165548	7868.81	1302672347	3147.82
GS -SAT	0.04	5.24	26.90	6.29E-08	3.30E-07	83243	5.13	427248888.3	45.53
GS SAT	0.74	2.48	629.97	2.39E-07	5.95E-07	10375388.2	253.44	2629590787	790.48
GS +SAT	0.04	0.46	44.0	1.73E-06	8.12E-07	269374.68	94.26	25393483.74	47.26
FS -SAT	2.49	1.71	1871	2.78E-07	4.76E-07	6140085.70	1093.46	6713992201	2636.03
FS SAT	1.02	0.97	2271	4.57E-06	4.44E-06	211972.35	2340.27	496073830.7	1058.21
FS +SAT	0.47	0.25	1098	2.04E-05	5.29E-06	12675.36	4239.83	53741408.02	475.69